This is to certify that the
dissertation entitled

ELECTROSPINNING CELLULOSE BASED NANOFIBERS
FOR SENSOR APPLICATIONS

presented by

Steven Nartker

has been accepted towards fulfillment
of the requirements for the

Doctoral degree in Chemical Engineering

Lawrence T. Drzal
Major Professor's Signature

12-08-2009
Date

ELECTROSPINNING CELLULOSE BASED NANOFIBERS FOR SENSOR APPLICATIONS

By

Steven Nartker

A DISSERTATION

Submitted to
Michigan State University
in partial fulfillment of the requirements
for the degree of

DOCTOR OF PHILOSOPHY

Chemical Engineering

2009

ABSTRACT

ELECTROSPINNING CELLULOSE BASED NANOFIBERS FOR SENSOR APPLICATIONS

By

Steven Nartker

Bacterial pathogens have recently become a serious threat to the food and water supply. A biosensor based on an electrochemical immunoassay has been developed for detecting food borne pathogens, such as *Escherichia coli (E. coli)* O157:H7. These sensors consist of several materials including, cellulose, cellulose nitrate, polyaniline and glass fibers. The current sensors have not been optimized in terms of microscale architecture and materials. The major problem associated with the current sensors is the limited concentration range of pathogens that provides a linear response on the concentration conductivity chart. Electrospinning is a process that can be used to create a patterned fiber mat design that will increase the linear range and lower the detection limit of these sensors by improving the microscale architecture. Using the electrospinning process to produce novel mats of cellulose nitrate will offer improved surface area, and the cellulose nitrate can be treated to further improve chemical interactions required for sensor activity.

The macro and micro architecture of the sensor is critical to the performance of the sensors. Electrospinning technology can be used to create patterned architectures of nanofibers that will enhance sensor performance. To date electrospinning of cellulose nitrate has not been performed and optimization of the electrospinning process will provide novel materials suitable for applications such as filtration and sensing. The goal of this research is to identify and elucidate the primary materials and process factors necessary to produce cellulose nitrate nanofibers using the electrospinning process that will improve the performance of biosensors.

Cellulose nitrate is readily dissolved in common organic solvents such as acetone, tetrahydrofuran (THF) and N,N dimethylformamide (DMF). These solvents can be mixed with other latent solvents such as ethanol and other alcohols to provide a solvent system with good electrospinning behavior. Using cellulose nitrate in biosensor materials provides excellent antibody binding characteristics that are resistant to pH changes.

Sensors will be constructed of electrospun materials and compared to existing materials. The main advantage of electrospinning fiber mats is the increased surface area, and controllable morphology, which ultimately affects biosensor performance. Characterization tools will include Environmental Scanning Electron Microscopy (ESEM), BET N_2 adsorption, X-Ray Photoelectron Spectroscopy (XPS), Dynamic Mechanical Analysis (DMA) and AC impedance.

ACKNOWLEDGEMENTS

My first acknowledgement goes to Professor Lawrence T. Drzal. I would like to thank him for providing the research tools, personal support, encouragement, mentoring which made my research enjoyable. I would also like to thank my Ph.D. committee members, professors Ilsoon Lee, Ramani Narayan, and Evangelyn Alocilja, and to the Department of Chemical Engineering and Materials Science.

I would like to extend a special thank you to Dr. Manju Misra, Dr. Hazel-Ann Hosein, Dr. Per Askeland, Brian Rook, Ed Drown, and Mike Rich in the Composite Materials and Structures Center for providing a safe, professional, and instructive work environment, and for their friendship along the years. I would especially like to thank Dr. Askeland for his support, expertise and guidance. I would also like to thank Sara and Michael Wiederoder for their assistance. I would also like to thank all the graduate students that I shared an office with.

I am very grateful for the unlimited support of my family through this process. I truly appreciate Amy who provided encouragement and support.

TABLE OF CONTENTS

LIST OF TABLES

LIST OF FIGURES

Images in this dissertation are presented in color.

CHAPTER 1

Introduction

Problem Statement

Bacterial pathogens have recently become a serious threat to the food and water supply. A biosensor based on an electrochemical immunoassay has been developed for detecting food borne pathogens, such as *Escherichia coli (E. coli)* O157:H7. These sensors consist of several materials including, cellulose, cellulose nitrate, polyaniline (PANi) and glass fibers. The major problem associated with the current sensors is the limited concentration range of pathogens that provides a linear response on the concentration conductivity chart. The current sensors have not been optimized in terms of microscale architecture and materials.

The macro and microscale architecture of the sensor is critical to the performance of the sensors. The commercial capture pad materials that are used do not optimize surface area or capillary flow properties, which are essential for efficient biosensor performance. Electrospinning technology can be used to create patterned architectures of nanofibers that will enhance sensor performance. Electrospinning is a process that can be used to create nanoscale

diameter fibers with large surface areas in a patterned design that will increase the linear range and lower the detection limit of these sensors by improving the microscale architecture. To date electrospinning of cellulose nitrate and cellulose nitrate functionalized with PANi has not been performed and optimization of the electrospinning process will provide novel materials suitable for applications such as filtration and sensing. Electrospinning is the preferred method for producing nanoscale fibrous materials since it can be controlled to produce various morphological structures within the overall capture pad size constraint of 20 mm X 5 mm.

Electrospinning to produce novel mats of cellulose nitrate has the potential to provide substrates with increased surface area and a preferred alignment to enhance pathogen transport and detection. Post-treatment of the electrospun cellulose nitrate fibers will be performed to further improve chemical interactions, and capillary flow properties required for sensor activity. Cellulose nitrate can serve as a core polymer and conductive polymers, such as PANi or polypyrrole (PPy) can be polymerized on the surface and the resultant core sheath fibers have potential for use as biosensor materials. Addition of biologically active materials to the cellulose nitrate membrane will provide a novel approach to creating biosensor materials with improved functionality. Controlling the electrospinning process to produce aligned homogenous nanoscale fibrous mats that offer optimal pore size, surface area, capillary flow and chemical properties will increase the detection limit and expand the concentration range inherent in current biosensor devices.

Research Goals

The goal of this research is to identify and elucidate the primary material variables and process parameters necessary to produce cellulose nitrate, and cellulose nitrate functionalized with PANi or PPy nanofibers using the electrospinning process in order to improve the performance of biosensors. Ultimately all the material and processing parameters will be evaluated to determine the optimal conditions to consistently produce nanofiber films that will be utilized as capture pad materials in biosensor devices.

Electrospinning cellulose nitrate has not been reported in the literature. Cellulose nitrate is readily dissolved in common organic solvents such as acetone, N, N' dimethylformamide (DMF) and tetrahydrofuran (THF). These solvents can be mixed with other latent solvents such as ethanol and other alcohols to provide a solvent system with good electrospinning behavior. The importance of this research then is to understand the conditions necessary to produce aligned homogenous cellulose nitrate nanofibers. Since cellulose nitrate has the potential to provide excellent antibody binding characteristics that are resistant to pH changes in biosensor devices, the initial emphasis will focus on electrospinning of pure cellulose nitrate. Following success in this aspect of the research, a core sheath fiber consisting cellulose nitrate with polyaniline or polypyrrole will be used to obtain conductive fiber networks.

Research Approach

Initial efforts to understand and model the electrospinning process will be conducted using a well-characterized water-soluble polymer system of poly (vinyl alcohol) (PVOH). The choice of PVOH as a model was dictated by its easy dissolution in deionized water and its documented predictable electrospinning behavior. The electrospinning processing parameters of the electric field strength, solution flow rate, viscosity and collector design will be investigated for their relationship to changes in the fiber diameter and morphology. Once the general electrospinning trends are understood, the system will be changed to the cellulose nitrate polymer solution.

In the case of cellulose nitrate, two solvents are necessary to provide the most stable electrospinning behavior. These solvents can be adjusted to balance the surface tension, viscosity, and volatility of the solution. Cellulose nitrate and cellulose nitrate functionalized with PANi or PPy will be characterized for morphological electrical, mechanical, thermal, surface area, capillary flow, surface chemistry and biosensor performance properties. The fiber morphology will be characterized first, using Environmental Scanning Electron Microscopy (ESEM). The ESEM will provide fiber size distribution data, fiber alignment properties as well as an optical verification of pore size distribution. Quantification of the surface area and pore size distribution will be accomplished by nitrogen adsorption coupled with analysis using the Brunauer, Emmett, and Teller (BET) equation. The electrospun fibers will also be investigated through the use of thermal gravimetric analysis (TGA) to quantify the polymer

degradation temperature, verify the PANi or PPy loading and quantify any residual solvents. Bulk chemical compositional information will be obtained by Fourier Transform infrared spectroscopy (FTIR) and the fiber surface chemical analysis will be performed using X-Ray Photoelectron Spectroscopy (XPS). Electrical characterization will be completed using AC impedance measurements. Physical properties such as capillary flow and water contact angle will also be measured. Methods such as plasma treatment will be employed to alter the capillary flow and water contact angle properties. The effects of post-treatment on the fiber morphology will also be understood.

Ultimately the electrospun nanofibrous materials will be fabricated into biosensors and compared to the commercially available existing materials. As a result of this research, the primary material variables and process parameters necessary to produce cellulose nitrate, and cellulose nitrate functionalized with PANi or PPy nanofibers using the electrospinning process in order to improve the performance of biosensors will be identified and utilized to optimize biosensor performance.

CHAPTER 2

BACKGROUND AND LITERATURE REVIEW

Abstract

This chapter provides a description of the electrospinning process, and the development of sensor devices, in particular biosensor devices using the electrospinning technique. The nanofibers that are produced generally improve the quality and performance of the device by producing an increased surface area, controllable architecture, and specific chemical incorporation that only electrospinning can provide. The development of models has allowed researchers to eliminate costly steps in creating new electrospun technologies. The electrospinning process has allowed for the creation of biosensors with lower detection limits, increased stability, improved specificity, and enlarged linear response regions. The electrospun biosensor is still in its infancy, but the future is full of promise as researchers focus on specific details of the process and its effects on the biosensor device performance.

Introduction

Nanotechnology is the study and development of materials at nanoscale levels. It is a rapidly growing scientific discipline due to its enormous potential in creating novel materials that have advanced applications, such as high value sensors. This technology has tremendously impacted many different science and engineering disciplines, such as electronics, materials science, and polymer engineering. Nanofibers, due to their high surface area and porosity, have applications as filter media, adsorption layers in protective clothing, and reinforcing materials. Electrospinning has been found to be a viable technique to produce nanofibers in an efficient manner.

Cellulose is the most abundant organic material on the surface of earth. It is the main constituent of paper and plant cell walls. Cellulose consists of linear glucose polymer chains, which form hydrogen bonded supramolecular structures. Cellulose is a renewable resource, but is not soluble in water and most organic solvents. Functionalized cellulose such as cellulose nitrate (CN) is soluble in many common organic solvents and is important for many industries with applications in packaging, coatings, adhesives and sensors.

Biosensors are an important application for electrospun cellulose based materials since they offer improved surface area over existing technologies. The improved surface area is responsible for lower the detection limit, decreasing the detection time and improving the sensitivity of the sensors. Surface nitro (NO_2) functional groups are essential for binding specific antibodies used in the biosensor construction.

Electrospinning

In textile and fiber science related scientific literature, fibers with diameters in the range 100 nm – 500 nm are generally referred to as nanofibers.[1] Electrospinning is a unique approach using electrostatic forces to produce nanoscale fibers. The advantages of the electrospinning process are its technical simplicity and its easy adaptability. In general electrospun fibers have small pore size and high surface area. There is also evidence that the relatively large static charges in electrospun fibers can be effectively handled to produce three-dimensional structures.[2]

The apparatus used for electrospinning is simple in construction, consisting of a high voltage electric source with positive or negative polarity, a syringe pump with capillaries or tubes to carry the solution from the syringe or pipette to the spinneret, and a conducting collector such as aluminum. The collector can be made of any shape according to the product requirements, such as a flat plate, rotating drum, or patterned collector. Fibrous structures can be produced as random, aligned or patterned networks, depending on the processing equipment used; in particular the collector choice is crucial for producing patterned electrospun architectures. Polymers, composites, ceramics and metals have all been created using either solution based or melt based electrospinning.[3] A schematic of the electrospinning process is shown in Figure 2.1.

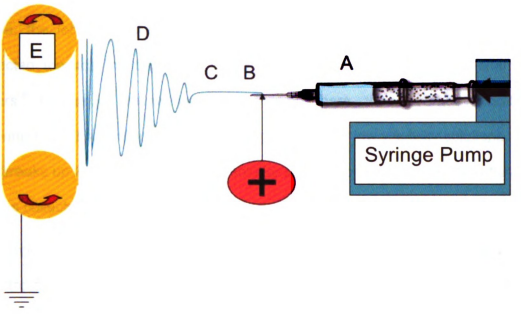

Figure 2.1 Electrospinning schematic showing A) the syringe, B) the Taylor Cone, C) the stable region, D) the instability region and E) the rotating drum style collector.

A polymer solution or melt is forced through a needle from a syringe pump to form a pendant drop of the polymer at the tip of the capillary. A high voltage potential is applied to the polymer solution inside the syringe through an attached electrode, thereby inducing free charges into the polymer solution. These charged ions move in response to the applied electric field towards the electrode of opposite polarity, thereby transferring tensile forces to the polymer liquid.[4] At the tip of the capillary, the pendant hemispherical polymer drop forms in the presence of an electric field; this is known as the Taylor cone.[5] When the applied potential reaches a critical value required to overcome the surface tension of the

liquid, a jet of liquid is ejected from the cone tip.[4] After the initiation from the cone, the jet undergoes a chaotic motion or bending instability and is field directed towards the oppositely charged collector, which collects the charged fibers.[6] As the jet travels through the atmosphere, the solvent evaporates, leaving behind a dry fiber on the collecting device. For low viscosity solutions, the jet breaks up into droplets, while for solutions with appropriate viscosity, it travels to the collector as a charged fiber jets.[2]

Anton Formhals first demonstrated production of synthetic filaments using electrostatic forces in 1934.[7] The use of electrostatic forces to create fibers from a polymer melt or solution was first known as electrostatic spraying. This name was condensed in the 1990's to the current name of electrospinning. It has been shown recently that the electrospinning process is capable of producing fibers in the submicron range.[6] Electrospinning has increased in popularity over the last ten years due to its flexibility to produce numerous polymeric fibers and the consistency and ease of producing fibers in the nanoscale. These fibers generally have higher surface area than regular fibers, and have applications in filtration, catalysis, biomedicine, protective clothing and sensors.

Research activity on the electrospinning of nanofibers has been successful in spinning submicron range fibers from different polymeric solutions and melts. Variations of the collector size and shape are crucial for developing the desired final fiber arrangement. Recently groups have used flat solid surfaces to obtain random arrays of fibers[8], while wire meshes[9], rotating drums[10] and patterned electrodes[11] can be used to create patterned or aligned fiber networks. In

conventional fiber spinning methods, the fiber is subjected to a group of tensile, gravitational, aerodynamic, rheological, and inertial forces.[4] In electrospinning, the tensile forces created in the axial direction of the flow of the polymer by the induced charges in the presence of an applied electric field accomplish the production of fibers. The collector design and electric field parameters are essential for obtaining the desired morphology of fibers.

Electrospinning is a relatively low volume operation, which typically produces materials with a small geometric footprint; therefore the desired products should be utilized in high value applications. The focus of this review is the exploitation of electrospinning technology for the development of biosensor devices. Reviews of the general electrospinning literature are readily available[12-15]. A review of nanofiber materials for biosensors is also available[16,17]. Information regarding the polymers that can be used, the processing equipment parameters and specifically the use of these fibers in biosensor devices will be discussed.

Modeling of the Electrospinning Process

The electrospinning process can be used to produce nanoscale fibers. These fibers have large aspect ratios, and high surface area per unit volume, which is important for many applications, such as sensors. The electrospinning process is very complex and the resultant fiber size is influenced by numerous processing parameters, material variables and equipment designs. The majority of the information regarding the electrospinning process has been obtained empirically,

but the complexity of the process makes empirical determination of the parameter effects very difficult, costly and often impractical. By using a suitable theoretical model, the effects of parameters on the fiber diameter can be evaluated in a more efficient manor.

The modeling data can be used to determine which parameters have the greatest influence on the resultant fiber diameter. Special concentration on the most influential factors can be conducted using empirical studies to determine relationships for the resultant fiber size. Empirical observations indicate that the smallest fiber diameters can be obtained at low flow rates, and low polymer concentrations, due to the small amount of material available. It has been determined that solution concentration is primarily responsible for final fiber diameter,[2] but this approach is limited to a narrow window of spinnable solution concentrations, and it is further reduced when defect free fibers are required.

Using a model that considers the stretching of a viscous charged fluid in the presence of an electric field could lead to a quicker approach for determining the final jet diameter. The model predicts the final diameter of the fluid arises from a force balance between the surface tension of the fluid and electrostatic charge repulsion. Several approaches based on stretching have been reported.[18-21] Simple scaling laws have also been proposed, but they are not as universally applicable as other more rigorous modeling techniques.[22-24] There have also been efforts to predict fiber alignment based on the applied electric fields.[25]

In the electrospinning process, a polymer solution is in contact with a large electric potential at the tip of a small capillary. The electrical charges that

develop and the fluid's free surface interact with the external electric field, resulting in the emission of a steady fluid jet that thins as it accelerates downfield as shown in Figure 2.1. The charged jet experiences a whipping instability, leading to bending and stretching of the jet, which is observed as loops of increasing size as the instability grows.[4] The whipping jet thins dramatically as it travels towards the collector. The solvent evaporates during the whipping process, and solid fibers are collected on the collector surface.

The goal of predictive models is to ascertain the approximate solution properties and electrospinning equipment variables before entering the laboratory. This method will reduce the amount of time, money and energy necessary to produce electrospun fibers. To date, the electrospinning modeling literature is somewhat limited. There are sources, which define basic scaling relationships for the resultant fiber diameters, describe the bending and stretching of the jet, and dimensionless analysis to correlate known properties to fiber diameters and morphologies. A brief review of several of the more common models is given below. In each case a table of the data will be shown followed by a graphical representation. A concise discussion of the advantages and drawbacks of each model will conclude each section.

Predicting Fiber Diameter using Solution Viscosity

Information regarding the solution viscosity is required as an initial basis to determine the resultant fiber diameter. There are numerous relations in the

literature for viscosity and its effect on fiber diameter.[26-28] The most common is a power law relation.[29, 30] More sophisticated approaches include understanding the force balances and relating solution to electrical forces. The final approach is to use dimensionless analysis.

The most basic predictive models have been proposed to correlate the fiber diameter with the solution viscosity or concentration. There is a minimal concentration necessary to produce homogenous fibers. Viscosity and concentration are related and increasing either variable tends to produce larger diameter fibers. If the viscosity of the solution is too low, beaded morphology will dominate, and if the viscosity is too high, fibers will tend to agglomerate.

Most viscosity values that are reported in the literature are zero-shear values. The experimental data show a strong dependence on viscosity for fiber morphology.[27, 31, 32] Nearly every referenced work concluded that increasing the zero-shear viscosity, using either a higher MW polymer or higher concentration, would increase the resulting fiber radius. The only exceptions to this rule would be in cases where the nozzle becomes partially plugged or flow is somehow decreased so that a full size droplet is not available at the needle tip. The initial elongational viscosity is weakly related to the zero-shear viscosity. It characterizes the stretching of the polymer solution, which is a transition from the tip of the Taylor cone to the beginning of the jet. The higher the initial elongational viscosity means a stronger stretching force must be applied to create charged fibers. This increased force is related to the applied voltage.[33]

Investigations of viscosity as it relates to fiber diameter are numerous.[29] There is a desire to quantify the relationships that connect the resultant fiber morphology and fiber diameter to the solution's rheological and electrical properties and the processing parameters. The goal of Daga's model was to determine if there is a correlation between the zero shear viscosity and electrospun fiber diameter for aqueous polymer solutions. Equation 2.1 shows the power law dependence for the diameter (D) based on the zero shear viscosity (η_0).

$$D = (127 \pm 6)\eta_0^{0.16\pm0.02} \qquad \text{(Equation 2.1)}$$

The data set that was used to evaluate the accuracy of the model is shown as Table 2.1. The data set includes values that were determined at the average values in Equation 2.1, that is the actual equation that was used in the modeling is shown as Equation 2.2.

$$D = (127)\eta_0^{0.16} \qquad \text{(Equation 2.2)}$$

Table 2.1 Daga model data set

Reference	Polymer	Wt%	Solvent	Zero Shear Viscosity (kg/ms)	Actual Fiber Radius (m)	Daga Model	
						Model Fiber Radius (m)	Percent comparison
This Work	CN	12	6:4 THF:DMF	12.85	2.25E-07	9.48.E-08	137%
This Work	CN	8	6:4 THF:DMF	8.45	9.50E-08	8.86.E-08	7%
This Work	CN	6	7:3 EtOh:Ace	6.50	1.75E-07	8.50.E-08	106%
This Work	CN	10	7:3 EtOh:Ace	15.20	6.00E-07	9.74.E-08	516%
This Work	CN	8	7:3 EtOh:Ace	11.65	4.50E-07	9.33.E-08	382%
This Work	CN	6	7:3 EtOh:Ace	9.25	1.65E-07	8.99.E-08	83%
This Work	PVOH	10	water	5.80	1.50E-07	8.35.E-08	80%
This Work	PVOH	10	water	5.80	1.40E-07	8.35.E-08	68%
Daga, 2006	PEO	2.52	water	0.18	4.20E-08	4.79.E-08	-12%
Daga, 2006	PEO	3.74	water	0.91	6.65E-08	6.21.E-08	7%
Daga, 2006	PEO	4.5	water	2.65	7.65E-08	7.36.E-08	4%
Daga, 2006	PEO	5.5	water	6.44	8.90E-08	8.49.E-08	5%
Daga, 2006	PEO	6.5	water	15.60	9.55E-08	9.78.E-08	-2%
Deitzel, 2001	PEO	7	water	4.00	1.13E-07	7.86.E-08	43%
Deitzel, 2001	PEO	10	water	16.00	2.00E-07	9.82.E-08	104%

A graphical representation of the data set is shown as Figure 2.2. The solid model prediction line shows a good fit with the PEO water data. The cellulose nitrate data points do not fit very well, with errors of actual fiber diameter as compared to model predicted diameters larger that 100%. The polyvinyl alcohol data points show a closer fit, with errors that are less than 100%. The general trend is observed for all data, that is, as the zero shear viscosity is increased, the fiber diameter increases.

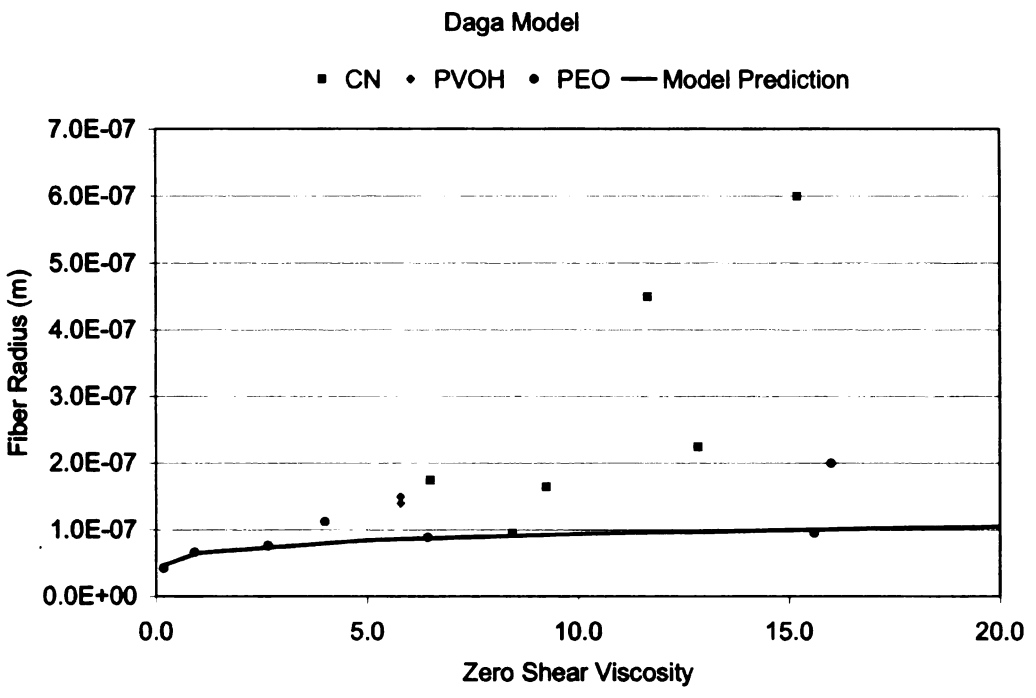

Figure 2.2 Daga data chart showing a good fit for PEO water, but a poor fit for CN and PVOH.

Another model relating the zero shear viscosity to the final fiber diameter was proposed by McKee.[30] As shown Equation 2.3, this model uses much stronger power law dependence. The data table that was used to test the validity of this model is shown in Table 2.2.

$$D = (0.05)\eta_0^{(0.8)} \qquad \text{(Equation 2.3)}$$

Table 2.2 McKee data table

Reference	Polymer	Wt%	Solvent	Electric Field Strength (kg*m/A*s3)	Zero Shear Viscosity (kg/ms)	Actual Fiber Radius (m)	McKee Model	
							Model Fiber Radius (m)	Percent comparison
This Work	CN	12	6:4 THF:DMF	1.67E+05	12.85	2.25E-07	4.E-07	-36%
This Work	CN	8	6:4 THF:DMF	1.33E+05	8.45	9.50E-08	3.E-07	-62%
This Work	CN	6	7:3 EtOh:Ace	1.25E+05	6.50	1.75E-07	2.E-07	-14%
This Work	CN	10	7:3 EtOh:Ace	1.00E+05	15.20	6.00E-07	4.E-07	49%
This Work	CN	8	7:3 EtOh:Ace	1.00E+05	11.65	4.50E-07	3.E-07	39%
This Work	CN	6	7:3 EtOh:Ace	1.00E+05	9.25	1.65E-07	2.70E-07	-39%
This Work	PVOH	10	water	8.00E+04	5.80	1.50E-07	1.86E-07	-19%
This Work	PVOH	10	water	1.10E+05	5.80	1.40E-07	1.86E-07	-25%
Daga, 2006	PEO	2.52	water	1.54E+05	0.18	4.20E-08	1.15E-08	264%
Daga, 2006	PEO	3.74	water	1.54E+05	0.91	6.65E-08	4.22E-08	58%
Daga, 2006	PEO	4.5	water	1.54E+05	2.65	7.65E-08	9.93E-08	-23%
Daga, 2006	PEO	5.5	water	1.54E+05	6.44	8.90E-08	2.02E-07	-56%
Daga, 2006	PEO	6.5	water	1.54E+05	15.60	9.55E-08	4.10E-07	-77%
Deitzel, 2001	PEO	7	water	4.24E+04	4.00	1.13E-07	1.38E-07	-18%
Deitzel, 2001	PEO	10	water	4.24E+04	16.00	2.00E-07	4.18E-07	-52%
Lee, 2003	PVC	15	THF	1.00E+05	1.00	3.00E-06	4.55E-08	6491%
Lee, 2003	PVC	15	6:4 THF:DMF	1.00E+05	1.00	4.00E-07	4.55E-08	779%
Lee, 2003	PVC	15	4:6 THF:DMF	1.00E+05	1.00	5.00E-07	4.55E-08	999%
Lee, 2003	PVC	15	DMF	1.00E+05	1.00	2.00E-07	4.55E-08	339%

A graphical representation of the data set is shown as Figure 2.3. The model shows a decent fit for all data points. The trend of increasing zero shear viscosity leads to increased fiber diameter is observed. This particular equation is a more accurate fit than the model proposed by Daga.[29]

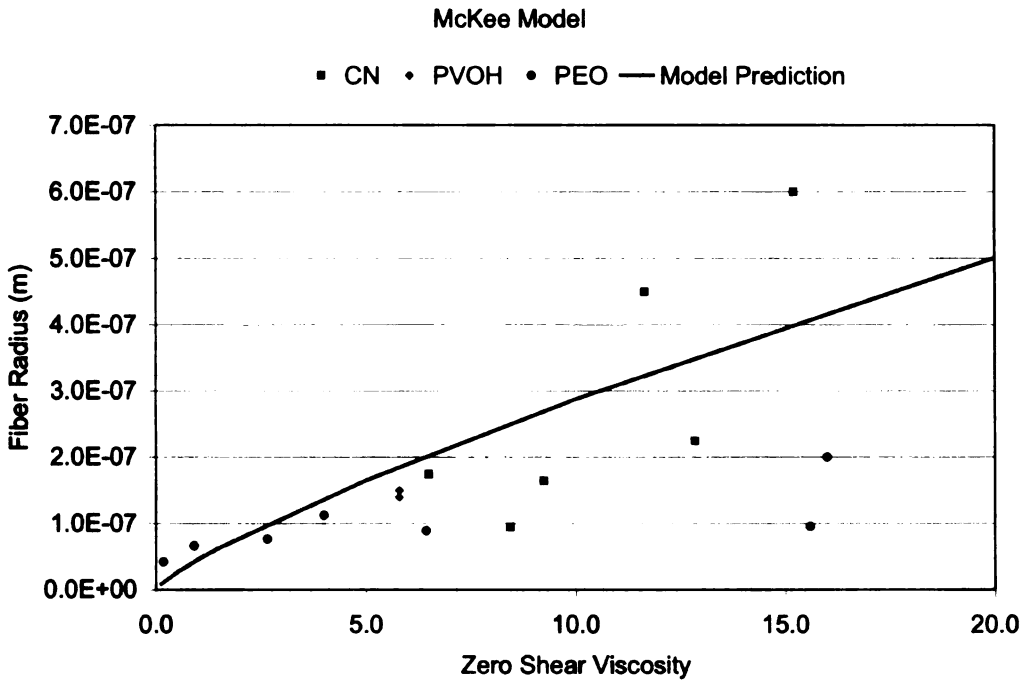

Figure 2.3 McKee model chat showing good correlation for PEO at low viscosity values and a relatively poor fit for CN and PVOH.

Correlations for the final fiber diameter as a function of zero-shear viscosity have been shown. In addition to the relationship shown above Equation 2.3, it was proposed that the viscosity dependence of the fiber diameter was due to the influence of polymer chain entanglements on the rheology of the solutions, and thus the fiber diameter correlated well with the polymer concentration scaled by the critical concentration for entanglements as shown in Equation 2.4.

$$D = \left[\frac{C}{C_e}\right]^{2.8}$$

(Equation 2.4)

Further work by McKee et al showed that for solutions with associative interactions, such as hydrogen bonding, the fiber diameter increases more strongly with polymer concentration than expected for nonassociative polymers.[34]

The advantage of these models is that it is relatively accurate and easy to calculate, rely solely upon the zero shear viscosity of the solution. In cases where crude estimations are necessary, this model would provide the appropriate results. The disadvantage is that the data set used is small, and does not vary much in terms of processing and solution variables. Most electric field strengths used in the data set are similar. This model may not be applicable to filled solutions, solutions with different conductivity, or different processing variables.

Fiber Diameter Predictions Using Force Balances

The model proposed by Fridrikh predicts a fiber diameter resulting from a force balance between electrostatic charge repulsion and surface tension forces.[35] This is shown as Equation 2.5 below. This model relies on parameters and data that are very difficult to obtain experimentally. For example the radius of whipping χ is only shown to hold for polymer solutions with sufficient

conductivity. Overall, it is clear that the model does not accurately predict the fiber diameter using electrostatics and solution rheology alone. The assumptions of Q/I scaling and the χ value are too severe and limited to specific cases.

The model considers the whipping jet a slender viscous object. The equations that describe the motion of the whipping jet have been successfully applied to the linear analysis of electrostatically driven jets.[36, 37] These equations are only relevant to the initial stages of the whipping phenomenon. To determine the final diameter of the charged jet, the nonlinear instability region needs to be modeled. The model solves equations of motion for the jet as a function of the material properties (conductivity (K), dielectric permittivity (ε), dynamic viscosity (μ), surface tension (γ) and density (ρ)), as well as processing parameters (flow rate (Q), electric field strength (E_∞) and electric current (I)). The current is determined by fluid, equipment and processing parameters. The model assumes that the fluid is Newtonian and neglects elastic effects due to drying of the jet. The outside medium is assumed to be air and has a dielectric constant ε, and provides a uniform external pressure. The model also assumes that the elastic effects and fluid evaporation are negligible. The model assumes that there is minimal jet thinning after the initiation of the whipping instability. The thinning jet is characterized by the jet diameter h and radius of curvature R. Analysis of the thinning jet shows that the characteristic length scale of the thinning is the contour length of the jet L, which is typically much larger than the radius of curvature R of whipping, therefore $h/L << 1$ and $h/R << 1$, which is generally observed in the lab.[35] These assumptions lead to the terminal radius of the jet as

defined by Equation 2.5 below. Spivak et al used a similar approach with similar results.[38, 39]

$$h_t = \left(\gamma \varepsilon \frac{Q^2}{I^2} \frac{2}{\pi(2\ln\chi - 3)} \right)^{\frac{1}{3}} \qquad \text{(Equation 2.5)}$$

In Equation 2.5 above, γ is the surface tension (g/s^2), ε is the permittivity constant (8.85x10-12 (C^2*s^2 / $kg*m^3$)), Q is the volumetric flow rate (m^3/s), I is the electric current (C/s) and χ is a characteristic length scale defined as the radius of curvature / jet diameter (dimensionless). Since χ is difficult to measure, it is often assumed to have a value of 100. It has been observed to vary from 10 to 1000, but the ln of χ varies slightly over this entire range.[35]

Using Equation 2.5 above, a decision can be made to either combine the Q/I term into a constant, which typically varies as 2/3, or to substitute the values of Q and I. In most cases since Q/I is not known and is very difficult to measure, the 2/3 assumption is reasonable. Q is simply the volumetric flow rate, but to obtain a value for I, electrical properties of the solution must be known, as well as the fiber jet velocity. Equation 2.6 is the relationship for electric current I (C/s).

$$I = 2\pi\sigma_0 h\upsilon + \pi E k h^2$$ (Equation 2.6)

In Equation 2.6, σ_0 is the electrical charge (C/m^2), h is the jet diameter (m), υ is the jet velocity (m/s), E is the applied electric field (V/m) and K is the conductivity of solution ($C^2*s / kg*m^3$). In order to solve for the electrical charge I, the permittivity of the solution σ_0, must be known. This is difficult to measure and is not commonly reported in the literature. The speed of the jet has been reported in the literature but it is not common.[40] Therefore this model is limited by the assumption of the 2/3 scaling. The data set used to verify this model is shown as Table 2.3.

Table 2.3 Fridrikh model data set.

Reference	Polymer	Wt%	Solvent	Surface Tension (kg/s2)	Actual Fiber Radius (m)	Fridrikh Model	
						Model Fiber Radius (m)	Percent Comparison
This Work	CN	8	6:4 THF:DMF	0.0034	8.00E-08	2.600.E-07	-69%
This Work	CN	8	6:4 THF:DMF	0.0034	9.50E-08	2.600.E-07	-63%
This Work	CN	8	6:4 THF:DMF	0.0034	9.50E-08	2.600.E-07	-63%
This Work	CN	8	6:4 THF:DMF	0.0034	8.00E-08	2.600.E-07	-69%
This Work	CN	8	6:4 THF:DMF	0.0034	5.50E-08	2.600.E-07	-79%
This Work	CN	8	6:4 THF:DMF	0.0034	6.00E-08	2.600.E-07	-77%
This Work	CN	6	7:3 EtOh:Ace	0.0026	7.00E-07	1.965.E-07	256%
This Work	CN	6	7:3 EtOh:Ace	0.0026	2.00E-07	1.965.E-07	2%
This Work	CN	6	7:3 EtOh:Ace	0.0026	1.75E-07	1.965.E-07	-11%
This Work	CN	6	7:3 EtOh:Ace	0.0026	1.65E-07	1.965.E-07	-16%
This Work	CN	6	7:3 EtOh:Ace	0.0026	1.85E-07	1.965.E-07	-6%
This Work	CN	6	7:3 EtOh:Ace	0.0026	2.25E-07	1.965.E-07	15%
This Work	CN	6	7:3 EtOh:Ace	0.0026	2.10E-07	1.965.E-07	7%
This Work	CN	6	7:3 EtOh:Ace	0.0026	2.10E-07	1.965.E-07	7%
This Work	CN	6	7:3 EtOh:Ace	0.0026	1.65E-07	1.96E-07	-16%
This Work	PVOH	10	water	0.0053	1.50E-07	4.08E-07	-63%
This Work	PVOH	10	water	0.0053	1.40E-07	4.08E-07	-66%
Fridrikh, 2003	PAN	8	DMF	0.0037	2.50E-07	2.83E-07	-12%
Fridrikh, 2003	PAN	10	DMF	0.0037	4.00E-07	2.83E-07	42%
Fridrikh, 2003	PCL	8	3:1 CHCl3:MeOH	0.0025	7.00E-07	1.91E-07	267%
Fridrikh, 2003	PCL	12	3:1 CHCl3:MeOH	0.0028	1.10E-06	2.15E-07	413%
Fridrikh, 2003	PEO	2	water	0.0062	2.50E-07	4.73E-07	-47%
Daga, 2006	PEO	2.52	water	0.0075	4.20E-08	5.73E-07	-93%
Daga, 2006	PEO	3.74	water	0.0075	6.65E-08	5.73E-07	-88%
Daga, 2006	PEO	4.5	water	0.0075	7.65E-08	5.73E-07	-87%
Daga, 2006	PEO	5.5	water	0.0075	8.90E-08	5.73E-07	-84%
Daga, 2006	PEO	6.5	water	0.0075	9.55E-08	5.73E-07	-83%
Deitzel, 2001	PEO	7	water	0.0043	1.13E-07	3.28E-07	-66%
Deitzel, 2001	PEO	10	water	0.0037	2.00E-07	2.83E-07	-29%
Lee, 2003	PVC	15	THF	0.0035	3.00E-06	2.71E-07	1005%
Lee, 2003	PVC	15	6:4 THF:DMF	0.0032	4.00E-07	2.47E-07	62%
Lee, 2003	PVC	15	4:6 THF:DMF	0.0036	5.00E-07	2.74E-07	82%
Lee, 2003	PVC	15	DMF	0.0043	2.00E-07	3.33E-07	-40%

The advantage of the Fridrikh model is that it predicts a terminal jet diameter, which is a consequence of balance between normal stresses due to surface tension and surface charge repulsion and can be determined from knowledge of the flow rate, electric current, and the surface tension of the fluid. The 2/3 scaling with the inverse volume charge density Q/I predicted by the model can be

confirmed experimentally using several concentrations and several various types of polymer solutions, from hydrogen bonding aqueous systems of PVOH and PEO to DMF solvent systems of PCL, PAN and CN. These provide convincing evidence for the correctness of the model by the reasonable prediction of the dry fiber diameter for PCL, PEO, and PAN as shown in Figure 2.4.

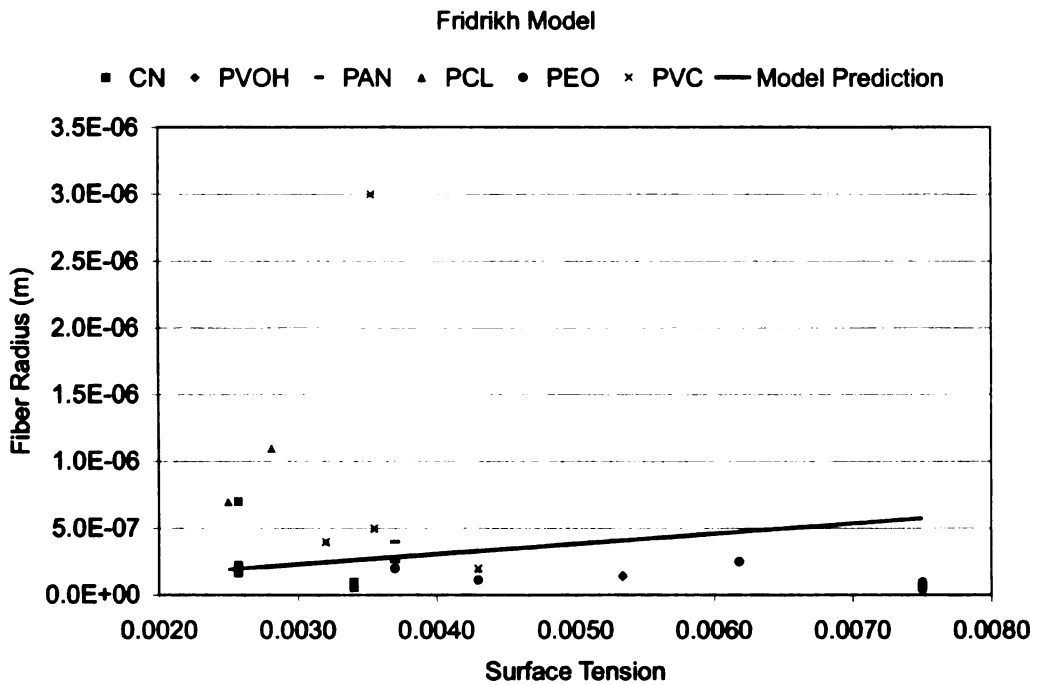

Figure 2.4 Fridrikh model chart showing correlations for PCL, PEO and PAN.

Dimensional Analysis approach

Several analytical models for electrospinning based on slender body electrohydrodynamic theory have been previously proposed that attempt to predict jet behavior.[41] Stability analysis of electrostatically driven jets by led to the

development of operating maps over which different operating regimes could be predicted, such as: whipping instability, varicose instability, and stable jetting.[36, 37] There have also been more detailed analyses reported that attempt to predict the final fiber diameter of electrospinning jets.[19, 35, 39] The main disadvantage of these models is that they all involve internal parameters that are impossible to know a priori and are very difficult to measure in practice. For example, Spivak et al.[39] and Feng[19] developed models to predict the asymptotic behavior of the jet radius in terms of an initial jet radius, which is not known. Similarly, Fridrikh et al.[35] proposed a force balance model for the final diameter of electrospun fibers, but it implicitly contains χ, the radius of whipping, which has proven difficult to measure or predict, and introduces further approximations for mass transfer to ultimately compare with experimental data. This model also assumes a polymer flow to electrical current scaling estimation. As a result, these models and analyses do not allow for a priori prediction of electrospun nanofiber morphology. They do provide a theoretical foundation for the development of a simple scaling analysis relating fiber morphology to spinning solution properties and controllable process parameters.

Several empirical relationships have been proposed for the prediction of electrospun fiber morphology from one fluid property. For example, McKee et al. showed that the diameter of electrospun polymer fibers displays a uniform power law scaling with the zero-shear viscosity.[30, 34] Shenoy et al.[27] identified the important need to be above the critical entanglement concentration of the polymer to form uniform fibers.

However, later results by McKee et al.[34] and Daga et al.[29] show that this result is not universal, especially for fibers spun from hydrogen-bonding systems as well as aqueous polyethylene oxide (PEO). When comparing fiber diameter versus zero shear viscosity for various neat polymer-solvent systems at different operating conditions, a large variation in behavior is observed.

Feng[42] identified the following dimensionless groups as governing parameters for electrospinning in a model developed from conservation equations for mass, momentum, and electrical charge applied to an electrospinning jet of a Newtonian fluid:

The Peclet number (Pe) is a ratio of the electrical conduction to convective time scales and represents the motion of the free electrical charges relative to the jet motion.

$$Pe = \frac{2\bar{\varepsilon}v_0}{kR_0} \qquad \text{(Equation 2.7)}$$

The jet Reynolds number (Re) is a ratio of the inertial to viscous stresses and represents the kinetic energy of the jet relative to the viscous dissipation.

$$\mathrm{Re} = \frac{\rho v_0 R_0}{\eta_0}$$ (Equation 2.8)

The Weber number (We) is a ratio of the inertial to surface stresses.

$$We = \frac{\rho v_0^2 R_0}{\gamma}$$ (Equation 2.9)

The dimensionless field strength (Ψ) is a ratio of the electrostatic to inertial stresses.

$$\Psi = \frac{\bar{\varepsilon} E_0^2}{\rho v_0^2}$$ (Equation 2.10)

These dimensionless groups contain internal variables that cannot be directly controlled or readily measured, namely, R_0 and v_0. It is standard engineering practice to eliminate these internal variables in order to develop useful

correlations between dimensionless groups that contain only measurable spinning fluid properties and measurable electrospinning parameters.[43] The dimensionless stress that drives jet elongation, Π_1, is a ratio of the electrostatic to the viscous stresses. This dimensionless group contains only solution variables that are measurable and controllable processing parameters.

$$\Pi_1 = \frac{2\bar{\varepsilon}^{-2}\phi_0^2}{k\eta_0 L^2} \qquad \text{(Equation 2.11)}$$

A second dimensionless group arises by considering a dimensionless electrospun fiber radius R_{jet}/R_0. Elimination of the initial jet radius using the dimensionless groups yields the dimensionless electrospun fiber diameter.

$$\Pi_2 = \frac{\rho\gamma R_{jet}}{\eta_0^2} = Oh^{-2} \qquad \text{(Equation 2.12)}$$

Where Oh is the Ohnesorge number, which can be used to characterize the stability and morphology of electrospinning jets.

$$Oh = \frac{\eta_0}{(\rho\gamma R_{jet})^{1/2}}$$ (Equation 2.13)

The characteristic wet radius R_{jet} of the electrospinning jet can be calculated knowing the dry fiber radius R_f and the initial concentration of the polymer in solution W_S.

$$R_{jet} = R_f\sqrt{\frac{1}{Ws}}$$ (Equation 2.14)

$$\Pi_1 Oh = \frac{2\bar{\varepsilon}^{2}\phi_0^2}{kL^2(\rho\gamma R_{jet})^{1/2}}$$ (Equation 2.15)

These dimensionless groups are functions of the dielectric permittivity of atmosphere (ε); conductivity (K), density (ρ), zero-shear viscosity (η_0), and surface tension (γ) of the electrospinning fluid; the applied electric field (E_0); and characteristic jet radius (R_0) and velocity (v_0) scales. The characteristic electric field strength E_0 is taken here to be the average field defined as the voltage applied to the capillary tip divided by the working distance between the capillary

tip and collecting target, Φ_0/L. Table 2.4 below shows the values required for the dimensionless analysis, or Helegeson's Model. The values of conductivity of cellulose nitrate solutions were measured using a simple handheld conductivity meter. For samples consisting of 8 wt% CN in a 60 : 40 mixture of THF : DMF, the conductivity was determined to be 7.1 μs/cm. The density of cellulose nitrate was measured by weighing known volumes of solutions. This data was plotted to accurately determine the density of the particular solution. It was determined that the 8 wt% CN in a 60:40 mixture of THF:DMF had an average density of 0.995 g/cm^3. Zero shear viscosity was obtained from plotting the rotational viscosity versus concentration and extrapolating back to the y intercept. Measuring the 8 wt% CN in 60:40 mixture of THF:DMF resulted in a zero shear viscosity of 8.65 Pa*s.

Table 2.4 Helgeson data table

Reference	Polymer	Wt%	Solvent	Zero Shear Viscosity (kg/ms)	Actual Fiber Radius (m)	Helgeson Model			
						PI 1	Oh	Fiber Radius (m)	Percent Comparison
This Work	CN	12	6:4 THF:DMF	12.8500	2.25E-07	4.8E-11	8661.29	2.07.E-07	9%
This Work	CN	8	6:4 THF:DMF	8.4500	9.50E-08	4.6E-11	7920.61	1.84.E-07	-48%
This Work	CN	6	7:3 EtOh:Ace	6.5000	1.75E-07	5.3E-11	5163.36	1.37.E-07	28%
This Work	CN	10	7:3 EtOh:Ace	15.2000	6.00E-07	1.5E-11	7408.84	5.38.E-08	1016%
This Work	CN	8	7:3 EtOh:Ace	11.6500	4.50E-07	1.9E-11	6201.31	5.87.E-08	666%
This Work	CN	6	7:3 EtOh:Ace	9.2500	1.65E-07	2.4E-11	7567.25	9.02.E-08	83%
This Work	PVOH	10	water	5.8000	1.50E-07	1.7E-10	3486.62	3.01.E-07	-50%
This Work	PVOH	10	water	5.8000	1.40E-07	3.3E-10	3608.99	5.90.E-07	-76%
Daga, 2006	PEO	2.52	water	0.1800	4.20E-08	2.6E-09	127.78	1.69.E-07	-75%
Daga, 2006	PEO	3.74	water	0.9100	6.65E-08	4E-10	566.65	1.14.E-07	-42%
Daga, 2006	PEO	4.5	water	2.6500	7.65E-08	1.3E-10	1611.34	1.04.E-07	-27%
Daga, 2006	PEO	5.5	water	6.4400	8.90E-08	4.9E-11	3817.25	9.31.E-08	-4%
Daga, 2006	PEO	6.5	water	15.6000	9.55E-08	1.9E-11	9307.23	8.64.E-08	11%
Deitzel, 2001	PEO	7	water	4.0000	1.13E-07	5.4E-12	2958.18	8.01.E-09	1305%
Deitzel, 2001	PEO	10	water	16.0000	2.00E-07	1.1E-12	10459.34	5.75.E-09	3377%
Lee, 2003	PVC	15	THF	1.0000	3.00E-06	1.6E-09	191.2383	1.50.E-07	1903%
Lee, 2003	PVC	15	6:4 THF:DMF	1.0000	4.00E-07	1.6E-09	550.07	4.31.E-07	-7%
Lee, 2003	PVC	15	4:6 THF:DMF	1.0000	5.00E-07	1.6E-09	467.11	3.66.E-07	37%
Lee, 2003	PVC	15	DMF	1.0000	2.00E-07	1.6E-09	671.08	5.26.E-07	-62%

The advantage of the Helgeson dimensionless analysis model is that the elimination of internal variables in a dimensional analysis of the electrospinning of a Newtonian fluid provides a strong correlation between the dimensionless fiber radius, as characterized by the Ohnesorge number, and a new dimensionless group Π_1, which relates controllable operating parameters and measurable solution spinning properties as shown in Figure 2.5. A stable jet-operating regime has been defined above a critical Ohnesorge number of 100. Above this value, the fibers are typically homogenous with uniform diameter, since the operation is stable. Below Ohnesorge numbers of 100, the process is much less stable, as and fiber inhomogenieties including beading are common.

Since this is a relatively recent publication (2007) the applicability and accuracy has yet to be challenged.

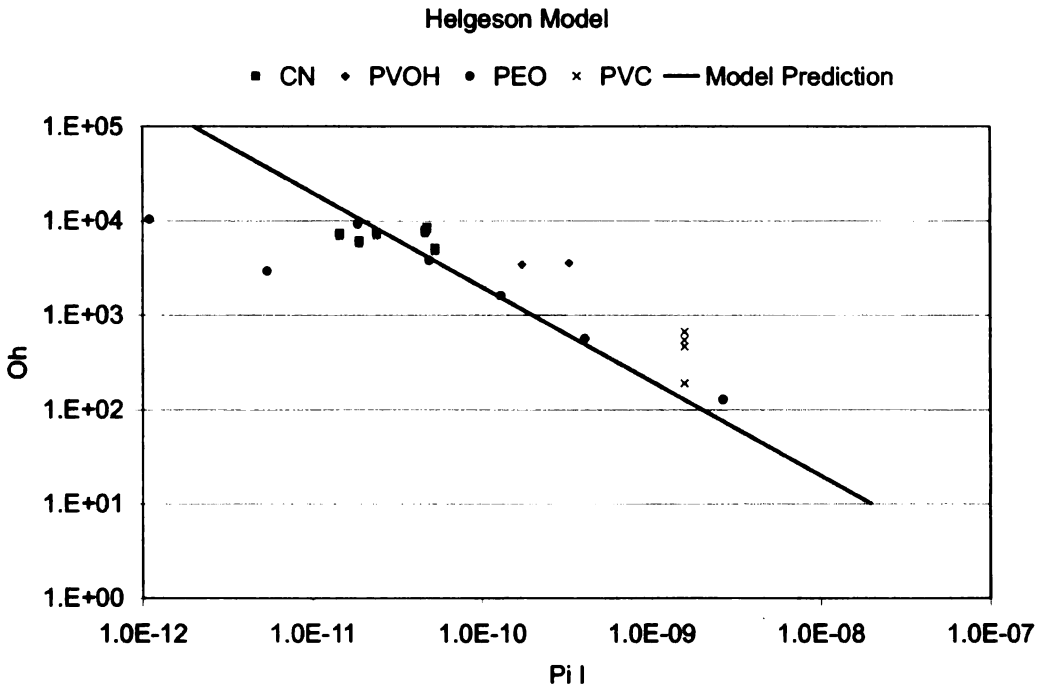

Figure 2.5 Helgeson chart showing good correlation for almost all data sets

The disadvantage to using the Helgeson dimensional analysis model is that several solution parameters must be known. The values of conductivity, zero shear viscosity and surface tension are relatively simple to obtain, but they are often not reported in the literature. Once these values are known, the model does provide relatively good accuracy, especially when using the Helgeson data set.[43]

Modeling Summary

A crucial factor for producing nanoscale fibers using the electrospinning apparatus involves knowing a priori the expected fiber diameter. Several models have been proposed to calculate the fiber diameter based on solution and processing variables. The models vary in complexity and accuracy. The McKee model is a simple zero shear viscosity relation that proves to be accurate for the data set chosen. A more detailed dimensional analysis provides a more accurate approach to determining the fiber diameter and operating conditions through its definition of the Ohnesorge number. Using the models presented can quickly eliminate experimental steps and provide expected results for the solution chosen. The modeling shows that concentration or solution viscosity is an important variable to consider, but other factors, such as electric field strength and conductivity must be considered to accurately estimate fiber diameters.

Biosensors

Biosensors are composed of three major parts: the sensitive biological element, the transducer or detector element and an electronic interface. Figure 2.6 shows a schematic illustration of a biosensor device.

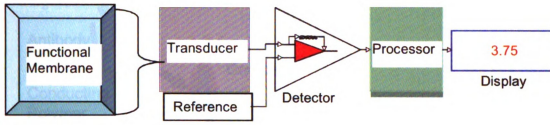

Figure 2.6 Biosensor schematic

The biological element is a biologically derived or biomimic compound that has highly specific interactions for the biological molecules to be detected. This specificity makes the biosensor a powerful tool when a high selectivity is required. The biological element is also known as the bioreceptor. Figure 2.7 shows an antibody as an example of the biological element in a fiber based biosensor device. The biological element is closely associated with a transducer that converts the physicochemical signal occurring during the molecular recognition phenomenon into an electrical signal. The electrical signal is then transferred to a device that allows for quantification of the interactions. The ability of biomolecules to react with very low concentrations of substances allows biosensors to be used in various applications such as the monitoring of impurities in water, air, soil, foods, and in the detection of medically important molecules such as hormones, sugars, and peptides in body fluids.

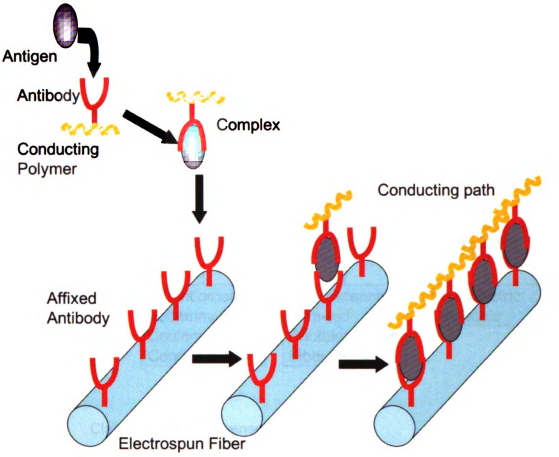

Figure 2.7 Biosensor consisting of an antibody as the biological element, conducting polymer chain as the transducer and electrospun fibers as the matrix.

There are many applications and classifications of biosensors. The main design criteria for the biosensor device include low cost disposable material, reliable identification of a target molecule, availability of a suitable biological recognition element, and high sensitivity. Detection mechanisms include, photometric, piezoelectric, electrochemical and immunoassay. Immunoassay

detection mechanisms are most prevalent in the electrospinning literature and are often detected electrochemically. Figure 2.8 shows an illustration of the biosensor classifications.

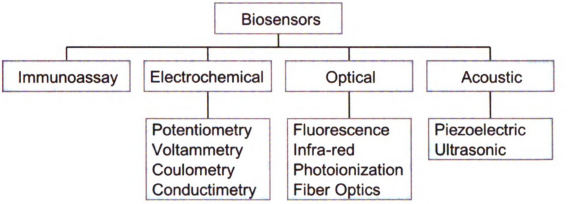

Figure 2.8 Classification of biosensors

Acoustic

Piezoelectric sensors utilize crystals, which undergo a phase transformation when an electrical current is applied to them. An alternating current (A.C.) produces a standing wave in the crystal at a characteristic frequency. This frequency is highly dependent on the surface properties of the crystal, such that if a crystal is coated with a biological recognition element the binding of a large target analyte to a receptor will produce a change in mass which in turn alters the resonant frequency, which gives the binding signal.

Polymer thin films are used extensively in acoustic biosensors. Nanofiber films can be used as a sensing interface for thickness shear mode (TSM) piezoelectric sensors. TSM sensors coated with nanofiber films made of poly-lactic acid-co-glycolic acid (PLAGA) polymers were studied under various ambient conditions and were reported to possess better sensitivities than their thin film counterparts [44]. For TSM resonators, the resolution varies linearly with the surface area of the sensing interface. It was concluded that electrospun polymer nanofibers would be an ideal material for this purpose. Another publication from this group showed that piezoelectric biological sensors that were electrospun from PLAGA offered a unique advantage [45]. The PLAGA membranes consisted of fibers with diameters of approximately 500 nm. These fibers were deposited on the gold surface of a thickness shear mode (TSM) micro viscoelastic sensor operating at 10 MHz. The NF thin film coated TSM sensors were exposed to gaseous and liquid media under various ambient conditions. The most interesting result was the different response of the NF coated TSM sensor to hydrophilic and hydrophobic liquid loading. The aerial density of water is larger than that of propanol, but the NF coated TSM sensors showed more loading from propanol. This effect is very unique and presents a very advantageous feature of NF thin films as a chemical or biochemical-sensing interface.

Optical

Photometric biosensors are optical devices that are based on the phenomenon of surface plasmon resonance. Specifically, gold and other materials absorb laser light when thinly coated on the surface of glass. The absorption of laser light produces electron waves called surface plasmons. This only occurs at a specific wavelength of incident light and at a specific angle. When target analytes are bound to the surface of gold, the angle of light changes thus producing a measurable signal. The principle of this sensor is that any change in the concentration of its surroundings produces a change in its optical properties. Therefore, there is a noticeable change in the amount of radiation reflected or emitted. Infrared, UV, and fluorescence are the spectra commonly used. Fluorescence is the most applied method for optical biosensors.

Optical sensors are relatively new and not much work has been carried out in this field. From first principles, the sensitivity of an optical sensor would depend on the amount of fluorescence emitted, which in turn is proportional to the available area of the interface. Thus by change in morphology, if porosity could be increased, the sensitivity would also increase proportionately. Electrospun nanofibers can promote an increase in porosity, especially if porous fibers are created. Electrospun nanofibers would be the optimal choice in architecture and materials for the fabrication of optical sensors.

The design and fabrication of the electrospun nanofibers is crucial for the preparation of highly sensitive optical sensors [46]. Combining the techniques of electrospinning and electrostatic layer-by-layer adsorption, highly sensitive

fluorescent sensors were fabricated. A fluorescent probe was electrostatically assembled onto the surface of electrospun nanofibrous membranes whose fluorescence could be quenched on using extremely low concentrations of aqueous methyl viologen (MV2+) and cytochrome C solutions. The high sensitivity is attributed to the high surface area-to-volume ratio of the electrospun membrane and efficient interaction between the fluorescent conjugate polymer and the analytes [47].

Another combination technique utilized both wet spinning and electrospinning to create virus-based microscale and nanoscale fibers. When M13 viruses were blended with polyvinyl pyrolidone PVP fibers, an intact structure of the viruses was formed. These fibers demonstrated that novel biomaterials can be fabricated from a programmed organism to extend the dimension of engineered viruses into fibers providing useful biological functions and highly sensitive catalytic functions in the future for biomedical biosensor applications [48].

Optical chemical sensors were fabricated by electrospinning a mixture of PAA-PM and thermally cross-linkable polyurethane latex in one solution. These sensors showed high sensitivities due to the high surface area-to-volume ratio of the nanofibrous membrane structures. Electrospun nanofiber membranes with individual fiber diameters of 400 nm were prepared. A fluorescent polymer poly(acrylic acid) - poly(pyrene methanol) (PAA-PM) was employed for the detection of metal ions (Fe3+ and Hg2+) and 2,4-dinitrotulene (DNT). The electrospun fibrous material exhibited a sensitivity of almost three orders of magnitude higher than that of films of the same material [46].

A variation of the multiple component electrospinning technique utilizes multiple syringes or core and shell nozzles to deliver different solutions, which result in the formation of a composite fiber network. A novel dual syringe electrospinning method was employed to prepare a composite fiber network of a semiconducting, electroluminescent polymer MEH-PPV and mesoporous SBA-15 silica [49]. The idea behind using two different solutions was to make an interwoven network of fibers containing a polymer and a molecular sieve material and study the optical properties of the resulting composites. The composite fibers obtained by electrospinning MEHPPV and SBA-15 silica together exhibit a blueshift in the emission, which can also be altered by introducing organic moieties into the inorganic material. The shift in emission is mainly attributed to non-aggregation of the polymer chains, which occurs due to the polymer chain conformation. The silica mesoporous fibers acted as a nanospacer thereby reducing interchain interactions, resulting in the blueshift in the emission. Hence, dual syringe electrospinning is a way to alter the optical properties of the fluorescent polymers in fibrous form, which will have interesting applications in molecular electronics.

Electrochemical

In the electrochemical method the conductance of a solution or fibrous network is measured, using inert electrodes, alternating current, and an alternating null current. However, it is noteworthy that there is no electric current

or potential gradient and the concentration of the analyte is measured as a function of the conductance of ions.

Recent efforts were undertaken in the production of nanofibers for electrochemical sensors using electrospinning as shown in Table 2.5. Metal ions such as Pd, Pt, and Au can be coated or electrodeposited onto the surface of the fibers to improve the conductivity and resolution. The literature shows that polymers such as polyaniline, polypyrrole, and polyamic acid have been electrospun and successfully used as sensing interfaces [50]. For electrochemical sensors, the resolution varied in proportion to the conductivity of the interface; in this case, it is the number of electrons transferred that governs the sensitivity. Therefore, nanofibers that have a very high surface area would be idealistic for electrochemical biosensors as well.

Recently, many kinds of nanomaterials such as gold and SiO_2 nanoparticles have been widely used in constructing electrochemical biosensors [51-55]. Bharathi and co-workers have demonstrated that gold nanoparticles can self-assemble both inside the network and on the surface of the silica gel [56]. The gold nanoparticles immobilized by a silica gel three-dimensional network can act as tiny conducting centers and facilitate the electron transfer [55]. It has also been reported that gold nanoparticles not only promote the electron transfer between the analyte and the electrode surface but could also act as a conducting base for the assembly of biomolecules [57]. They can provide a favorable microenvironment for the active immobilization of glucose oxidase (GOx) due to their excellent biocompatibility.

Immunoassay

Immunoassay biosensors are a general classification of sensors that embody antibodies as their selective binding components. They take advantage of the high selectivity provided by the molecular recognition of antibodies. Immunoassay biosensors can be divided in principle into two categories: non-labeled and labeled immunoassay biosensors. Non-labeled immunoassay biosensors are designed so that the immunocomplex that is the antigen–antibody complex is directly determined by measuring the physical changes induced by the formation of the complex. In contrast, in a labeled immunoassay biosensor, a sensitively detectable label is incorporated.

Microelectronics has sufficiently minimized the instrumentation and made the sensing device portable, but the sensing interface is still the most crucial component of the biosensor device. Therefore, the available surface area of the biosensor should be optimized in order to maximize the number of active sites. The design approach is to adapt such a morphology that is small yet possesses a large surface area for interaction. The choice to use electrospun nanofibers is obvious since they can provide these advantages with ease. Nanofibers have been recently tested for biomedical applications as well as for fabrication of nanofiber-based immunoassay biosensors [58]. Specific target molecules such as antibodies can be tailored on the surface of the nanofibers at high concentrations. It is also possible to attach more than one antibody on the

nanofiber mesh, which would create a basis for multiple analyte detection capability.

Electrochemical Immunoassay

The electrochemical immunoassay biosensor combines the reactivity of the antibody and its antigen with the detection method of an electrochemical sensor. Electrochemical immunoassays are biosensors constructed with antibodies as biological elements, attached to an electrochemical transducer [59]. Conductive materials used to carry out electrochemical events include silver, gold, and organic polymers [60, 61]. Biosensors based on electrochemical immunoassays using conductive polymers such as polyaniline, polypyrrole, polyacetylene, and polythiophene have gained industrial acceptance [62]. The conductive polymer acts as the electrochemical transducer to convert the biological signal into an electrical signal [63]. Polyaniline in particular, has been one of the most extensively investigated conducting polymers, due to its excellent stability in liquid form, promising electronic properties [64], and strong biomolecular interactions [65].

These biosensors only have two electrodes and are extremely sensitive, robust and accurate. There are two basic fiber structures used for the production of these biosensors, conductive fiber networks, and non-conductive fiber networks. Figure 2.7 above shows the non-conductive fiber network and Figure 2.9 shows the conductive fiber alternative.

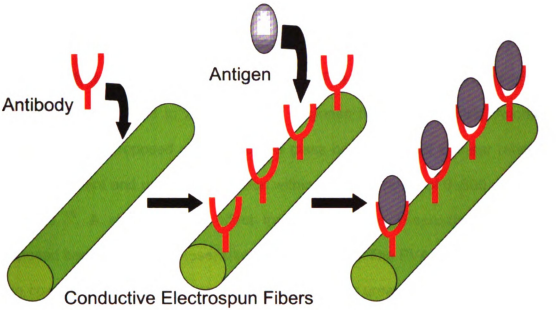

Figure 2.9 Conductive nanofiber biosensor schematic.

A sensing material of hydrolyzed poly(2-(3-thienyl) ethanol butoxy carbonylmethyl urethane) (H-PURET) was recently assembled onto the surface of electrospun nanofibrous cellulose acetate membrane [66]. The electrospun fibers had diameters from 100 – 400 nm. High sensitivity in detecting extremely low concentration (ppb) of methyl viologen (MV2+) and cytochrome c (cyt c) was reported. It is believed that the high surface area to volume ratio of electrospun nanofibrous membrane and efficient interaction between sensing material and detected substance are responsible for this significant improvement.

There are several technologies proposed for urea detection through use of immobilized urease. Most of them offer a narrow detection limit in either low or

high concentrations of urea. A urea biosensor utilizing urease immobilized on gelatin beads was reported [67]. This system was successful at achieving long storage stability, with a half-life of 240 days. The sensors' drawbacks were a detection limit from 0.8 to 23 mM and a response time of 6 minutes. Another sensing system proposed was on porous glass beads showed a linear relation between current and urea concentration within a narrow range of 0–600 μM urea solutions [68]. A chemical field effect transistor with a pH-sensitive gate was proposed based on the photosensitive layers of PVA. The PVA was cast using a spin coating technique and was capable of detecting urea at concentrations of 5 to 25 mM [69]. Composite electrically conductive PAn–PBMA homogenous films by were prepared by casting, these films offered the detection limits of 3–20 mM [70]. Urea has been immobilized on SiO_2 film as a pH-sensitive layer in light addressable potentiometric sensors (LAPS) and once again had a narrow range of detection from 5 to 15 mM. A detailed discussion of longevity for the mentioned product was not provided[71].

Nanocomposite fibers of urease and PVP were prepared by the electrospinning technique [72]. The non-woven mat formed with fibers from 7 to 100 nm in diameter, has potential as a urea biosensor. The immobilized enzyme remained active inside the polymer solution, and more importantly the reactivity was maintained inside the electrospun non-woven mats. The electrospun membrane acted as catalyst in the hydrolysis of various urea solutions. The biggest improvement over prior technology is the fast response time, sensitivity to low concentrations of urea, and a more versatile design.

The electrospinning method can be both convenient and efficient to produce enzymatic electrodes for biosensors. Biocomposite nanofibers were prepared by electrospinning glucose oxidase (GOD) with Poly(vinyl alcohol) PVA solution [73]. The immobilized glucose oxidase enzyme remained active inside the biocomposite (PVA/GOD) membrane. The glucose biosensors fabricated using the electrospun PVA/GOD exhibited a rapid response time (1 s) and a higher output current (IA level) to glucose in the normal and diabetic level. The linear response range from 1 to 10 mM and the lower detection limit (0.05 mM) of the sensor can meet the demand in the detection of the glucose in medical diagnosis.

Nanofibrous glucose electrodes have also been fabricated by using an electrospun composite membrane consisting in part of polymethylmethacrylate [74]. The nanofiber electrodes showed an excellent detection limit, wide linear range response, and operational stability and were free from electrochemical interference of co-existing species. These features provide advantages for utilizing the electrospinning technique to obtain structures suitable for the immobolization of biomolecules in the process of fabricating new and unique biosensor devices. Electrospinning has also been used to prepare the nanofibrous membranes composed of poly(vinylidene flouoride) and poly(aminophenylboronic acid) [75]. The nanofibrous membrane displayed an excellent linear response to the detection of glucose for the concentration range of 1 to 15mM and a very rapid response time of less than 6 seconds. The electrospun nanofibrous membranes were subjected to interference studies

using uric acid, ascorbic acid, acetaminophen, fructose, and mannose. It was determined that the interferents did not give significant overlapping current signal during the determination of glucose. The electrospun nanofibrous mats also provide improved reproducibility toward glucose detection and storage stability.

Nanoporous silica nanofibers have been prepared using tetramethyl orthosilicate (TMOS) as a silica precursor, poly (vinyl alcohol) (PVA) and β-D-glucose [76]. The enzyme immobilized inside the mesoporous silica fibers was horseradish peroxidase (HRP). The PVA aids in the formation of fibers since it increases viscosity of the solution. Fibers were formed with small diameters from 100 to 200 nm. The resultant nonwoven mats exhibited extreme porosity of 2 to 4 nm, most likely due to the glucose template present in solution. The fibers with mesoporosity showed a fourfold increase in activity as compared to the conventional nontemplated silica samples, and threefold increase in activity as compared to the HRP immobilized silica powders. The improved surface area, mechanical flexibility, thermal stability, reusability and freedom of encapsulating various enzymes make porous silica nanofibers excellent candidates for biosensor substrates.

Biotin has been successfully incorporated into PLA nanofibers through electrospinning without significantly changing the morphology and size of the resulting nanofibers [77]. The fibers were approximately 200 nm in diameter. The nanofiber membranes were characterized with Electron Probe Microanalyzer (EPMA) to confirm biotin incorporation in the fibers. Although biotin is dispersed throughout the nanofiber membranes the distribution is heterogeneous and

regions of locally high biotin concentration are evident. Confocal microscopy analysis indicates that both specific and non-specific binding occur between streptavidin and the biotin incorporated PLA nanofiber membranes. With blocking reagent, non-specific binding can be suppressed effectively. Fluorescence labeled streptavidin binds along the surface of PLA-biotin fibers providing evidence that biotin incorporated via electrospinning is available at the fiber surface. Biosensor assay experiments confirm that the PLA nanofiber membranes can successfully transport analyte solutions via wicking. A biotinylated DNA probe was successfully captured by immobilized streptavidin in a preliminary biosensor assay using an electrospun PLA nanofiber membrane as substrate.

Nylon-6 nanofibers have been electrospun, impregnated with Au nanoclusters to increase the conductivity and immobilized with glucose oxidase [16]. The results show that electrospun nanofibers can offer a quick response time within 130 seconds. The new biosensors can selectively and accurately detect glucose levels with resolution of 0.113-μV/ mM. The sensors were also stable; the membrane with immobilized enzyme gave results with less than 5% absolute error after two months.

Table 2.5 Summary of electrospun material used for biosensor applications

Spinning Solution	Electric Field Strength (kV/cm)	Flow Rate (mL/h)	Fiber Size (nm) / Pattern	Reference
5 wt% PLAGA in DMF	1.33	---	500 / Aligned	Kwoun 2001
9 wt% CA in 2:1 Acetone:DMAC	1.25 - 1.33	---	100 - 400 / Random	Wang 2004
M13 Virus + PVP in aqueous buffer	2.00	0.18 - 0.36	100 - 200 / Random	Lee 2004
7-10 wt% MEH-PPV in 1,2 dichloroethane	0.83 - 0.91	---	200 / Random	Madhugiri 2003
18.6 wt% PAA-PM + 36.5 wt% PU in DMF	1.00	---	100 - 400 / Random	Wang 2002
3:7 Urease:PVP in Ethanol	1.00	0.9	7 - 100 / Random	Sawicka 2005
8 wt% PVA + GOD in PBS Buffer	1.00	0.2	70 - 250 / Random	Ren 2006
PMMA + MWCNT(PDDA) in 7:3 DMF:Acetone	1.67	10	200 - 400 / Random	Manesh 2008
PVDF + PAPBA in 7:3 DMF:Acetone	1.67	10	150 / Random	Manesh 2007
Glucose+PVA+HRP in PBS Buffer	1.33	---	200 / Random	Patel 2006
6-8 wt% PLA +Biotin in 3:1 Chloroform:Acetone	1.25 - 1.5	0.3 - 0.6	150 - 5,000 / Random	Li 2006

Summary

This chapter gives a brief description of electrospinning, and the development of biosensor devices using the electrospinning technique. The nanofibers that are produced generally improve the quality and performance of the device. These improvements are due to the increased surface area, controllable architecture, and specific chemical incorporation that only electrospinning can provide. The electrospinning process has allowed for the creation of biosensors with lower detection limits, increased stability, improved specificity, and enlarged linear response regions. The electrospun biosensor is still in its infancy, but the future is full of promise as researchers focus on specific details of the process and its effects on the biosensor device performance.

References

1. MacDiarmid, A. G.; Jones, W. E.; Norris, I. D.; Gao, J.; Johnson, A. T.; Pinto, N. J.; Hone, J.; Han, B.; Ko, F. K.; Okuzaki, H.; Llaguno, M., Electrostatically-generated nanofibers of electronic polymers. *Synthetic Metals* **2001,** 119, (1-3), 27-30.

2. Deitzel, J. M.; Kleinmeyer, J.; Harris, D.; Tan, N. C. B., The effect of processing variables on the morphology of electrospun nanofibers and textiles. *Polymer* **2001,** 42, (1), 261-272.

3. Lyons, J.; Li, C.; Ko, F., Melt-electrospinning part I: processing parameters and geometric properties. *Polymer* **2004,** 45, (22), 7597-7603.

4. Reneker, D. H.; Chun, I., Nanometre diameter fibres of polymer, produced by electrospinning. *Nanotechnology* **1996,** 7, (3), 216-223.

5. Taylor, G., Disintegration of water drops in electric field. *Proceedings of the Royal Society of London Series a-Mathematical and Physical Sciences* **1964,** 280, (138), 383.

6. Koombhongse, S.; Liu, W. X.; Reneker, D. H., Flat polymer ribbons and other shapes by electrospinning. *Journal of Polymer Science Part B-Polymer Physics* **2001,** 39, (21), 2598-2606.

7. Formhals, A. Process and apparatus for preparing artificial threads. 1975504, 1934.

8. Kim, J. S.; Reneker, D. H., Polybenzimidazole nanofiber produced by electrospinning. *Polymer Engineering and Science* **1999,** 39, (5), 849-854.

9. Katta, P.; Alessandro, M.; Ramsier, R. D.; Chase, G. G., Continuous electrospinning of aligned polymer nanofibers onto a wire drum collector. *Nano Letters* **2004,** 4, (11), 2215-2218.

10. Sundaray, B.; Subramanian, V.; Natarajan, T. S.; Xiang, R. Z.; Chang, C. C.; Fann, W. S., Electrospinning of continuous aligned polymer fibers. *Applied Physics Letters* **2004,** 84, (7), 1222-1224.

11. Li, D.; Ouyang, G.; McCann, J. T.; Xia, Y. N., Collecting electrospun nanofibers with patterned electrodes. *Nano Letters* **2005,** 5, (5), 913-916.

12. Tan, S.; Huang, X.; Wu, B., Some fascinating phenomena in electrospinning processes and applications of electrospun nanofibers. *Polymer International* **2007,** 56, 1330-1339.

13. Li, D.; Xia, Y. N., Electrospinning of nanofibers: Reinventing the wheel? *Advanced Materials* **2004,** 16, (14), 1151-1170.

14. Huang, Z. M.; Zhang, Y. Z.; Kotaki, M.; Ramakrishna, S., A review on polymer nanofibers by electrospinning and their applications in nanocomposites. *Composites Science and Technology* **2003,** 63, (15), 2223-2253.

15. Teo, W. E.; Ramakrishna, S., A review on electrospinning design and nanofibre assemblies. *Nanotechnology* **2006,** 17, (14), R89-R106.

16. Ramakrishna, S.; Lala, N.; Garudadhwaj, H.; Ramaseshan, R.; Ganesh, V. K., Polymer Nanofibers for Biosensor Applications. In *Molecular Building Blocks for Nanotechnology*, 2007; pp 377-392.

17. Mohanty, S. P. K., E., Biosensors: a tutorial review. **2006,** 25, (2), 40.

18. Wan, Y. Q.; Guo, Q.; Pan, N., Thermo-electro-hydrodynamic model for electrospinning process. *International Journal of Nonlinear Sciences and Numerical Simulation* **2004,** 5, (1), 5-8.

19. Feng, J. J., The stretching of an electrified non-Newtonian jet: A model for electrospinning. *Physics of Fluids* **2002,** 14, (11), 3912-3926.

20. Reneker, D. H.; Yarin, A. L.; Fong, H.; Koombhongse, S., Bending instability of electrically charged liquid jets of polymer solutions in electrospinning. *Journal of Applied Physics* **2000,** 87, (9), 4531-4547.

21. Shin, Y. M.; Hohman, M. M.; Brenner, M. P.; Rutledge, G. C., Experimental characterization of electrospinning: the electrically forced jet and instabilities. *Polymer* **2001,** 42, (25), 9955-9967.

22. Wan, Y. Q.; He, J. H.; Yu, J. Y., Experimental verification of scaling law between current and applied voltage in electrospinning. *Iranian Polymer Journal* **2006,** 15, (3), 265-268.

23. He, J. H.; Wane, Y. Q., Allometric scaling for voltage and current in electrospinning. *Polymer* **2004,** 45, (19), 6731-6734.

24. Carroll, C. P.; Joo, Y. L., Electrospinning of viscoelastic Boger fluids: Modeling and experiments. *Physics of Fluids* **2006,** 18, (5).

25. Bunyan, N. N.; Chen, J.; Chen, I.; Farboodmanesh, S., Electrostatic effects on electrospun fiber deposition and alignment. *Polymeric Nanofibers* **2006,** 918, 106-120.

26. Doshi, J.; Reneker, D. H., Electrospinning Process and Applications of Electrospun Fibers. *Journal of Electrostatics* **1995,** 35, (2-3), 151-160.

27. Shenoy, S. L.; Bates, W. D.; Frisch, H. L.; Wnek, G. E., Role of chain entanglements on fiber formation during electrospinning of polymer solutions: good solvent, non-specific polymer-polymer interaction limit. *Polymer* **2005,** 46, (10), 3372-3384.

28. Koski, A.; Yim, K.; Shivkumar, S., Effect of molecular weight on fibrous PVA produced by electrospinning. *Materials Letters* **2004,** 58, (3-4), 493-497.

29. Daga, V. K.; Helgeson, M. E.; Wagner, N. J., Electrospinning of neat and laponite-filled aqueous poly(ethylene oxide) solutions. *Journal of Polymer Science Part B-Polymer Physics* **2006,** 44, (11), 1608-1617.

30. McKee, M. G.; Wilkes, G. L.; Colby, R. H.; Long, T. E., Correlations of Solution Rheology with Electrospun Fiber Formation of Linear and Branched Polyesters. *Macromolecules* **2004,** 37, (5), 1760-1767.

31. Deitzel, J. M.; Kleinmeyer, J. D.; Hirvonen, J. K.; Tan, N. C. B., Controlled deposition of electrospun poly(ethylene oxide) fibers. *Polymer* **2001,** 42, (19), 8163-8170.

32. Fong, H.; Chun, I.; Reneker, D. H., Beaded nanofibers formed during electrospinning. *Polymer* **1999,** 40, 4585-4592.

33. Drew, C.; Wang, X.; Samuelson, L. A.; Kumar, J., The Effect of Viscosity and Filler on Electrospun Fiber Morphology. *Journal of Macromolecular Science, Part A* **2003,** 40, (12), 1415 - 1422.

34. McKee, M. G.; Hunley, M. T.; Layman, J. M.; Long, T. E., Solution rheological behavior and electrospinning of cationic polyelectrolytes. *Macromolecules* **2006,** 39, (2), 575-583.

35. Fridrikh, S. V.; Yu, J. H.; Brenner, M. P.; Rutledge, G. C., Controlling the fiber diameter during electrospinning. *Physical Review Letters* **2003,** 90, (14).

36. Hohman, M. M.; Shin, M.; Rutledge, G.; Brenner, M. P., Electrospinning and electrically forced jets. I. Stability theory. *Physics of Fluids* **2001,** 13, (8), 2201-2220.

37. Hohman, M. M.; Shin, M.; Rutledge, G.; Brenner, M. P., Electrospinning and electrically forced jets. II. Applications. *Physics of Fluids* **2001,** 13, (8), 2221-2236.

38. Spivak, A. F.; Dzenis, Y. A., Asymptotic decay of radius of a weakly conductive viscous jet in an external electric field. *Applied Physics Letters* **1998,** 73, (21), 3067-3069.

39. Spivak, A. F.; Dzenis, Y. A.; Reneker, D. H., A model of steady state jet in the electrospinning process. *Mechanics Research Communications* **2000,** 27, (1), 37-42.

40. Leon, M. B.; Harold, G. C.; Juan, P. H., Direct measurement of fluid velocity in an electrospinning jet using particle image velocimetry. *Journal of Applied Physics* **2007,** 102, (9), 094308.

41. Saville, D. A., ELECTROHYDRODYNAMICS:The Taylor-Melcher Leaky Dielectric Model. *Annual Review of Fluid Mechanics* **1997,** 29, (1), 27-64.

42. Feng, J. J., Stretching of a straight electrically charged viscoelastic jet. *Journal of Non-Newtonian Fluid Mechanics* **2003,** 116, (1), 55-70.

43. Helgeson, M. E.; Wagner, N. J., A correlation for the diameter of electrospun polymer nanofibers. *Aiche Journal* **2007,** 53, (1), 51-55.

44. Kwoun, S. J. L., R.M.; Han, B. and Ko, F.K. In *Polymer Nanofiber Thin Films for Biosensor Applications*, IEEE 27th Annual Northeast Bioengineering Conference, 2000; 2000; pp 9-10.

45. Kwoun, S. J. L., R.M.; Han, B. and Ko, F.K., A Novel Polymer Nanofiber Interface for Chemical and Biochemical Sensor Applications. In *Modeling and Simulation of Microsystems*, 2001; pp 338-341.

46. Wang, X.; Drew, C.; Lee, S. H.; Senecal, K. J.; Kumar, J.; Samuelson, L. A., Electrospun Nanofibrous Membranes for Highly Sensitive Optical Sensors. *Nano Letters* **2002,** 2, (11), 1273-1275.

47. Wang, X. K., Y-G.; Drew,C., Ku,B-C., Kumar,J., Samuelson L.A., Electrostatic Assembly of Conjugated Polymer Thin Layers on Electrospun Nanofibrous Membranes for Biosensors. *Nano Letters* **2004,** 4, (2), 331-334.

48. Lee, S. W.; Belcher, A. M., Virus-Based Fabrication of Micro- and Nanofibers Using Electrospinning. *Nano Letters* **2004,** 4, (3), 387-390.

49. Madhugiri, S.; Dalton, A.; Gutierrez, J.; Ferraris, J. P.; Balkus, K. J., Electrospun MEH-PPV/SBA-15 Composite Nanofibers Using a Dual Syringe Method. *Journal of the American Chemical Society* **2003,** 125, (47), 14531-14538.

50. Jianrong, C.; Yuqing, M.; Nongyue, H.; Xiaohua, W.; Sijiao, L., Nanotechnology and biosensors. *Biotechnology Advances* **2004,** 22, (7), 505-518.

51. Qhobosheane, M.; Santra, S.; Zhang, P.; Tan, W. H., Biochemically functionalized silica nanoparticles. *Analyst* **2001,** 126, (8), 1274-1278.

52. Hilliard, L. R.; Zhao, X. J.; Tan, W. H., Immobilization of oligonucleotides onto silica nanoparticles for DNA hybridization studies. *Analytica Chimica Acta* **2002,** 470, (1), 51-56.

53. Yu, A.; Liang, Z.; Cho, J.; Caruso, F., Nanostructured Electrochemical Sensor Based on Dense Gold Nanoparticle Films. *Nano Letters* **2003,** 3, (9), 1203-1207.

54. Xiao, Y.; Ju, H. X.; Chen, H. Y., Hydrogen peroxide sensor based on horseradish peroxidase-labeled Au colloids immobilized on gold electrode surface by cysteamine monolayer. *Analytica Chimica Acta* **1999,** 391, (1), 73-82.

55. Chen, Z. J.; Ou, X. M.; Tang, F. Q.; Jiang, L., Effect of nanometer particles on the adsorbability and enzymatic activity of glucose oxidase. *Colloids and Surfaces B-Biointerfaces* **1996,** 7, (3-4), 173-179.

56. Bharathi, S.; Nogami, M.; Ikeda, S., Novel electrochemical interfaces with a tunable kinetic barrier by self-assembling organically modified silica gel and gold nanoparticles. *Langmuir* **2001,** 17, (1), 1-4.

57. Zhang, S.; Wang, N.; Niu, Y.; Sun, C., Immobilization of glucose oxidase on gold nanoparticles modified Au electrode for the construction of biosensor. *Sensors and Actuators B: Chemical* **2005,** 109, (2), 367-374.

58. Huang, J.; Virji, S.; Weiller, B. H.; Kaner, R. B., Polyaniline Nanofibers: Facile Synthesis and Chemical Sensors. *Journal of the American Chemical Society* **2003,** 125, (2), 314-315.

59. Tahir, Z. M.; Alocilja, E. C.; Grooms, D. L., Polyaniline synthesis and its biosensor application. *Biosensors & Bioelectronics* **2005,** 20, (8), 1690-1695.

60. Brunelle, S., Electroimmunoassay technology for foodborne pathogen detection. *Detection Technology* **2001**, 55-62.

61. kim, J. H., Cho, J.H., Cha, G.S., Conductimetric membrane strip immunosensor with polyaniline-bound gold colloids as signal generator. *Biosensors & Bioelectronics* **2000,** 14, 907-915.

62. Hoa, D. T. K., T.N.; Punekar, N.S.; Srinivasa, R.S.; Lal, R. and Contractor, A.Q., Biosensor Based on Conducting Polymers. *Analytical Chemistry* **1992,** 64, 2645-2646.

63. Chiang, J. C.; Macdiarmid, A. G., Polyaniline - Protonic Acid Doping of the Emeraldine Form to the Metallic Regime. *Synthetic Metals* **1986,** 13, (1-3), 193-205.

64. Syed, A. A. D., M. K., Polyaniline - A novel Polymeric Material. *Talanta* **1991,** 38, (8), 815-837.

65. Imisides, M. D. J. R. W., G.G., Microsensors based on conducting polymers. *Chemtech* **1996,** 26, (5), 19-25.

66. Wang, X., Kim,Y-G., Drew,C., Ku,B-C., Kumar,J., Samuelson, L.A., Electrostatic Assembly of Conjugated Polymer Thin Layers on

Electrospun Nanofibrous Membranes for Biosensors. *Nano Letters* **2004,** 4, (2), 331-334.

67. Srivastava, P. K.; Kayastha, A. M.; Srinivasan, Characterization of gelatin-immobilized pigeonpea urease and preparation of a new urea biosensor. **2001,** 34, (Pt 1), 55-62.

68. Yoneyama, K.; Fujino, Y.; Osaka, T.; Satoh, I., Amperometric sensing system for the detection of urea by a combination of the pH-stat method and flow injection analysis. *Sensors and Actuators B-Chemical* **2001,** 76, (1-3), 152-157.

69. Sant, W.; Pourciel, M. L.; Launay, J.; Do Conto, T.; Martinez, A.; Temple-Boyer, P., Development of chemical field effect transistors for the detection of urea. *Sensors and Actuators B-Chemical* **2003,** 95, (1-3), 309-314.

70. Castillo-Ortega, M. M.; Rodriguez, D. E.; Encinas, J. C.; Plascencia, M.; Mendez-Velarde, F. A.; Olayo, R., Conductometric uric acid and urea biosensor prepared from electroconductive polyaniline-poly(n-butyl methacrylate) composites. *Sensors and Actuators B-Chemical* **2002,** 85, (1-2), 19-25.

71. Seki, A.; Ikeda, S.; Kubo, I.; Karube, I., Biosensors based on light-addressable potentiometric sensors for urea, penicillin and glucose. *Analytica Chimica Acta* **1998,** 373, (1), 9-13.

72. Sawicka, K.; Gouma, P.; Simon, S., Electrospun biocomposite nanofibers for urea biosensing. *Sensors and Actuators B-Chemical* **2005,** 108, (1-2), 585-588.

73. Ren, G. L.; Xu, X. H.; Liu, Q.; Cheng, J.; Yuan, X. Y.; Wu, L. L.; Wan, Y. Z., Electrospun poly(vinyl alcohol)/glucose oxidase biocomposite membranes for biosensor applications. *Reactive & Functional Polymers* **2006,** 66, (12), 1559-1564.

74. Manesh K.M., K. H. T., Santhosh P., Gopalan A.I., Lee K.P., A novel glucose biosensor based on immobilization of glucose oxidase into multiwall carbon nanotubes-polyelectrolyte-loaded electrospun nanofibrous membrane. *Biosensors & Bioelectronics* **2008,** 23, (6), 771-779.

75. Manesh, K. M.; Santhosh, P.; Gopalan, A.; Lee, K. P., Electrospun poly(vinylidene fluoride)/poly(aminophenylboronic acid) composite nanofibrous membrane as a novel glucose sensor. *Analytical Biochemistry* **2007,** 360, (2), 189-195.

76. Patel, A. C.; Li, S. X.; Yuan, J. M.; Wei, Y., In situ encapsulation of horseradish peroxidase in electrospun porous silica fibers for potential biosensor applications. *Nano Letters* **2006,** 6, (5), 1042-1046.

77. Li, D. P.; Frey, M. W.; Baeumner, A. J., Electrospun polylactic acid nanofiber membranes as substrates for biosensor assemblies. *Journal of Membrane Science* **2006,** 279, (1-2), 354-363.

CHAPTER 3

ELECTROSPINNING POLY(VINYL ALCOHOL) PVOH

Abstract

Submicron poly(vinyl alcohol) (PVOH) fiber mats were prepared by electrospinning of aqueous PVOH solutions in 6– 12 wt% concentration. Fumed silica was added to the electrospinning solution as nanoscale reinforcements for the electrospun fibers. Fiber morphology was observed using electron microscopy and effects of electrospinning parameters including electric voltage, separation distance, flow rate and solution parameters such as concentration were evaluated. Results showed that, when PVOH was electrospun at larger separation distances, the fiber diameter variation increased. Altering the solution flow rate can also change the morphological structure. At high voltages above 10kV, electrospun PVOH fibers exhibited a broad diameter distribution. When the solution concentration was increased, the morphology was changed from beaded fiber to uniform fiber and the average fiber diameter could be increased from 250 nm to 1200 nm. It was also found that additions of silica had significant effects on the fiber diameter and the morphology of electrospun PVOH fibers because of

the different solution conductivity, surface tension and viscosity. Thermal and mechanical properties of the electrospun PVOH mats were also measured.

Introduction to Electrospinning Poly(vinyl alcohol)

Poly(vinyl alcohol) (PVOH) is a semi-crystalline, hydrophilic polymer with good chemical and thermal stability.[1] A number of grades of PVOH are commercially available, which can be divided into two types: fully hydrolyzed and partially hydrolyzed PVOH, which depend on the amount of acetate groups left in the backbone.[2] PVOH is highly biocompatible, is non-toxic and it dissolves easily in water. [3] These properties have led to the use of PVOH in a wide range of applications in medical, cosmetic, food, pharmaceutical and packaging industries. PVOH has been electrospun for applications such as drug delivery systems, contact lenses and artificial organs. It is also used in more traditional applications, such as adhesives, paper coatings, and stabilizers.[4] Recently, Ding et al. [5] have used electrospinning as a processing technique to produce nanoscale fibrous aggregates. The molecular weight of the PVOH has significant effects on the solution properties, including the viscosity, surface tension and electrical conductivity. [6] These solution properties can have drastic impacts on the electrospinning process. [7] Experiments have been conducted at several molecular weights and solution concentrations to highlight the range of structures that may be produced by electrospinning.[1, 8]

Electrospinning PVOH over a range of pH values has also been performed.[9] PVOH can also be mixed with inorganic materials such as silver to make composite nanofibers with antimicrobial activity.[10] PVOH can also be mixed with silica for use as a silica wire precursor or as composite fibers.[11, 12]

The need for nanofibrous materials with high surface area, small pore size, and the production of patterned three - dimensional structures has increased the interest in nanofibers. While various groups have conducted theoretical modeling studies of the electrospinning process, other groups have focused on efforts to characterize the structure and morphology of nanofibers as a function of process parameters and material characteristics. The successful production of nanofibers by electrospinning resulted from a balance of the electrostatic forces and the viscoelastic behavior of the polymer.

The structure and properties of electrospun fibers were influenced by processing parameters, such as solution feed rate, applied voltage, nozzle to collector distance, spinning environment; and material properties, such as solution concentration, viscosity, surface tension, conductivity, and solvent vapor pressure. Substantial work has been done to characterize the properties of fibers as a function of processing and material parameters. The goal of this experimental work was to compare the results obtained varying the solution and processing variables to published reports. PVOH dissolved in water served as a simple model system to understand the electrospinning process. Varying the parameters in a controlled pattern provided results similar to the trends shown in Table 3.1. Increasing viscosity and flow rate provided more polymeric material to

undergo the electrospinning process, resulting in increased fiber diameters. When solvent volatility, solution conductivity and electric field strength were increased, the fiber diameters decreased. Upper and lower limits exist for all solution and processing variables and these values will be explained in further detail.

Table 3.1 Effect of increasing the electrospinning variables on the resultant fiber morphology.

Variable Increasing	Fiber Diameter	Morphology
Electric Field Strength	Decrease	Less Homogenous
Polymer Flow Rate	Increase	Less Homogenous
Solution Viscosity	Increase	More Homogenous
Solution Conductivity	Decrease	More Homogenous
Solvent Volatility	Decrease	Less Homogenous

Experimental

The driving force of the charged jet was provided by two high voltage sources. The high voltage sources were used that were capable of generating up to 30 kV DC of potential difference, and the setup was designed to be able to run on positive or negative polarity or a combination. Typically a total of 8 – 12 kV was applied over a distance of 8 to 12 cm to produce uniform fibers. This research proved a combination of positive polarity at the syringe and negative polarity at the collector yielded the most predictable fiber morphology. The negative polarity at the collector typically maintained at a constant 1 kV.

Adjusting the flow rate of the fluid and the magnitude of the electric field controlled the spinning rate, which influenced the resultant fiber size. The syringe pump rate was varied from 0.01 ml/hr up to 4.0 ml/hr. The needle diameter could have also been altered, which would change the initial fiber jet size, which would ultimately affect the final fiber diameter, but for these experiments a 20-gauge needle tip was employed.

Materials

Poly(vinyl alcohol) (PVOH) was donated by the Celanese Corporation. 10 wt % solutions of Celvol 425 PVOH were prepared in deionized water by vigorous mixing for 12 hours at 90°C. This PVOH solution had 96.5 % degree of hydrolysis and 580 cps viscosity, which was determined using a Brookfield viscometer. Pendant drop shape analysis of this solution, in this research work, yielded an average surface tension of 53.4 mN/m. Fumed silica (Cab-O-Sil M5) was purchased from Cabot Corporation.

Morphology

An Electroscan 2020 Environmental Scanning Electron Microscope (ESEM) was used to obtain sample images. The samples were first mounted on ESEM pedestals, then sputter coated with gold. The samples were imaged at 15 kV from 500 x to 10,000 x magnification to obtain alignment and size distribution

information. Alignment efforts were made so that the electrospun fibers could be used as fillers in composite materials. Preliminary experiments have shown that a high degree of alignment is possible.

Transmission electron microscope (TEM) (JEOL 2100FEF 200 kV field emission) was used to obtain images for the silica-loaded samples. The goal was to determine how effective the silica loading was, the dispersion of silica particles can be seen in the electrospun fibers.

Thermal Properties

A TA Instruments 2950 TGA was used to evaluate the thermal properties of the electrospun materials. The goal of the thermal analysis was to determine the degradation temperature, if any residual water was present in the system and the residue values.

Mechanical Properties

A TA instruments 2980 Dynamic Mechanical Analyzer (DMA) was used to evaluate the mechanical properties of the electrospun materials. The goal was to determine the modulus for the neat electrospun PVOH and silica filled electrospun PVOH fibers. To date, accurate and reliable mechanical property analysis has not been fully realized. The initial measurements obtained in this research were compared to published literature values.

Results and Discussion

Morphology

The electrospinning setup was tailored to provide nanofiber mats that were either aligned or randomly oriented. Aligned mats could be produced in several ways, including using high speed rotating collectors, a parallel array of collectors, or auxiliary electric fields.[13] One of the objectives of this research was to be able to reproducibly produce aligned electrospun fibers of uniform diameter to serve as the basis of the sensors. Electrospun fibers are highly charged and undergo a chaotic 'whipping' motion between the needle tip and the collector due to their interaction with the electric field. A series of experiments were organized in which the collector and the location of the field were varied in order to reduce the motion of the fibers and collect an ordered array. This involved collection on a flat plate, rotating drum and parallel electrode "C" shaped collector. Aligned fibers were demonstrated by harvesting the fibers that spanned the gap of a "C" shaped collector as shown in Figure 3.1. In Figure 3.1, the polymeric solution was loaded in a glass syringe fitted with a metal needle, which was attached to the syringe pump. The syringe pump supplied a constant flow of solution through the needle. At the needle, a high voltage (positive) connection is made to the high voltage power supply. The positively charged fibers were deposited on a collector that was either grounded, or held at negative potential. Collecting the fibers across a void gap enabled the fibers to be easily gathered for future processing and evaluation.

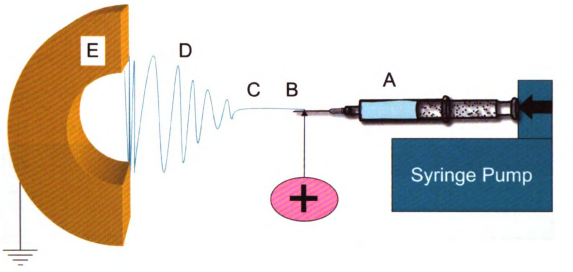

Figure 3.1 Electrospinning schematic showing (A) the polymer solution in the syringe, (B) the Taylor Cone at the needle tip, (C) the stable region of the charged jet, (D) the unstable region of the charged polymer jet and (E) the C-shaped void gap collector

The collector can be replaced with various geometrical designs. The designs and orientations of the collectors affect the fiber deposition process. A schematic illustration of the collectors used is shown as Figure 3.2.

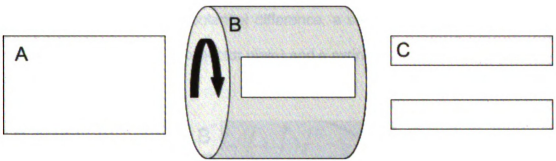

Figure 3.2 Various collectors used in the electrospinning of PVOH. A) A flat plate of aluminum, B) a rotating steel drum with a slot milled in the surface, C) a parallel set of copper electrodes.

Using a flat plate (Figure 3.2 (A)) as a collector provided a simple collection device that could be used to provide morphology information easily. The flat plate collector was used to produce a random array of fibers. This technique provided a facile method to understand the effects of altering the solution and electrospinning parameters on the fiber morphology. Once a satisfactory set of parameters was chosen, a rotating drum was added to improve the fiber alignment (Figure 3.2 (B)). Difficulties were encountered using the rotating drum to obtain aligned fibers. It was thought that the high speed generated turbulence in the air, which forced the fibers into an undesirable unaligned pattern. As a result, the parallel electrode design (Figure 3.2 (C)) was employed. This design

allowed the fibers to span the gap between the top and bottom electrode, which resulted in a high degree of alignment. A comparison of fibers collected from a various styles of collectors is shown in Figure 3.3. The solution parameters were adjusted to final values of 10 wt% PVOH in water. The electrospinning setup was operated with 10 kV potential difference, a separation distance of 8.0 cm (between the needle tip to collector plate) and a syringe pump rate of 1.0 ml/h.

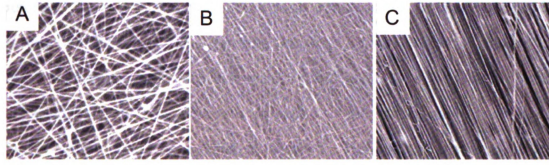

Figure 3.3 ESEM comparison of electrospun PVOH. A) Stationary collector, B) Rotating drum collector with slot, C) Stationary parallel electrode collector.

As Figure 3.3 shows, a drastic difference in alignment was observed by changing the collector design. The stationary flat plate (Figure 3.3 (A)) provided a random distribution of electrospun fibers. Alignment of fibers was improved in the rotating drum setup (Figure 3.3 (B)), but the highest degree of alignment was obtained in the parallel electrode setup (Figure 3.3 (C)).

The goal of fiber alignment was essential since the fibers were to be incorporated into composites. A 90 mm rotating drum that was capable of 2500 rpm was used as the rotating collector. This provided a speed of 22 m/s at the face of the collector. It was determined that the rotating drum collector provided the highest throughput of electrospun fibrous material, but the collection of material was difficult. To alleviate this problem, a 25 mm slot was milled in the surface of the drum. This allowed fibers to span the gap as the drum was rotating. The gap allowed fibers to be easily transferred to a different backing for testing and evaluation. The gap also produced a fan effect, which caused too much interference and instabilities in the air to obtain truly aligned fibers. As the lightweight polymer jet approached the surface of the rotating drum, it was forced into a random patter as a result of the wind. The platform that was used to mount the motor, axle and collector was also vibrating erratically at high speed, which was thought to further increase the instability of the process.

From the idea of the slotted rotating drum, the parallel electrode evolved. The idea was to use the open gap that was advantageous to the rotating drum, but hold the device stationary. The parallel electrode produced very highly aligned fiber mats, but the throughput was extremely limited. At this point it was determined that operating the collector at a slight negative potential, the fiber morphology and throughput would improve. This was due to the fact that the positively charged fibers that deposited on the collector built up charge and would repel incoming positively charged fibers. By adding a negative charge at the collector the positive charge build up would be eliminated and the aligned

network could be realized. The morphology of the optimized aligned parallel electrode setup is shown in Figure 3.4.

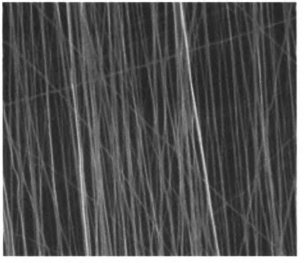

Figure 3.4 ESEM micrograph of electrospun 10 wt% PVOH fibers. 10 cm Separation distance, 500 X magnification, scale bar shown is 100 micrometers

ImagePro software [14] was utilized to aid in the fiber diameter and alignment analysis. ESEM images were used with ImagePro to count and size the individual fibers. The classical method of viewing the samples from the top down was chosen and it was assumed that the fibers were circular in cross section. [15] The purpose of the top down method is for easy alignment characterization and fiber size estimation.

Fiber Size Distribution

An important advantage of the electrospinning process is that the device parameters in conjunction with the solution properties could be tailored to accurately produce fibers of the desired size. These experiments have shown that altering the solution concentration was an effective method to alter the fiber diameters. Several variables have been explored to determine their effects on the resultant fiber size. It was expected that increasing the electric field strength would induce more instability, thus reducing the fiber diameter. Increasing the polymer flow rate would increase the amount of material available and increase the fiber diameter. Increases in viscosity or concentration would also provide larger diameter fibers. The morphology of the fibers is also dependent upon the volatility of the solvent. Highly volatile solvents, such as THF are difficult to continuously electrospin, due to rapid solvent evaporation, but have been known to result in highly porous fiber structures.[16] In order to accurately determine the fiber sizes, a higher magnification image is required. An example of a high magnification image used for fiber size analysis is shown in Figure 3.5.

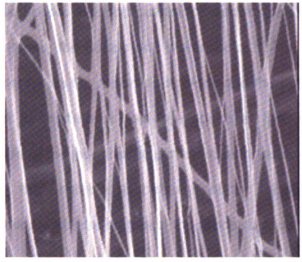

Figure 3.5 High magnification (2,000X) ESEM image of electrospun PVOH. The scale bar is 25 μm.

Effect of Electric Field Strength

Baumgarten observed that increasing the applied voltage resulted in a doubling of fiber length with small changes in fiber diameter.[17] Megelski et al. investigated the fiber diameter dependence on applied voltage using polystyrene (PS). The PS fiber size decreased from about 20 μm to 10 μm with an increase in voltage from 5 KV to 12 KV, while there was no significant change observed in the pore size distribution.[18] These results concur with the interpretation by Buchko et al., who observed a decrease in the fiber diameter with an increase in the applied field while spinning silk -like polymer fiber (SLPF) with fibronectin functionality.[19] Generally, it has been accepted that an increase in the applied voltage increases the deposition rate due to higher mass flow from the needle tip.

Jaeger et al. used a two-electrode setup for electrospinning by introducing a ring electrode in between the nozzle and the collector.[20] The ring electrode was set at the same potential as the electrode immersed in the polymer solution. This setup was thought to produce a field-free space at the nozzle tip to avoid changes in the shape of the jet-initiating surface due to varied potential. Although this setup reduced the unstable jet behavior at the initiation stage, bending instability is still dominant at later stages of the process, causing a chaotic motion of the jet before depositing itself as a non-woven matrix on the collector. Deitzel et al. experimented with a new electrospinning apparatus by introducing eight copper rings in series in between the nozzle and the collector for dampening the bending instability.[7] The nozzle and the ring set were subjected to different potentials (ring set at a lower potential) of positive polarity, while the collector was subjected to a negative polarity. The idea behind this setup was to change the shape of the macroscopic electric field from the jet initiation to the collection target in such a way that the field lines converge to a center line above the collection target by the applied potential to the ring electrodes. The authors have suggested that the bending instability of fibers was dampened by the effect of the converging field lines producing straight jets. Controlled deposition helps to produce specific deposition patterns and also yarn like fibers. Deitzel et al. investigated the spinning of polyethylene oxide (PEO) in aqueous solution using multiple electric fields, which resulted in fibers deposited over a reduced area due to the dampening of bending instability. The multiple field technique was also shown to produce fibers of smaller diameter than the conventional

electrospinning method, which consists only of a positive needle tip and grounded collector.

The structure and morphology of electrospun fibers was easily affected by the nozzle to collector distance because of their dependence on the deposition time, evaporation rate, and whipping or instability interval. Buchko et al. examined the morphological changes in SLPF and nylon electrospun fibers with variations in the distance between the nozzle and the collector screen. They showed that regardless of the concentration of the solution, decreased nozzle to collector distance produced wet fibers and beaded structures. SLPF fiber morphology changed from round to flat with a decrease in the nozzle collector distance from 2 cm to 0.5 cm.[19] This result showed the effect of the nozzle to collector distance on fiber morphology. The work also showed that aqueous polymer solutions require more distance for dry fiber formation than systems that use highly volatile organic solvents. Megelski et al. observed that decreasing the nozzle to collector distance resulted in bead formation, while preserving the ribbon shaped morphology of PS fibers.[18]

Several studies specifically focused on using PVOH and understanding the effect of electric field strength.[2, 5, 21] Lee et al conducted a very thorough study of the PVOH system and concluded that the diameter of the electrospun fibers decreased with an increase in the electric field strength, and the diameters also decreased with decreasing the solution concentration.[8] A summary of these results is shown in figure 6. The data shown in Figure 3.6 was generated using a lower molecular weight PVOH of 54,400 grams per mole as compared to 65,000

grams per mole PVOH used in this study. It was determined that higher molecular weight samples follow the same trend.[8]

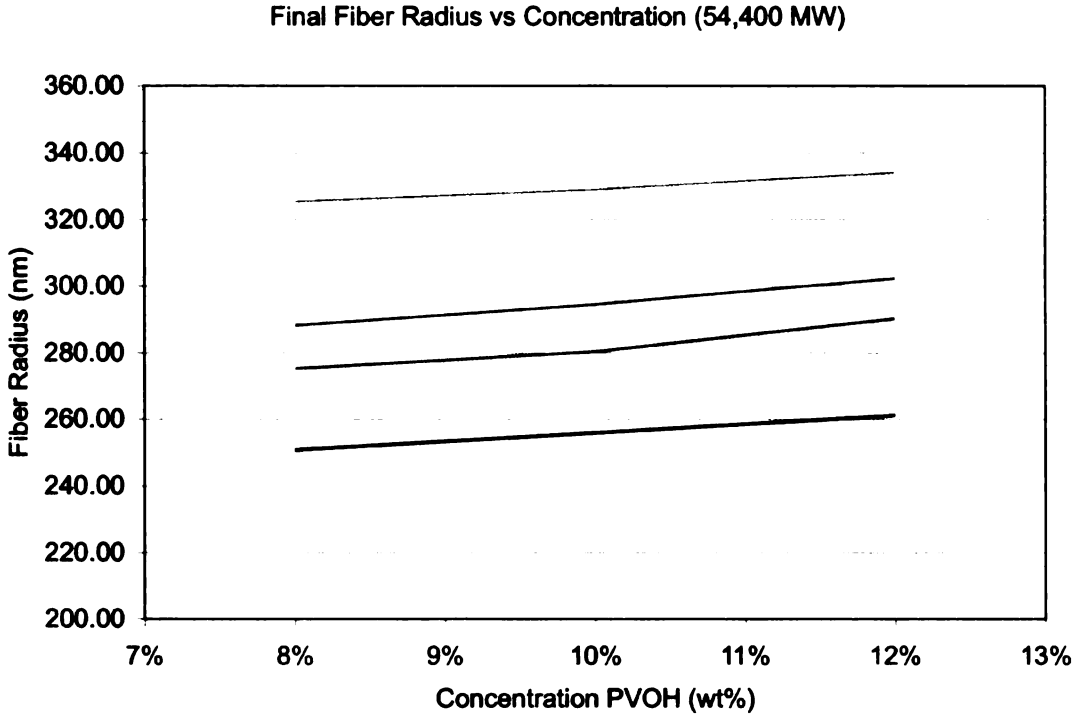

Figure 3.6 Fiber size as a function of electric field strength and concentration for 54,400 MW PVOH. Increases in electric field strength reduce fiber diameters.

Fiber Diameter Summary

Three different electric field strength experiments have been employed to examine the effect on fiber morphology. The applied voltage was maintained constant at 10 kilovolts (kV), while the separation distance was varied from 8 to 12 cm. In all cases the applied voltage was 10 kV, the syringe pump rate was 0.1 ml/h, the collection time was 1 hour, and the solution was 10 wt% PVOH in water. Variation in the electric field strength resulted in fiber size and relative fiber alignment differences. There is a broad range of fiber diameters for the 8 and 12 cm separation distance and the smallest variation of fiber diameter occurred at a separation distance of 10 cm. A summary of the results is shown in Table 3.2. As expected, the 8 cm separation distance produced fibers with the largest diameter, but on average, the 10 cm separation distance produced the smallest diameter fibers. The 12 cm separation distance was expected to produce fibers with the smallest diameters, but they were found to be similar in size to the 10 cm. The fibers collected at 12 cm had undergone the most instability, resulting in a wide range of fiber diameters. The alignment of fibers collected at 12 cm indicated that they are the most random, showing that the instability region was not controlled well; therefore fiber size did not agree with expected results.

Table 3.2 Separation distance affects the fiber diameter and alignment. Applied voltage 10 kV, syringe pump rate 0.1 ml/h, 10 wt% PVOH in water.

Separation Distance	**8 cm**	**10 cm**	**12 cm**
Average Diameter (nm)	599	355	380
Standard Dev. Dia. (nm)	116	43	73
Fibers within 10 deg. Of average (%)	93	80	69
Standard Dev. Angle (deg)	6.5	9.5	14

The fiber morphology was only slightly different when comparing the ESEM images. As shown Figure 3.7, the 10 cm separation distance produced the highest number of fibers in the same collection time. The 8 cm separation distance produced the largest diameter fibers. This was due to the limited space for the whipping phenomenon to occur. The whipping phenomenon was the part of the process responsible for the rapid fiber thinning. The 12 cm separation distance produced the widest range of fiber diameters with a lower relative alignment. This is a result from collecting fibers from a separation distance that is too large. The whipping phenomenon, which is also the instability region, dominates and the fibers collected are various in size and shape. The fibers that were collected from a separation distance of 10 cm were the most uniform in

size and shape due to a proper balance of electric field strength and solution properties.

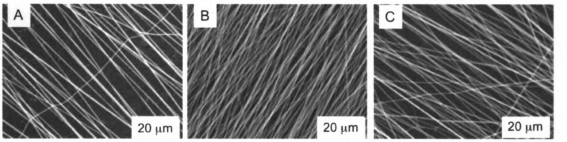

Figure 3.7 ESEM images of electrospun PVOH fibers, showing variation with separation distance A) 8 cm, B) 10 cm, and C) 12 cm. Applied voltage 10 kV, pump rate 0.1 ml/h, 10 wt% in water

The average fiber diameter of electrospun 10 wt % PVOH ranges from 300 to 450 nm. This was determined by viewing samples in the ESEM coupled with image analysis. Higher magnification is crucial for accurately determining the fiber size and alignment. A series of high magnification images were required to obtain statistically significant measurements.

An experimental protocol was developed to understand the effect of each variable (separation distance, electric field strength and solution flow rate) on the resultant fiber diameter. In order to ascertain which variable has the most significant effect on fiber morphology, all variables were held constant except the variable of interest. A larger separation distance at a fixed applied voltage will result in a lower electric field strength, which should have increased the fiber

diameter. Samples were prepared at separation distances of 8, 10 and 12 cm. A summary table of the variables and the resultant fiber diameters is shown as Table 3.3. The variable of interest for each data set is highlighted.

Table 3.3 The effect of variables on the diameter and variability (standard deviation) of electrospun PVOH fibers.

Concentration (wt%)	Electric Field Strength (kV/cm)	Syringe Pump Rate (ml/h)	Diameter (nm)	Diameter Std. Dev. (nm)
8	1.00	0.1	500	260
10	1.00	0.1	280	60
12	1.00	0.1	1100	960
10	0.83	0.1	380	80
10	1.00	0.1	360	40
10	1.25	0.1	600	120
10	1.00	0.1	800	240
10	1.00	0.2	780	400
10	1.00	0.3	1180	720

In the first set of experiments, the concentration was varied from 8 wt% to 12 wt%. This represented a 50% increase in the concentration, yielding a 120% increase in the fiber diameter as compared to the 8 wt% data. This variable provided the most significant change in fiber diameter. The upper limit of concentration (12 wt%) was not stable and produced a very large distribution of fiber diameters as evidenced by the standard deviation. The electric field strength was 1.0 kV/cm, (8 kV, 8 cm) the syringe pump flow rate was 0.1 ml/hr through a 2 inch 20 gauge blunt tip needle.

In the second set of experiments, all of the experimental parameters were maintained constant from the 10 wt% trial, and the electric field strength was varied. Using a separation distance of 12 cm with an applied voltage of 10 kV resulted in an electric field strength of 0.83 kV/cm. When the electric field strength was increased to 1.0 kV/cm (10 kV, 10 cm) the fiber diameter did not change significantly, but the variability (standard deviation) was reduced. A separation distance of 8 cm with an applied voltage of 10 kV yielded an electric field strength of 1.25 kV/cm. This relatively large field strength increased fiber diameter variability and resulted in larger diameter fibers. The fiber diameter increased with increasing field strength, which is not expected. The fiber diameter should decrease with increased electric field strength due to more electric forces to induce charged fiber whipping. The fact that fiber diameter increased is explained by the short distance (8cm) between the needle tip and collector. There was a geometric limitation, and the expected whipping phenomenon, which greatly reduces fiber diameter, could not occur.

The third set of experiments varied the syringe pump rate while maintaining all other variables constant. In general, increasing the polymer flow rate resulted in larger diameter fibers. The lower limit 0.01 ml/h and even the middle value of 0.2 ml/h produced fibers with a large amount of variation in their diameters. The flow rate chosen for the other experiments (0.1 ml/h) was the best choice for homogenous fiber production.

Another set of electric field strength experiments was run using a lower applied electric voltage of 8 kV. Table 3.4 shows the statistics for the three

different separation distances. Since the applied voltage is constant for the three different cases, as the distance changes, the electric field strength is altered.

Table 3.4 Summary of various electric field strengths and the resultant fiber morphology.

	8 cm (1.0 kV/cm)	10 cm (0.8 kV/cm)	12 cm (0.67 kV/cm)
Average Diameter (nm)	600	355	380
Standard Deviation (nm)	115	40	70
Diameter Range (nm)	450	170	380

The expected trend of higher electric field strength producing smaller diameter fibers is not apparent in this data set either, as shown in Table 3.4. The trend is slightly present when comparing the 10 cm (0.8 kV/cm) and 12 cm (0.67 kV/cm) data. The decreased electric field strength resulted in larger diameter fibers. The large variability in the 8 cm separation distance (1 kV/cm) data was the reason for the inconsistencies.

Figure 3.8 shows the percentage of analyzed fibers that are within a 50 nm diameter range. The 0.8 kV/cm data shows that 80% of the fibers are within the range of 200-300 nm and furthermore 92% of the fibers are within 100 nm from the mean diameter. The goal of creating uniform fibers was for the intended application of composite materials. Uniform materials also aid in estimating individual fiber properties based on bulk sample data. The data shows that uniform fiber shape was attainable with this experimental setup.

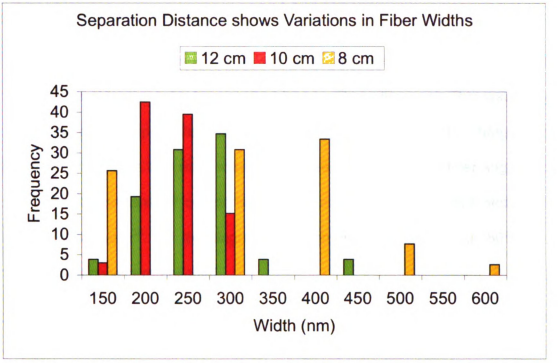

Figure 3.8 Fiber diameter comparison for 10 wt% PVOH fibers electrospun from separation distances of 8 cm, 10 cm and 12 cm.

Alignment Distribution

Collection of aligned fibers has been shown to be important for composite and biomedical applications. Aligned electrospun fibers can significantly improve the mechanical properties of the composite. The importance of a high degree of alignment was essential to fully realize the reinforcing effect of the materials.[22]

Aligned fibers are important in biomedical applications, since the morphology can control tissue growth rates.[23]

Previous research has shown that not using the proper setup, and in our case the negative potential collector, resulted in poor fiber alignment. This was likely due to charge buildup on the collector, which repelled the incoming charged jet. The number of fibers that were within 10 degrees of the average fiber angle was chosen as a standard for comparison and fiber angles were determined using ImagePro software[14]. If the degree of alignment was larger than 80%, the network was considered aligned.

The 8 cm separation distance, (1 kV/cm) data had the lowest range and the least amount of standard deviation. 92% of the fibers from this sample were within 10 degrees of the average. The mean angle parameter was arbitrary; it depended upon how the sample was loaded in the ESEM for analysis. As expected, the fibers collected at 8 cm were the most aligned, since they had traveled less distance through the instability region. As Table 3.5 shows, decreasing the electric field strength, broadened the range and lowered the relative amount of alignment. At 10 cm, (0.8 kV/cm), 79% of the fibers are still within 10 degrees of the average fiber. At 12 cm (0.67 kV/cm), only 69% of the fibers are within 10 degrees of the average angle of alignment. The fibers collected at 12 cm experience the greatest instability and were therefore the most random in size and alignment. These fibers appeared nearly parallel in most regions examined with the ESEM.

The alignment distribution results indicate that closer distances between source and collector result in a smaller number of stray fibers. The increased field strength forces the charged fibers to be aligned by the collector rather than going astray. It has also been shown that the void gap plays a significant role in how the charged fiber behaves near the collector.[24] Void gap was defined as the distance between the electrodes of the collector. Separation distance was defined as the distance between the collector and the needle tip, or origin of the electrospinning process.

Table 3.5 Summary of alignment distributions.

	8 cm (1.0 kV/cm)	**10 cm (0.8 kV/cm)**	**12 cm (0.67 kV/cm)**
Average Angle (deg)	43	121	30
Standard Deviation (deg)	6	9	13
Range (deg)	22	52	54
AN (10)	92	79	69

Table 3.5 shows a summary of the alignment distributions for fibers that were electrospun from 8, 10 and 12 cm separation distances. The mean angle was an arbitrary value, which was just the average angle of the fibers observed in the

ESEM. The standard deviation and range values were measures of the statistical variation of the alignment. The 8 cm separation distance provided the smallest range and the smallest standard deviation. AN(10) is a value defined as the percentage of fibers within 10 degrees of the average fiber alignment. In the case of the 8 cm separation distance, 92% of the fibers were within 10 degrees of the average, which is considered highly aligned. As Figure 3.9 shows, the alignment distribution proves that closer distances result in less stray fibers. In this chart, the majority of the fibers in all electric field strength scenarios are within 5 degrees from the average fiber angle.

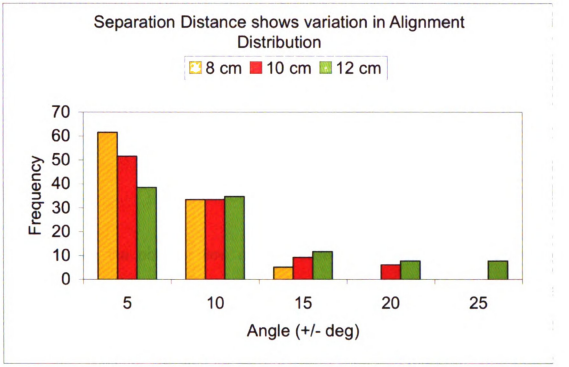

Figure 3.9 Angle distribution of 10 wt% electrospun PVOH fibers from separation distances of 8 cm, 10 cm, and 12 cm.

Effect of Polymer Flow Rate on Morphology

The flow rate of the polymer from the syringe was an important process parameter since it influenced the jet velocity and the material transfer rate. In the case of PS fibers, Megelski et al. observed that the fiber diameter and the pore diameter, the open areas on the individual fibers, increased with an increase in the polymer flow rate.[18] As the flow rate increased, fibers had pronounced beaded morphologies and the mean pore size increased from 90 to 150 nm.

The conservation of mass for the electrospun jet states that volumetric flow rate (Q) was based on the initial jet radius (R) and the constant axial fluid velocity υ as shown in Equation 3.1.

$$\pi R^2 \upsilon = Q \qquad \text{(Equation 3.1)}$$

Increasing the polymer flow rate increased the jet size, which ultimately increased the size of the collected fiber.[25] Increasing the flow rate increased the velocity of the jet and the size of the jet, and if the separation distance was maintained constant, the time for solvent evaporation was reduced. This lead to structures that contained more entrapped solvent molecules and were more agglomerated than fibers produced at lower syringe flow rates.

The effect of polymer flow rate, varied by the syringe pump rate, on the fiber morphology was studied for the 10 wt% PVOH in water system. As the flow rate increased, the fibers became less uniform. At low flow rates of 0.01 ml/h, the amount of fibers formed over a 1-hour time span were inconsequential. A flow rate of 0.1 ml/h resulted in homogeneous fiber formation. The flow-rate was increased to 0.2 ml/h and 0.3 ml/h. All other processing parameters were kept constant: 10 kV applied voltage, 10 cm separation distance, and 1-hour collection time. The results of the experiments are shown in Figure 3.10. Figure 3.10showed a broad range of syringe pump rates. In panel A of Figure 3.10, the

syringe pump rate was too low (0.01 ml/h) and there was insufficient material available to be electrospun into fibers. The density of material collected was much lower as compared to the other flow rates examined. Due to the low flow rate, large variations in shape and size were observed. In panel B of Figure 3.10, the syringe pump rate (0.1 ml/h) was ideal. The fibers appeared homogenous in shape and size, with very few imperfections. The density of the fiber mat was much greater than the mat obtained using the lower flow rate. In panel C of figure 10, the flow rate was slightly too large. The fibers appeared to be agglomerating, resulting in shape and size in homogeneities. In panel D of Figure 3.10, the flow rate was too high, which resulted in numerous agglomerations and fiber imperfections. It is clear that faster flow rates lead to agglomerated fiber structures since the solvent cannot be volatilized sufficiently from the larger mass of material constrained by the process parameters.

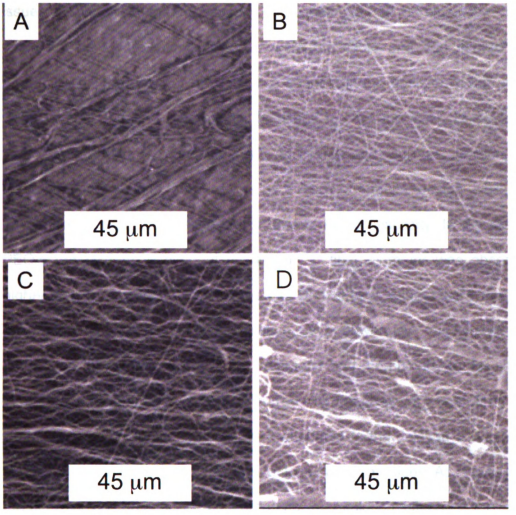

Figure 3.10 ESEM images of electrospun PVOH fibers, showing the variation with syringe pump flow rate A) 0.01 ml/h, B) 0.1 ml/h, C) 0.2 ml/h, and D) 0.3 ml/h. Applied voltage 10 kV, 10 cm separation distance, 10 wt% PVOH in water.

Effect of Solution Viscosity on Morphology

The viscosity had a dramatic effect on the electrospinning process. Highly viscous solutions could not be successfully electrospun due to needle clogging

issues and insufficient pump capacity. Solutions that had extremely low viscosity could not be electrospun since they were too dilute and had a much lower probability for the polymer molecules to connect in the fiber formation process. Solution concentration determines the limits for the formation of electrospun fibers due to its relationship with viscosity and surface tension.[7] Low concentration solutions form droplets as a result of surface tension, while higher concentration prohibits fiber formation due to higher viscosity. In the case of a PEO/water system, a bimodal distribution in fiber diameter was observed at higher concentrations. In the PEO system, Dietzel et al. related the average fiber diameter and the solution concentration by a power law relationship[7]. They interpreted the variations in the fiber diameter and morphology to the shape of the jet-originating surface, which concurred with the observations of Zong et al.[26] Undulating morphologies in fibers were attributed to the delayed drying and the stress relaxation behavior of the fibers at lower concentrations. As is evident from the discussions, the concentration of the polymer solution influences the spinning of fibers and controls the fiber structure and morphology.

As shown in Equation 3.2, the viscosity was directly related to the fiber diameter. The actual value of the exponent varies for each polymer system, and is also dependent on other solution and process variables. To date, there is not a reliable, accurate equation of state relating viscosity to fiber diameter, but as a general estimate Equation 3.2 is acceptable.

$$d = \eta^{0.5}$$

(Equation 3.2)

Molecular weight and viscosity are related, and their effects on morphology are comparable. In general when a polymer with a higher molecular weight is dissolved in a solvent, the viscosity is higher. Molecular chain entanglements are necessary to produce continuous fibers. The entanglement of the molecular chains prevents the electrically driven jet from breaking up, thus maintaining a continuous fiber jet. Buchko observed that monomeric solutions did not produce fiber structures when using the electrospinning process.[19] When molecular weight and viscosity increased, the fiber morphology changed from beads on a string, to smooth continuous fibers to agglomerated structures.

Varying the concentration of the polymer solution directly affected the viscosity of the solution and showed a non-linear dependence. Fibers could only be formed in a specific viscosity range of 200 cps (8 wt%) to 900 cps (12 wt%) as shown in Figure 3.11.

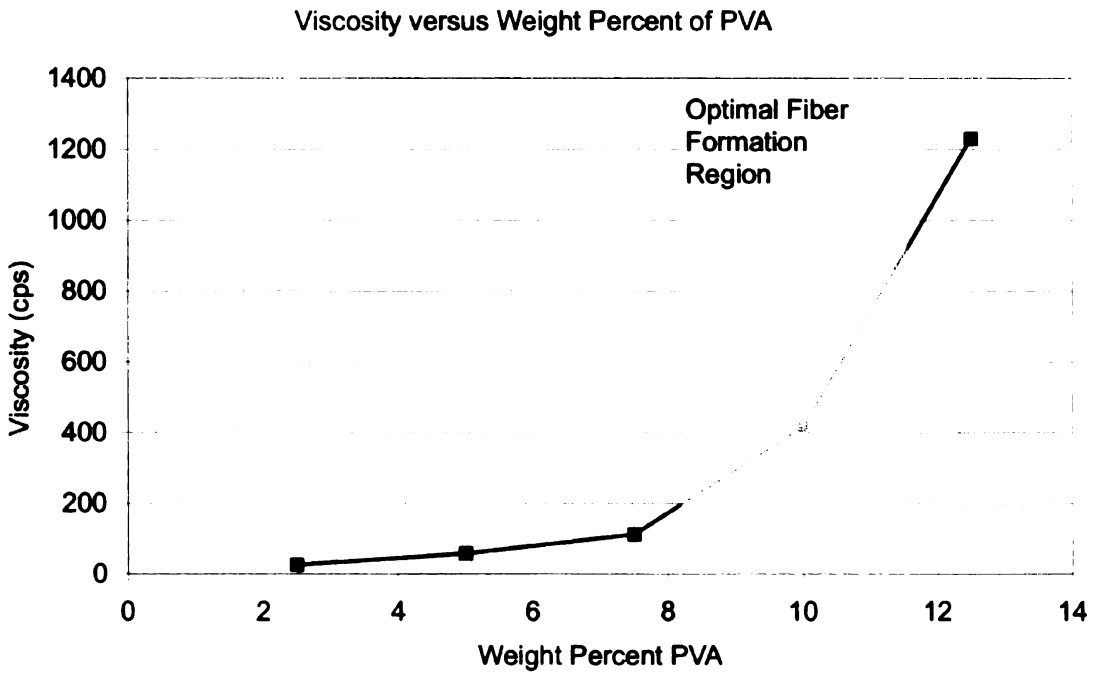

Figure 3.11 Viscosity chart of PVOH, indicating the viscosity range in which fibers can be readily formed.

Figure 3.12 compared ESEM images of electrospun PVOH at various concentrations. The low concentration (8 wt%) resulted in bead-on-string morphology, 10 wt% produced nearly homogeneous fibers and 12 wt% resulted in larger fibers with some agglomerations and some non-fibrous structures. It was determined that 10 wt% was the optimal concentration for homogeneous fibers.

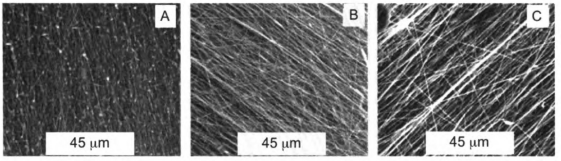

Figure 3.12 ESEM images of electrospun PVOH fibers, showing the variation with concentration A) 8 wt%, B) 10 wt%, and C) 12 wt%. Applied voltage 10 kV, syringe pump rate 0.1 ml/h, 10 cm separation distance

The results of the experiments showed that electrospinning 10 wt% PVOH at a syringe pump rate of 0.1 ml/h, a separation distance of 10 cm and an applied voltage of 10 kV resulted in the most homogeneous fiber structure. The optimized processing parameters lead to fibers shown in Figure 3.13. These fibers were optimized for alignment and homogeneous fiber diameter. The fiber diameter was determined to be 360 nm with a very small deviation of only 40 nm. In this case, 97% of the fibers are aligned within 10 degrees of the average fiber. There are only 3% of the fibers that are not considered aligned. The fiber mat appears uniaxially aligned and homogenous in diameter with very few imperfections. The detailed specifications are summarized in Table 3.6.

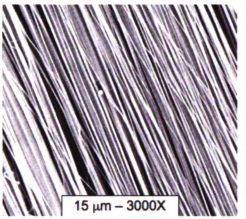

Figure 3.13 ESEM image of electrospun PVOH fibers, showing the optimized morphology. Applied voltage 10 kV, syringe pump rate 0.1 ml/h, 10 wt% PVOH in water, 10 cm separation distance.

Table 3.6 Summary of processing parameters and their effects on the fiber diameter. Results avg. ± SD, n = 40.

Parameter	Processing Condition	Fiber Diameter (nm)
Electric Field Strength	1.3 kV/cm (10 kV 8 cm)	600 ± 120
	1.0 kV/cm (10 kV 10cm)	360 ± 40
	0.8 kV/cm (10 kV 12 cm)	380 ± 80
Syringe Pump Rate	0.01 ml/h	800 ± 240
	0. 1 ml/h	560 ± 200
	0.2 ml/h	780 ± 400
	0.3 ml/h	1180 ± 720
Solution Concentration (Viscosity)	8 wt% (200 cps)	500 ± 260
	10 wt% (400 cps)	280 ± 60
	12 wt% (900 cps)	1100 ± 960

Effect of Electrospinning Environment on Morphology

Environmental conditions around the spinneret, like the surrounding air, its relative humidity (RH), vacuum conditions, surrounding gas, etc., also influenced the fiber structure and morphology. Baumgarten observed that acrylic fibers spun in an atmosphere of relative humidity more than 60% did not dry properly and get entangled on the surface of the collector.[27] The breakdown voltage of the atmospheric gases is said to influence the charge retaining capacity of the fibers. Srinivasan et al. proposed a new mechanism for pore formation by evaporative cooling called "breathe figures". Breathe figures are pores that occurred on the fiber surfaces due to the imprints of condensed moisture droplets caused by the evaporative cooling of moisture in the air surrounding the spinneret. Megelski et al. investigated the pore characteristics of PS fibers at varied RH and emphasized the importance of phase separation mechanisms in explaining the pore formation of electrospun fibers.[18]

Effect of Solution Conductivity on Morphology

Most polymers are slightly conductive, with the exception of insulating materials. The charged ions in the polymer increase the charge-carrying capacity of the jet, thereby subjecting it to higher elongational tension with the applied electric field. Baumgarten showed that the jet radius varied inversely as the cube root of the electrical conductivity of the solution.[17] Zong et al. added ionic salts to the electrospinning solution to increase conductivity. They found that poly (D,L-

lactic acid) PDLA fibers with added ionic salts such as KH_2PO_4, NaH_2PO4, and NaCl produced bead-less fibers with relatively smaller diameters ranging from 200 to 1000 nm.[28]

Effect of Solvent Volatility on Morphology

Solvent volatility plays a major role in the formation of nanostructures. Electrospinning involves rapid solvent evaporation and phase separation due to jet thinning. Solvent vapor pressure critically determined the evaporation rate and the drying time. Bognitzki et al. found that the use of highly volatile solvents like dichloromethane yielded poly (L – lactic acid) PLLA fibers with pore sizes of 100 nm in width and 250 nm in length along the fiber axis.[29] Lee et al. evaluated the effect of volume ratio of the solvent on the fiber diameter and morphology of electrospun PVC fibers.[30] Average fiber diameters decreased with an increase in the amount of DMF in the THF/DMF mixed solvent. Lee et al. found the electrolytic nature of the solvent to be an important parameter in electrospinning. Megelski et al. studied the characteristics of electrospun fibers with respect to the physical properties of solvents. The influence of vapor pressure was evident when PS fibers were spun with different THF/DMF ratios. The vapor pressure of THF is 129 mm Hg, while DMF is only 2.7 mm Hg. A large amount of THF resulted in a porous film being formed, while a large amount of DMF resulted in smooth homogenous fibers to be formed

Effect of Solution Rheology on Morphology

The rheological parameters of the solution are most strongly affected by the entanglement characteristics of the polymer. Addition of nanoscale fillers, such as silica particles, altered the entanglement characteristics of the polymer and can significantly alter the viscoelastic parameters of the electrospinning solution. The filler-polymer interactions resulted in a change in the entanglement density and distribution. It was found that adding untreated silica particles offered more hydrogen bonding opportunities that influenced the rheology of solutions. This phenomenon was similar to increasing the molecular weight or increasing the degree of polymerization in unfilled systems. The critical processing parameter was the applied electric field and how it affected the diameter of the fiber jet. A TEM image of the PVOH with silica in solution is shown in Figure 3.14. This image of silica shows that it is still agglomerated in solution. The individual silica particles are not well dispersed. This leads to fiber imperfections after the solution has undergone the electrospinning process.

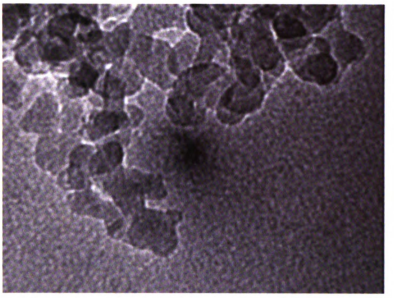

Figure 3.14 PVOH Silica solution. Image shows that silica is agglomerated in solution.

The mixing method had a significant impact on the dispersion of silica particles in the solution and ultimately in the electrospun fiber. A simple stir-bar mixing at maximum level for 3 hours did not provide enough energy to fully disperse the silica particles. Ideally the particles would have been 20 – 30 nm in size, with minimal agglomerations. Ultrasonication was necessary to improve the dispersion of the particles in solution. A Cole-Parmer 750 watt utrasonicator operated at power level of 20 for 3 hours with continuous stir-bar mixing was used as the ultrasonication treatment. Dispersion of silica particles in PVOH solution can be verified using surface tension and viscosity measurements. Improved dispersion increases the hydrogen bonding opportunities, which increase the surface tension and viscosity of the solutions. As an example, 10

wt% PVOH in water solution was prepared with a surface tension of 53 mN/m and a viscosity of 580 cps. The addition of 10 wt% silica (as a percentage of PVOH content) was mixed using a simple magnetic stir bar method. The stir bar mixed solution had a surface tension of 55 mN/m and a viscosity of 600 cps. To improve the dispersion, ultrasonication was used on the same solution (10wt% Silica) and the surface tension was 60 mN/m and the viscosity was 740 cps. It is clear that the addition of silica increases solution surface tension and viscosity and the increase can be amplified with the ultrasonication mixing method. A TEM image of the electrospun fiber is shown in Figure 3.15. The agglomerations are still present in the fiber after the electrospinning process.

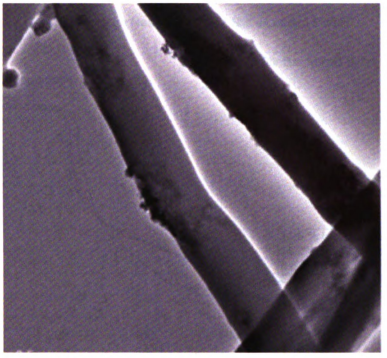

Figure 3.15 TEM image of electrospun PVOH with silica. Image shows that silica aggregations are still present in final fiber.

Thermal Properties

Thermal gravimetric analysis (Figure 3.16) showed the silica-modified fibers contained approximately 14 wt% residuals, as compared to 2 wt% residuals for the neat PVOH. It was concluded that ultrasonication alone might not be sufficient to obtain individual particles in solution. The use of a surfactant to limit aggregation may be required for this system.

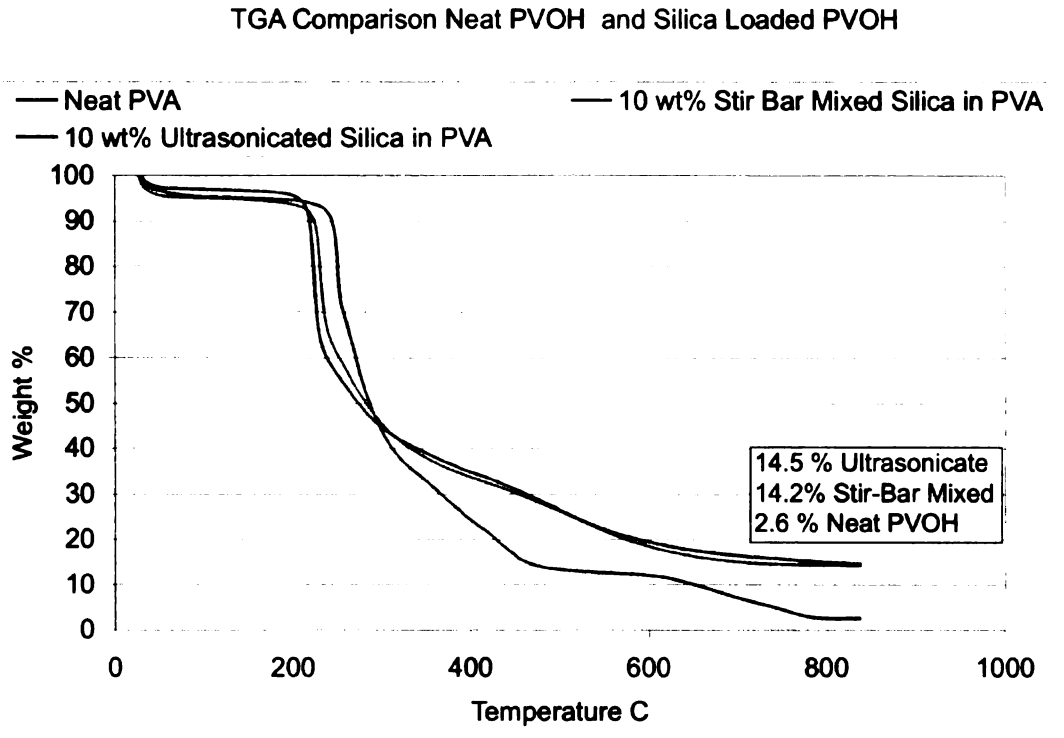

Figure 3.16 Thermal analysis of electrospun PVOH and silica loaded PVOH.

Mechanical Properties

Mechanical properties were measured to characterize the strength of the electrospun fiber mats relative to the bulk material. These values were generated from a collection of aligned fiber samples. The data produced was then compared to literature data.

A table of tensile strength and modulus is shown as Table 3.7. There is a wide variation in the values reported, due in part to the wide variation in fibers produced using the electrospinning process and variations in starting material.

In general, it is expected that increasing the molecular weight of the PVOH would improve the mechanical behavior. This was evident in the work of Lee et al, PVOH with a molecular weight of approximately 75,000 g/mole exhibited a tensile modulus and yield strength of 1.0 GPa and 16 MPa, respectively, and were increased to 1.2 GPa and 18 MPa for a PVOH with a molecular weight of 175,000 g/mole.[8] These two data points were produced from PVOH that was polymerized to form an atactic polymer. This was the first publication that measured the mechanical properties of electrospun PVOH fibers, so the test method may have resulted in values that were higher than actual values. All other tensile strength values reported in table 7 are similar to each other.

The molecular weight trend cannot be extended to the work of Jirawut, which showed that a similar molecular weight of 75,000 g/mole produced a tensile modulus and yield strength of 4.3 MPa and 35.3 MPa.[31] It should be noted that the fiber size in Jirawut's work is much larger than Lee et al., and the degree of hydrolysis was not listed for Lee et al, but was 98% in Jirawut's work. The tensile modulus values for electrospun fiber mats were significantly lower than the reported value of 1.9 GPa for solvent cast PVOH films.[32] The results showed a high degree of variation, since mechanical testing of electrospun materials is still a new procedure. The alignment method employed in the present study resulted in increased tensile modulus as compared to randomly oriented fiber networks. The tensile strength was comparable to other electrospun PVOH fiber materials as shown in Table 3.7.

Table 3.7 Mechanical properties of electrospun PVOH materials. MSU is a reference to this work.

PVOH Material [Ref]	Molecular Weight (g/mol)	Fiber Diameter (nm)	Tensile Strength (MPa)	Tensile Modulus (MPa)
Random Electrospun Fibers [5]	65,000	250	7.2	
Random Electrospun Fibers [31]	75,000	2000	4.3	35.3
Random Electrospun Fibers [33]	78,000	130	2.6	83
Random Electrospun Fibers [34]	74,800	270	16	1000
Random Electrospun Fibers [34]	176,000	280	18	1200
Aligned Electrospun Fibers [MSU]	65,000	300	5.2	225
Solvent Cast PVOH Film [32]	186,000	NA	83	1900

Tests were also performed to determine the effect of silica reinforcement, using two separate mixing methods, simple stir-bar mixing and ultrasonication. The dispersion was characterized by TEM microscopy as shown in Figure 3.15 above. In this micrograph, individual silica particles can be seen, but were still present in large groups. The agglomeration was much reduced as compared to the simple stir-bar mixing method. The stress strain behavior of the electrospun materials is shown in Figure 3.17.

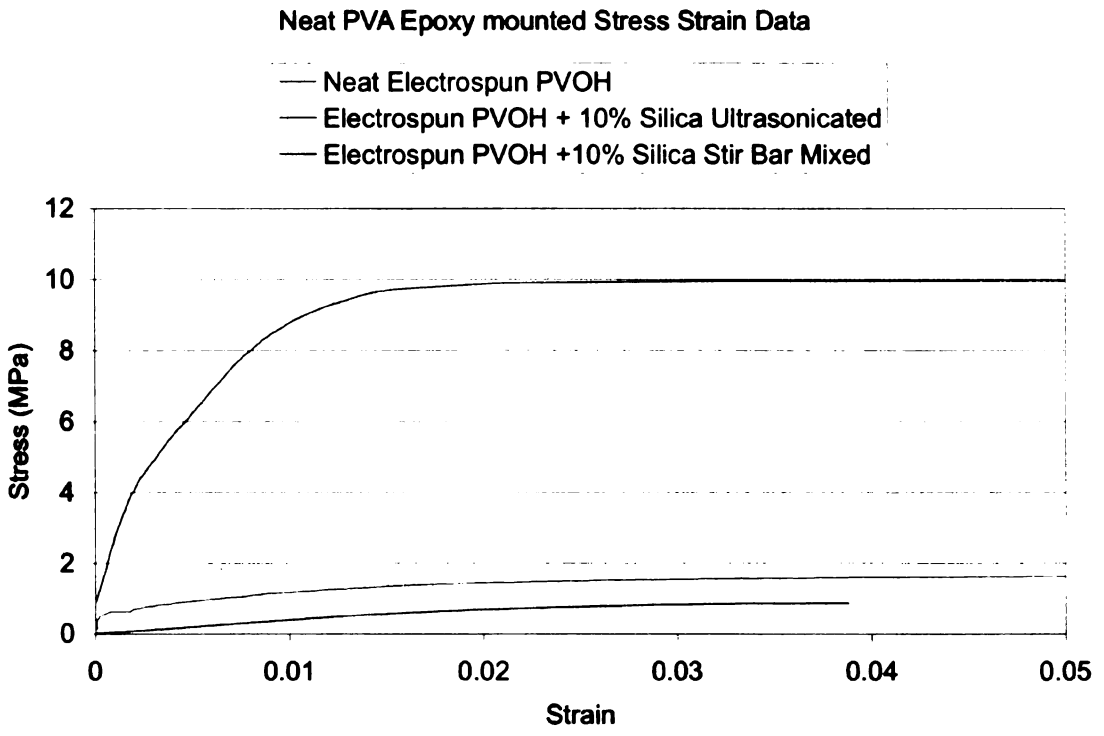

Figure 3.17 Stress strain chart for electrospun PVOH. Ultrasonic mixing of silica provides the best improvement.

The summary of the silica reinforcement is shown in Figure 3.18. It was clear that silica provided a reinforcement effect and this effect was maximized with the better stirring method of ultrasonication.

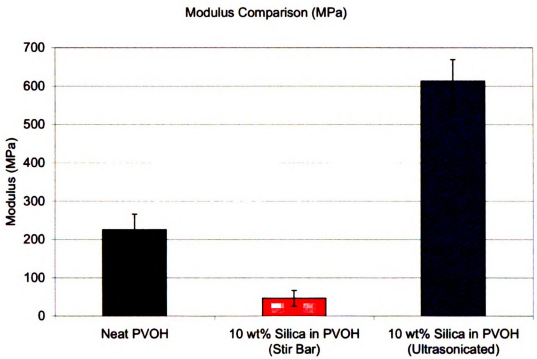

Figure 3.18 Modulus comparison for the electrospun PVOH and silica reinforced PVOH.

Electrospinning resulted in mechanical property values that were lower than expected, and since the dispersion of silica was relatively poor, the reinforcement effect was also limited. When perfectly dispersed and wetted in the matrix, filler particles can maximize the possible attachment points with the polymer, that is the apparent crosslink density of the matrix, and then maximize the hardness and modulus.[35] The surface interaction with the polymer matrix was critical with these fillers since their high-surface area could have lead to a very large number of attachment points with the matrix, and the tensile properties

were expected to increase with the filler volume fraction.[36] The addition of silica particles to the electrospinning solution has produced fibers with increased elastic forces. Specifically in this experiment; the addition of silica particles increased the hydrogen bonding opportunities, which allowed the material to recover better from deformation after stress has been released. The modulus data is shown in figure 18. It was determined that ultrasonication provided a more uniform dispersion of the silica particles, which is proved by improving the modulus. Ultrasonication improved the dispersion of the silica particles as compared to simple stir-bar mixing. The modulus data confirmed this effect.

Conclusions

Aligned nanofibers are essential for developing high strength nanocomposites. Aligned fibers with a narrow width distribution were obtained through careful control of the experimental parameters. The use of PVOH as a model compound has allowed the variables affecting the electrospinning process to be systematically varied and the process to be evaluated for consistency. Aligned fibers were demonstrated by harvesting the fibers that spanned the gap of a parallel electrode collector arranged with a positive voltage at the needle tip and negative voltage at the collector. Maintaining the collector at negative potential rather than at ground aids the fiber collection efficiency; fewer stray fibers are produced. Collecting the fibers across a void gap causes a high degree of alignment. The conductive strips of the collector enable the fibers to

be easily gathered for future processing and evaluation. As a result, the general trends discovered using this polymer system could be applied to other polymer solutions.

A summary of the most significant variables affecting the resultant fiber diameter is shown in Figure 3.19, using data from Table 3.6. The figure shows that concentration, also denoted by solution viscosity was the most dominant variable in this data set. Increases in concentration provided a positive effect by increasing fiber diameters significantly.

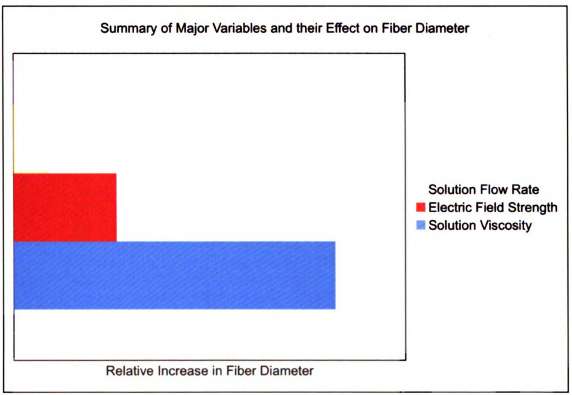

Figure 3.19 Relative increases in fiber diameter as a function of electrospinning variables.

Applied voltage was determined to give a positive response, which is counterintuitive. Theoretically, an increase in applied voltage, or electric field strength should reduce the fiber diameter. In this case, fiber diameters were found to increase. This can be explained by the large variability in the fiber diameters, as a result of a non-stable electrospinning process.

Increases in solution flow rate provided relatively low increases in fiber diameter. The actual diameters of the fibers increased slightly and since the

increased flow rate produced numerous fiber imperfections and agglomerations, the actual increase in diameters was exaggerated.

References

1. Koski, A.; Yim, K.; Shivkumar, S., Effect of molecular weight on fibrous PVA produced by electrospinning. *Materials Letters* **2004,** 58, (3-4), 493-497.

2. Zhang, C. X.; Yuan, X. Y.; Wu, L. L.; Han, Y.; Sheng, J., Study on morphology of electrospun poly(vinyl alcohol) mats. *European Polymer Journal* **2005,** 41, (3), 423-432.

3. Hodge, R. M.; Edward, G. H.; Simon, G. P., Water absorption and states of water in semicrystalline poly(vinyl alcohol) films. *Polymer* **1996,** 37, (8), 1371-1376.

4. Li, J. K.; Wang, N.; Wu, X. S., Poly(vinyl alcohol) nanoparticles prepared by freezing-thawing process for protein/peptide drug delivery. *Journal of Controlled Release* **1998,** 56, (1-3), 117-126.

5. Ding, B.; Kim, H. Y.; Lee, S. C.; Shao, C. L.; Lee, D. R.; Park, S. J.; Kwag, G. B.; Choi, K. J., Preparation and characterization of a nanoscale poly(vinyl alcohol) fiber aggregate produced by an electrospinning method. *Journal of Polymer Science Part B: Polymer Physics* **2002,** 40, (13), 1261-1268.

6. Mishra, R.; Rao, K. J., Electrical conductivity studies of poly(ethyleneoxide)-poly(vinylalcohol) blends. *Solid State Ionics* **1998,** 106, (1-2), 113-127.

7. Deitzel, J. M.; Kleinmeyer, J.; Harris, D.; Tan, N. C. B., The effect of processing variables on the morphology of electrospun nanofibers and textiles. *Polymer* **2001,** 42, (1), 261-272.

8. Lee, J. S.; Choi, K. H.; Do Ghim, H.; Kim, S. S.; Chun, D. H.; Kim, H. Y.; Lyoo, W. S., Role of molecular weight of atactic poly(vinyl alcohol) (PVA) in the structure and properties of PVA nanofabric prepared by electrospinning. *Journal of Applied Polymer Science* **2004,** 93, (4), 1638-1646.

9. Son, W. K.; Youk, J. H.; Lee, T. S.; Park, W. H., Effect of pH on electrospinning of poly(vinyl alcohol). *Materials Letters* **2005,** 59, (12), 1571-1575.

10. Hong, K. H., Preparation and properties of electrospun poly (vinyl alcohol)/silver fiber web as wound dressings. *Polymer Engineering and Science* **2007,** 47, (1), 43-49.

11. Shao, C. L.; Kim, H.; Gong, J.; Lee, D., A novel method for making silica nanofibres by using electrospun fibres of polyvinylalcohol/silica composite as precursor. *Nanotechnology* **2002,** 13, (5), 635-637.

12. Shao, C. L.; Kim, H. Y.; Gong, J.; Ding, B.; Lee, D. R.; Park, S. J., Fiber mats of poly(vinyl alcohol)/silica composite via electrospinning. *Materials Letters* **2003,** 57, (9-10), 1579-1584.

13. Teo, W. E.; Ramakrishna, S., A review on electrospinning design and nanofibre assemblies. *Nanotechnology* **2006,** 17, (14), R89-R106.

14. Image-Pro Software - MediaCybernetics - http://www.mediacy.com/.

15. Doshi, J.; Reneker, D. H., Electrospinning Process and Applications of Electrospun Fibers. *Journal of Electrostatics* **1995,** 35, (2-3), 151-160.

16. Park, J. Y.; Han, B. W.; Lee, I. H., Preparation of electrospun porous ethyl cellulose fiber by THF/DMAc binary solvent system. *Journal of Industrial and Engineering Chemistry* **2007,** 13, 1002-1008.

17. Baumgarten, P. K., Electrostatic spinning of acrylic microfibers. *Journal of Colloid and Interface Science* **1971,** 36, (1), 71-79.

18. Megelski, S.; Stephens, J. S.; Chase, D. B.; Rabolt, J. F., Micro- and nanostructured surface morphology on electrospun polymer fibers. *Macromolecules* **2002,** 35, (22), 8456-8466.

19. Buchko, C. J.; Chen, L. C.; Shen, Y.; Martin, D. C., Processing and microstructural characterization of porous biocompatible protein polymer thin films. *Polymer* **1999,** 40, (26), 7397-7407.

20. Jaeger, R.; Bergshoef, M. M.; Batlle, C. M. I.; Schonherr, H.; Vancso, G. J., Electrospinning of ultra-thin polymer fibers. *Macromolecular Symposia* **1998,** 127, 141-150.

21. Zhang, C. X.; Yuan, X. Y.; Wu, L. L.; Sheng, J., Properties of ultrafine fibrous poly(vinyl alcohol) membranes by electrospinning. *Acta Polymerica Sinica* **2006**, (2), 294-297.

22. Bergshoef, M. M.; Vancso, G. J., Transparent nanocomposites with ultrathin, electrospun nylon-4,6 fiber reinforcement. *Advanced Materials* **1999,** 11, (16), 1362-1365.

23. Xu, C. Y.; Inai, R.; Kotaki, M.; Ramakrishna, S., Aligned biodegradable nanofibrous structure: a potential scaffold for blood vessel engineering. *Biomaterials* **2004,** 25, (5), 877-886.

24. Li, D.; McCann, J. T.; Xia, Y. N., Uniaxial alignment of electrospun nanofibers. In *Polymeric Nanofibers*, Amer Chemical Soc: Washington, 2006; Vol. 918, pp 319-329.

25. Colman, P. C.; Yong Lak, J., Electrospinning of viscoelastic Boger fluids: Modeling and experiments. *Physics of Fluids* **2006,** 18, (5), 053102.

26. Zong, X. H.; Kim, K.; Fang, D. F.; Ran, S. F.; Hsiao, B. S.; Chu, B., Structure and process relationship of electrospun bioabsorbable nanofiber membranes. *Polymer* **2002,** 43, (16), 4403-4412.

27. Srinivasan, G.; Reneker, D. H., Structure and Morphology of Small-Diameter Electrospun Aramid Fibers. *Polymer International* **1995,** 36, (2), 195-201.

28. Zong, X. H.; Ran, S. F.; Fang, D. F.; Hsiao, B. S.; Chu, B., Control of structure, morphology and property in electrospun poly (glycolide-co-lactide) non-woven membranes via post-draw treatments. *Polymer* **2003,** 44, (17), 4959-4967.

29. Bognitzki, M.; Frese, T.; Wendorff, J. H.; Greiner, A., Submicrometer shaped polylactide fibers by electrospinning. *Abstracts of Papers of the American Chemical Society* **2000,** 219, U491-U491.

30. Lee, K. H.; Kim, H. Y.; La, Y. M.; Lee, D. R.; Sung, N. H., Influence of a mixing solvent with tetrahydrofuran and N,N-dimethylformamide on electrospun poly(vinyl chloride) nonwoven

mats. *Journal of Polymer Science Part B-Polymer Physics* **2002,** 40, (19), 2259-2268.

31. Jirawut, J.; Ratana, R.; Pitt, S., Fabrication of α-chitin whisker-reinforced poly(vinyl alcohol) nanocomposite nanofibres by electrospinning. *Nanotechnology* **2006**, (17), 4519.

32. Zhang, X.; Liu, T.; Sreekumar, T. V.; Kumar, S.; Moore, V. C.; Hauge, R. H.; Smalley, R. E., Poly(vinyl alcohol)/SWNT Composite Film. *Nano Lett.* **2003,** 3, (9), 1285-1288.

33. Wang, X.; Chen, X.; Yoon, K.; Fang, D.; Hsiao, B. S.; Chu, B., High Flux Filtration Medium Based on Nanofibrous Substrate with Hydrophilic Nanocomposite Coating. *Environ. Sci. Technol.* **2005,** 39, (19), 7684-7691.

34. Lee, J. S.; Choi, K. H.; Do Ghim, H.; Kim, S. S.; Chun, D. H.; Kim, H. Y.; Lyoo, W. S., Role of molecular weight of atactic poly(vinyl alcohol) (PVA) in the structure and properties of PVA nanofabric prepared by electrospinning. *Journal of Applied Polymer Science* **2004,** 93, (4), 1638-1646.

35. Westermann, S.; Kreitschmann, M.; Pyckhout-Hintzen, W.; Richter, D.; Straube, E.; Farago, B.; Goerigk, G., Matrix Chain Deformation in Reinforced Networks: a SANS Approach. *Macromolecules* **1999,** 32, (18), 5793-5802.

36. Guyard, A.; Persello, J.; Boisvert, J-P.; Cabane, B., Relationship between the polymer/silica interaction and properties of silica composite materials. *Journal of Polymer Science Part B: Polymer Physics* **2006,** 44, (7), 1134-1146.

CHAPTER 4

ELECTROSPINNING CELLULOSE NITRATE FOR BIOSENSOR APPLICATIONS

Abstract

Cellulose is the most abundant organic material on the surface of earth. It is the main constituent of paper and plant cell walls and is a renewable resource. Cellulose consists of linear glucose polymer chains, which form hydrogen bonded supramolecular structures. Cellulose is not soluble in water and most organic solvents but functionalized cellulose such as cellulose nitrate is soluble in many common organic solvents and is important for many industries with applications in packaging, coatings, adhesives, biochemistry and sensors.

Electrospinning is a method of producing nanoscale fibers from a polymer solution using high voltage electric forces. This technique is capable of producing fibers in the nanometer to micron diameter range. Electrospinning has been extensively investigated as a simple method to prepare fibers from polymer solutions or melts. The electrospinning process allows for alignment and patterning of the fibers through careful control of the processing parameters,

choice of suitable collector materials, and geometry. Electrospun fibers can be utilized in various applications including biosensors, filtration media, biomedical devices, and composites. The ability to control the alignment of fibers is essential for producing high flow membranes with a large surface area to volume ratio, which is crucial for biosensor applications

Cellulose nitrate has been electrospun into fibers with controllable diameters in the range of 100 to 1,000 nm. Collecting fibers with controllable size and orientation is essential for preparing biosensor devices. A unique rotating collector and a stationary parallel electrode void gap collector have been designed for collection of the fibers. The controllable size and alignment allow for properties such as pore volume, surface area and capillary flow to be managed.

Neat electrospun cellulose nitrate scaffolds were found to be hydrophobic in nature and unsuitable for capillary flow biosensor devices. This limitation was overcome by plasma treating the surface of the fibers. The surface chemistry modification allowed for improvements in capillary flow by altering the surface functional groups to ones that were more hydrophilic. This technique is ideally suited to electrospun scaffolds because, unlike other physical and chemical modification techniques, it did not compromise the bulk architecture of the material. Plasma treatments of electrospun cellulose nitrate scaffolds resulted in a significant increase in wettability due to the incorporation of oxygen-containing groups (hydroxyls, carbonyls, carboxyls), which were detected by XPS and FTIR.

The thermal, electrical, and mechanical properties of the electrospun fiber mats were examined. Thermal analysis proved that solvents were not present in the electrospun fiber mats and the onset of thermal degradation was 205 °C. Electrical characterization showed that the neat fibers were insulating, as expected. The mechanical behavior of the fiber mats was lower than films, due to the large amount of void spaces in the fiber mats, with tensile modulus values in the 10 – 13 MPa range.

Introduction

Cellulose is the most common organic polymer, and is considered an almost inexhaustible source of raw material for environmentally friendly and biocompatible products.[1] Many applications are available for cellulose, including the production of cellulose composites with synthetic and bio-based polymers.

Cellulose nitrate is prepared from cellulose through a nitration reaction involving nitric and sulfuric acid. Cellulose nitrate esters, also known as nitrocellulose, are commercially available with various degrees of esterification up to the maximum substitution degree of 3 nitrate ester groups per monomer (14% nitrogen). The degree of esterification influences its solubility properties. Cellulose nitrate can be dissolved in ether, aldehydes and some alcohols. Solutions of cellulose nitrate are commonly referred to as collodion. Collodion has been used extensively as a wound dressing material and a carrier for topical medications. Cellulose nitrate is also commonly used for immobilizing nucleic

acids in biochemistry applications. Cellulose nitrate also has the ability to immobilize proteins for applications in Western blots, due to its non-specific affinity for amino acids. Cellulose nitrate is also widely used in diagnostic tests where antigen-antibody binding occurs, such as pregnancy test and Albumin tests.

Background

Cellulose acetate has been the most widely researched and electrospun cellulose derivative.[2] The cellulose acetate can be deacetylated, resulting in a regenerated cellulose membrane. Lu et al., prepared cellulose acetate (CA) fibers using the electrospinning technique with acetone, acetic acid and dimethylacetamide (DMAC) as the solvents.[2] The source of cellulose for these experiments was cellulose acetate with a DS of 2.45 and a number average molecular weight of 30,000 Da (obtained from Aldrich). CA concentrations were varied from 10 wt% to 25 wt% depending on the solvent. Several mixtures of DMAC with either acetone or acetic acid produced suitable solvent systems for electrospinning CA. Fifteen percent CA in acetone:DMAC mixtures at ratios between 2:1 and 10:1 could be continuously electrospun into fibrous membranes. The highest concentration to yield homogeneous fibers was 20 wt% CA in a 2:1 ratio of acetone to DMAC. The 2:1 acetone: DMAC mixture was the most versatile mixing ratio because it allowed continuous electrospinning of CA solutions at concentrations between 12.5 and 20 wt%. The 12.5 and 20 wt% CA in 2:1 acetone:DMAC corresponded to a viscosity in the range of 1.2 to 10.2

poise and surface tension of 26 dyne/cm. Viscosities lower than 1.2 poise lead to beaded fiber formation, whereas a viscosity higher than 10.2 poise caused instability in electrospinning. Smooth fibers of uniform diameters from 100 nm to over 1,000 nm were generated using solutions with the appropriate viscosity. Fiber sizes were observed to decrease with decreasing CA concentrations, which was expected.

Ma et al. prepared cellulose acetate solutions suitable for electrospinning using a mixed solvent of acetone / dimethylformamide / trifluoroethylene (3/1/1).[3] The cellulose acetate source was from Fluka, M_r = 29,000 and 40% acetyl groups. The electrospinning solution was approximately 16 wt% CA in the mixed solvent. Fibers were formed in the range of 200 nm to 1,000 nm. The fiber network was subjected to a heat treatment, and then the resultant fiber network was characterized. It was determined that the tensile strength of the membranes was 7.6 Mpa. These membranes consisted of non-aligned fibers with a large diameter range and variation.

Son et al. electrospun ultrafine cellulose acetate fibers with various concentrations of silver nitrate ($AgNO_3$) for antimicrobial activity.[4] A 10 wt% CA solution, with an acetyl content of 40% and molecular weight of 30,000 in acetone water (80:20) was used as a baseline solution with 0.05, 0.3 and 0.5 wt% $AgNO_3$ added for functionalization. The addition of $AgNO_3$ increased the charge density in CA solutions and thus stronger elongational forces were imposed on the ejected jets under the electrical field, resulting in substantially

straighter and thinner CA fibers. The resultant fibers were 600 nm to 1,600 nm in diameter.

Ethyl cellulose (EC) has been successfully electrospun by Wu et al. using a mixed solvent. EC with Mn=72,000 and a substituted degree of ethyl of 2.2 was dissolved in various ratios of tetrahydrofuran (THF) and DMAC.[5] As the content of THF is increased in the solvent system, the fiber diameters increased. The increase in fiber diameter was due to an increase in the solution viscosity. In general concentrations from 7 up to 27 wt% of EC can be prepared and these solutions produced fibers that were 200 nm to 3,000 nm.

Hydroxypropyl cellulose (HPC) fibers have been electrospun by Shukla et al. from solutions of 2-propanol and ethanol.[6] Two separate spinning solutions were prepared, 15 wt% HPC in 2- propanol yielded homogeneous fibers without bead on string morphology, while the 15 wt% HPC in ethanol showed larger fiber variations including bead on string morphology. The purpose of these fibers is to provide a template for constructing tin oxide fibers. The fiber diameters ranged from submicron (>100 nm) to true nanofibers (< 100 nm).

In this research work cellulose nitrate fibers have been produced with diameters ranging from 100 nm to 1,000 nm. Highly aligned fibers are obtained using a patterned stationary collector, and partially aligned fiber networks can be obtained using a rotating drum collector. Literature suggests that high speed (>10 m/s) rotating collectors, gas flow, and electrical or mechanical shielding can also be used to increase alignment of fiber networks, but similar experiments were not attempted.[7] The rotating collector works well to obtain a larger yield of

aligned fibers in a shorter amount of time,[8] but the rotational speed must be fast enough to compare with the speed of the jet.[9] The current device provides fiber mats with 65% of the fibers within 10 degrees of the desired orientation. An aligned sample must consist of at least 90% of the fibers within 10 degrees of the desired orientation. A stationary collector with parallel electrodes can also be used to easily harvest aligned fibers, but is limited to a small area of coverage.[10] The stationary collector can provide alignment with greater than 90% fibers within 10 degrees of the desired orientation. A comparison of cellulose nitrate fiber morphology obtained using the stationary collector and rotating drum collector is shown as Figure 4.1. Typically a 4-hour collection time was used on the stationary collector, while the same fiber mat thickness could be produced in 2 hours on the rotating drum collector. This was most likely due to the fact that stray fibers were eliminated using the rotating drum collector. Stray fibers can collect on the electrode surface or other grounded objects near the electrospinning setup. Since the entire drum surface was the collector, there were virtually no stray fibers. Using the parallel electrode device, the top and bottom electrodes collect a large amount of material that is considered waste.

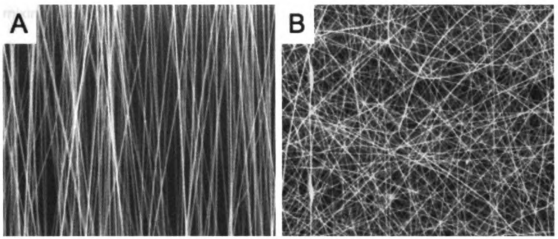

Figure 4.1 ESEM of electrospun cellulose nitrate comparing the alignment capabilities. A) Fibers were collected using a stationary parallel electrode collector design. B) Fibers were collected using a rotating drum.

Experimental

Materials

Cellulose nitrate was purchased from Scholle Corporation (College Park, GA). Cellulose nitrate had a nitrogen content of 12% which corresponds to a degree of substitution of 2.25. Solutions of cellulose nitrate were prepared in two different solvent systems: a 70:30 (wt:wt) mixture of ethanol : acetone and a 60:40 (wt:wt) mixture of tetrahydrofuran : N,N-dimethylformamide. All solvents were purchased from Sigma Aldrich (St. Louis, MO). Several different solutions were prepared by dissolving cellulose nitrate in each of the solvent systems by magnetic stir bar

mixing for 12 hours. The electrospinning unit was purchased from Kato – Tech Co (Kyoto, Japan) and was capable of 40 kV, syringe pump rates of 0.03 to 3.0 cm/min, rotating drum speeds of 0.01 to 9.0 m/min and collection times up to 4 hours.

Morphology

The cellulose nitrate was examined using Environmental Scanning Electron Microscopy (ESEM), and ImagePro image analysis software.[11] An Electroscan 2020 ESEM was used to obtain sample images. The samples were first mounted on ESEM pedestals, then sputter coated with gold. The samples were imaged at 15 kV from 500 to 10,000 times magnification to obtain morphological and size distribution information.

Field emission scanning electron microscopy (FESEM) was also used to aid in morphological characterization of electrospun cellulose nitrate. A JEOL 6300F FESEM was utilized to obtain images up to 100,000X magnification.

Surface Chemistry Properties

Contact angle measurements

Water contact angles were measured on electrospun fiber surfaces using a Kruss DSA10. The water droplet was placed on the surface of the material and an immediate image was captured. The captured image was used to calculate the contact angle. The samples were measured ten times and averaged. Samples were run as processed and after a plasma treatment procedure.

X-ray Photoelectron Spectroscopy

A Perkin Elmer Phi 5400 ESCA system was used for experimentation with a magnesium Kα X-ray source. Samples were analyzed at pressures between 10^{-9} and 10^{-8} torr with a pass energy of 29.35 eV and a take-off angle of 45°. The spot size was roughly 250 μm^2. Atomic concentrations were determined using previously determined sensitivity factors. All peaks were referenced to the signature C1s peak for adventitious carbon at 284.6 eV.

Plasma Treatment

Plasma treatments were carried out in Plasma Sciences system with a gas pressure of 0.29 torr and at 300W. The samples were presented for plasma treatment in the form of electrospun fiber bundles mounted on polycarbonate window frames on the outer surface to aid in handling. The samples were approximately 1 in x 1 in. These samples were laid flat in the plasma reactor. Plasma treatments were performed for 0, 90 and 360 seconds

Fourier Transform Infrared Spectroscopy

A Perkin Elmer Spectrum One FTIR was used to analyze the bulk chemistry of the electrospun cellulose nitrate materials. The bulk chemistry was important to analyze to ensure high quality samples were being produced without transformations or impurities. The FTIR spectra obtained were compared to neat cellulose nitrate materials.

Thermal Properties – Thermal Gravimetric Analysis

A TA Instruments 2950 was used to determine the amount of residual solvent in the electrospun fiber mat, and the thermal degradation temperature of the cellulose nitrate fiber bundle. The electrospun fibers will be used at room temperature, however thermal characterization is important to understand for heat assisted drying steps that may be necessary.

Electrical Properties – Electrical Impedance Spectroscopy

Electrical Impedance Spectroscopy was used to verify that the electrospun cellulose nitrate fiber bundles were non-conductive. A Gamry Instruments 300 series electrical impedance spectrometer was used to determine the resistance of electrospun samples at 1 Hz.

Mechanical Properties – Dynamic Mechanical Analysis

A TA instruments Q800 Dynamic Mechanical Analyzer (DMA) was used to evaluate the mechanical properties of the electrospun materials. The goal was to determine the modulus for various fiber sizes, which correspond to different fiber packing densities of electrospun cellulose nitrate. As the fiber packing density is increased, the tensile modulus is expected to increase.

Results and Discussion

Morphology

The concentration of cellulose nitrate in solution was found to be the most dominant factor controlling fiber size. Increasing the concentration resulted in increased fiber diameters. This is due to increased viscosity causing more entanglements leading to a structure that is more resistant to elongation under the external whipping and stretching forces.

Microscopic images were viewed perpendicular to the fiber mat for easy alignment characterization and fiber size estimation. It was assumed that the fibers were circular in cross section.[10] A typical FESEM micrograph is shown in Figure 4.2. The FESEM was used for high magnification images to accurately determine the fiber diameters.

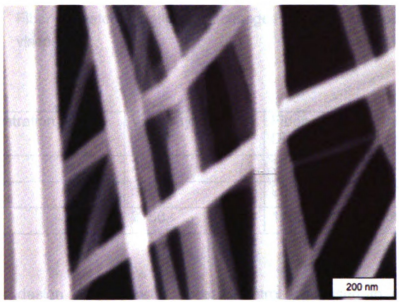

Figure 4.2 FESEM image showing that single fiber sizes are available less than 100 nm in diameter.

The electrospinning parameters were 8 cm separation distance, 0.02 mm/min syringe pump rate, a stationary collector and 30-minute collection time. The images verified that increasing the solution viscosity lead to larger diameter fibers. A 6 wt% (300 cps) cellulose nitrate solution produced fibers with an average diameter of 330 nm, while fibers electrospun from 8 wt% (500 cps) solution were on average 900 nm in diameter and from a 10 wt% (2800 cps) solution were approximately 1200 nm as shown in Table 4.1. The alignment is in terms of percentage within 10 degrees of the average angle when observed using electron microscopy.

Table 4.1 Fiber diameter and alignment changes as a result of solution viscosity.

Concentration (wt%)	Viscosity (cps)	Fiber Diameter (nm)	Alignment (%)
6	280	350 ± 50	82
8	510	900 ± 85	51
10	2750	1200 ± 80	68

Collector design coupled with process control was used to control fiber patterns.[12] Figure 4.3 displays an aligned cross-patterned design using a perpendicular electrode array requiring rotating the collected fiber mat 90 ° after a fixed amount of time. The advantage to collecting fibers in this fashion was that the procedure provided a fiber network structure with adjustable porosity. The layered morphology can be controlled by collecting fibers for longer times in each direction to build up fiber layer thickness.

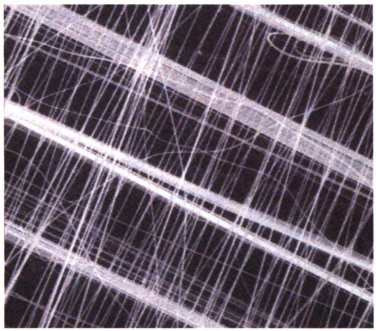

Figure 4.3 ESEM image of patterned electrospun fibers using a stationary collector.

Effect of Electric Field Strength

The electric field strength can be controlled by altering the separation distance, the distance between the needle tip and collector, or by adjusting the applied voltage. Typically the electric field strength was maintained near 1 kV/cm. Figure 4.4 shows the effect of varying the electric field strength while maintaining a constant applied voltage of 10 kV. A slight negative charge (1 kV) was maintained at the collector to reduce to residual charging phenomenon and promote thicker electrospun fiber mats with fewer stray fibers. In this experiment, the solution was 6 wt% cellulose nitrate in a 70 : 30 ethanol : acetone mixed

solvent system. The solution flow rate was maintained at 0.5 ml/h through a 22 gauge needle and collection times were 2 minutes. Fibers were harvested from a parallel void gap electrode with a 2.5 cm distance between top and bottom electrode.

Figure 4.4 shows that there was a range of electric field strengths that could be used to produce homogenous aligned fiber networks. As the electric field strength values increased, there was a slight decrease in fiber diameter, but the fiber diameter trend is not statistically significant. The electric field strength was determined to be an ineffective means to control the fiber diameter.

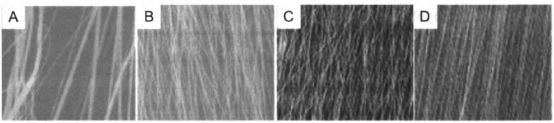

Figure 4.4 ESEM of electric field strength variations, A) 12 cm (0.9 kV/cm), B) 10 cm (1.1 kV/cm), C) 8 cm (1.4 kV/cm) and D) 6 cm (1.8 kV/cm).

Electric field strength can be used to alter the fiber alignment. At longer separation distances, the instability region was more prominent and resulted in a lower number of aligned fibers. As shown in Table 4.2, the alignment improved from 38% at 12 cm to nearly 90% at 6 cm. The alignment is defined as the percentage of fibers that are within 10 degrees of the average fiber angle as determined using ESEM images and ImagePro image analysis software. The

general trend of improved alignment as the separation distance was decreased was verified. Limiting the distance between source and collector and thereby decreasing the instability improved the bulk fiber alignment. The higher electric field strength would likely increase the polymer chain orientation on the molecular level since it provides higher elongation forces.[13]

Table 4.2 The effect of separation distance on the fiber diameter and alignment.

Sample	Separation Distance (cm)	Electric Field Strength (kV/cm)	Fiber Diameter (nm)	Alignment (%) within 10 degrees)
A	12	0.9	1405 ± 950	38
B	10	1.1	400 ± 110	81
C	8	1.4	340 ± 85	82
D	6	1.8	350 ± 10	90

Effect of Solution Viscosity on Morphology

As the viscosity increased, the polymer chains became more entangled and were more resistant to the stretching phenomenon common in the electrospinning process. This resulted in fibers with larger diameters. There was also more charge repulsion in the larger fibers, which lead to more randomly distributed fiber networks. Figure 4.5 shows the ESEM images for 6,8 and 10 wt% cellulose nitrate dissolved in a mixed solvent system of 60:40 THF:DMF.

The electric field strength was 1.8 kV/cm and the flow rate was 1.0 ml/h. Figure 4.5 shows that increasing the viscosity of the solution increased the fiber diameter and also decreased the alignment of the fiber mat.

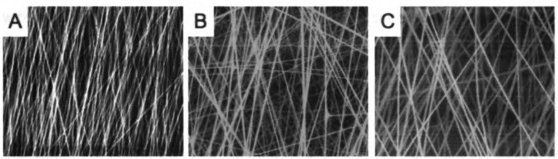

Figure 4.5 ESEM images of 6,8 and 10 wt% cellulose nitrate electrospun fibers.

Table 4.1 shows that when the viscosity is increased, the fiber diameter increases. There is also a trend of increasing randomness, as the fiber diameter gets larger. The fiber diameter trend was modeled with the Helgeson model (Chapter 2). This model provided a reasonable prediction for the resultant fiber diameters often with errors less than 50%.

Effect of Solvent Volatility on Morphology

Cellulose nitrate is shipped in 100% acetone and although this can be electrospun directly, the process is discontinuous, resulting in many fiber mat deformations. This is due to the rapid evaporation of acetone. Using acetone as

the only solvent results in clogged needle tips and makes the electrospinning process difficult to control. Ethanol was added to acetone to reduce the volatility of the solvent system. Ethanol cannot be used as the only solvent for cellulose nitrate due to solubility limitations. It was determined that a 70 wt% ethanol, 30 wt% acetone solvent system provided the most controllable process. This solvent was named 70:30 Ethanol:Acetone based on the weight composition of each solvent. Figure 4.6 shows the difference in morphology when using ethanol and acetone blends. The processing conditions were not optimized in this study; the purpose was to determine what solvent blend ratio provided the most uniform fiber diameters. As Figure 4.6 shows, 100% acetone is too volatile and results in agglomerated fibers and clogged needle tips. 70:30 Ethanol:Acetone provided the longest time between clogged needles, greater than 6 hours. As Figure 4.6 and Table 4.4 show, the 50:50 Ethanol:Acetone appears to provide the least fiber imperfections, but it still resulted in clogged needle tips. The 70:30 blends were optimized in other experiments to yield fiber mats with little or no inhomogeneities. The processing conditions were 10 wt% cellulose nitrate, 8 kV applied voltage, 8 cm separation distance (1.0 kV/cm) and a 2.0 ml/h flow rate.

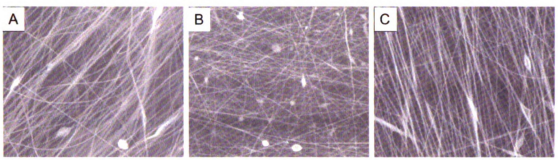

Figure 4.6 The effect of solvent volatility on fiber morphology. Variation in solvent vapor pressure results in various volatility A) 100% Acetone, B) 70:30 Ethanol:Acetone, C) 50:50 Ethanol:Acetone.

The reduction in vapor pressure generally reduced the fiber diameter as shown in Table 4.3. The goal of altering the solvent vapor pressure was to improve the electrospinning process, making it continuous, without interruption by eliminating the problem of clogged needle tips. It was determined that a 70:30 ethanol:acetone blended solvent provided the longest time between needle clogs, while still producing homogenous fiber networks.

Table 4.3 Solvent volatility effect on fiber diameter and alignment

Sample	Solvents	Vapor Pressure (mm Hg)	Fiber Diameter (nm)	Alignment (% within 10 degrees)
A	Acetone	230	350 ± 50	54
B	70:30 Ethanol:Acetone	145	160 ± 140	21
C	50:50 Ethanol:Acetone	110	220 ± 120	72

Surface Properties

Plasma Treatment

The surfaces of the electrospun cellulose nitrate fibers are composed of alkyl (C-C) and ether (C-O-C) functional groups. Plasma treatments are necessary to increase the hydrophilic nature fibers by forming groups such as carbonyls (C=O), and carboxyl (COOH) functional groups. The nitrogen containing functional groups are also affected by plasma treatment; the surface nitrate (NO3) functional groups are converted to nitroso (N=O) and amine (N-N). The exact functional groups cannot be identified from XPS alone. The changes to the fibers from the plasma treatment allowed for capillary flow to be realized.

Plasma chemistry, even of a simple gas such as oxygen, is extremely complex. When plasma contacts an organic surface, the number of possible reactions that may occur is very large. There are two main reactions that occur: (1) etching reactions that result in the removal of the surface material; (2) reactions that result in modification of the surface chemistry. Plasma treatment was chosen over solution-based methods due to fiber mat strength limitations. It was found that repeated washing cycles damaged the morphology of the fiber mat.

Etching results from either energy deposition from the plasma into the polymer surface, or from reactions between the polymer surface and the reactive

species in the plasma. There is sufficient energy in glow-discharge plasma to cause bond breakage, if enough of this energy is deposited from the plasma into the surface, bond breakage will occur.

Energy transfer from the plasma to the cellulose nitrate surface occurs by two mechanisms: (1) direct energy transfer, from the inelastic collisions of high-energy particles with the surface; (2) radiative energy transfer. The reactions of cellulose nitrates in argon plasmas have been used since argon cannot chemically react with the surface like oxygen can. The effect of energy transfer without the complication of chemical reactions by reactive species in the plasma was studied. Argon plasma treatments were shown to induce considerable changes in the surface chemistry of cellulose nitrate.[14] However, little or no weight loss in the cellulose nitrates was observed. It can therefore be assumed that at about 100 W, energy transfer from the glow discharge plasmas was not primarily responsible for etching; this was most likely to have arisen from oxidation at the surface, resulting in the formation of small volatile fragments that were pumped away in the plasma gas. There were significant weight changes, or etching when using oxygen plasma.[15]

Contact Angle

Cellulose nitrate films and fibers were subjected to contact angle measurements in order to measure their surface energy and change in surface energy with surface treatment. Water based solutions must be able to wet the

fiber surface in order to achieve capillary flow in the biosensor device. A contact angle less than 90 ° is required for wetting. As the contact angle decreases, the wetting increases and capillary flow is generally increased.

The contact angles for the cellulose nitrate film and electrospun cellulose nitrate fibers from both glass and plastic lab ware is shown in Table 4.4. The film was cast in a glass Petri dish directly from the stock solution and the electrospun fibers were prepared using either a plastic syringe assembly or glass syringe assembly. It was determined that using plastic syringe produced contact angles higher than expected as a result of plastic contaminants being extracted and mixing with the cellulose nitrate solutions. Plastic syringes were replaced with glass to eliminate the contamination effect. The neat electrospun cellulose nitrate contact angle was still much larger than 90 °, this effect can be explained using the Cassie equation and an areal density parameter.

For a Cassie drop, the contact angle is an average between the value of air (180°) and on the solid (θ), which can be calculated for geometric textures such as posts, fibers or dots.[16] Denoting φ_s as the fraction of solid in contact with the liquid (φ_s is dimensionless, but smaller than unity), we find:

$$\cos\theta^* = -1 + \phi_s(1 + \cos\theta) \qquad \text{(Equation 4.1)}$$

Cellulose nitrate solvent cast films exhibited a contact angle of 65°, which is the value used for θ. Examining the electrospun fiber morphology using ESEM and ImagePro image analysis (Figure 4.7), the fraction of solid in contact with the

water droplet (ϕ_s) was determined. Using ImagePro software, the images were first contrast normalized using the best fit contrast enhancement procedure, which assigns the bottom 3% of the pixels to the shadow value (0) and the top 3% to the highlight value (255). The remaining pixels are evenly distributed, providing the contrast enhancement. Finally a threshold value was set (128 for plastic and 102 for glass) to yield the images shown in Figure 4.7. These images represent the areas of the fiber mats expected to make contact with the water droplet in the contact angle experiments. The plastic syringe produced a more dense fiber mat as compared to the glass syringe, with all other experimental parameters being held constant. The plastic syringe produced a fiber coverage φ_s of 0.37, which means that 37% of the area under the water droplet during contact angle analysis is solid cellulose nitrate fiber. Using a glass syringe yielded φ_s of 0.32. Substituting these values Equation 4.1 yielded an apparent contact angle of 118° for the plastic syringe and 122° for the glass syringe. These values were relatively close to the experimentally measured data (Table 4.4). The plastic syringe measured value was for electrospun cellulose nitrate fiber mats. This was consistent with values determined experimentally. Similar results have been observed in the literature using nylon as the material.

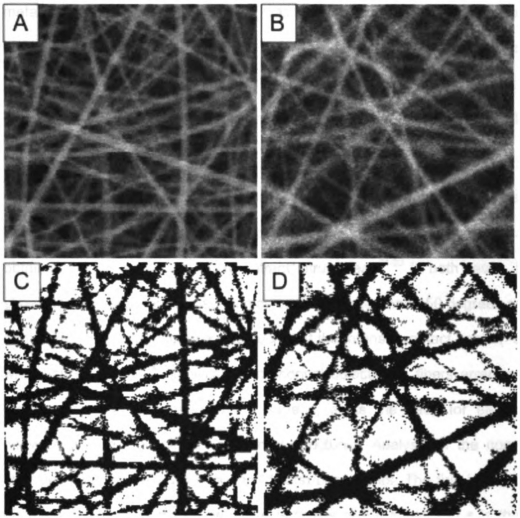

Figure 4.7 Electrospun cellulose nitrate shows an open fiber mat with air occupying the interfibrillar spaces. A) Fibers electrospun from plastic syringe, B) glass syringe C) image (A) after contrast enhancement and threshold screening, D) image (B) after processing.

According to Rutledge et al, electrospun nylon fiber mats exhibited an initial contact angle of 135°. This value was significantly higher than the contact angle of 69° measured for a smooth solvent cast nylon film.[17] This was the result of the

metastable Cassie state, in which air was trapped in the interfibrillar spaces.[18] It has been suggested that roughness promotes the trapping of air between the water droplet and fiber mat, which in turn prevents the water droplet from penetrating the mat.[19] This corresponds with the data obtained for the cellulose nitrate system.

Superhydrophobicity obtained from an intrinsically hydrophilic material has been proposed to be the consequence of a robust metastable state that can be obtained with "overhang" [20] or "re-entrant" structures. [21-23] In both cases, it was shown that the apparent contact angles could be larger than 150 degrees as long as the structure of the surface was such that the intrinsic contact angle (>0 deg) was realized locally.[24] Significantly, cylindrical objects like fibers arranged with their axes within the plane of the surface, as is the case for electrospun nonwovens, are examples of re-entrant structures. Analysis of the nonwoven fiber geometry reveals two important design parameters. The first is the scaled distance between fibers, s/d, where d is radius of the fibers and s is the half-distance between fibers, as shown previously[25]; this parameter is indicative of the areal density of fibers. Large (hydrophobic) contact angles are realized when the electrospun fiber mat has s/d >> 1. From this, the apparent contact angle, θ^*, can be calculated using Equation 4.2, where x=d/s.

$$\cos\theta^* = \frac{x(\pi-\theta)}{x+1}\cos\theta + \frac{x\sin\theta}{x+1} - 1 \qquad \text{(Equation 4.2)}$$

Figure 4.8 shows how these theoretical apparent contact angles for electrospun cellulose nitrate cylinders vary with *d/s*. The contact angle decreases as the separation distance decreases while the fiber diameter is fixed. Figure 4.8 also shows that the droplet sitting on spheres has a higher contact angle than that sitting on cylinders of comparable radius. Both of the predictions are consistent with the experimental data.[25] No attempt is made here to fit the data precisely since the random orientation of fibers in the real materials, as well as the three-dimensional nature of the mats imaged, complicates the determination of an appropriate value for the separation distance between fibers.

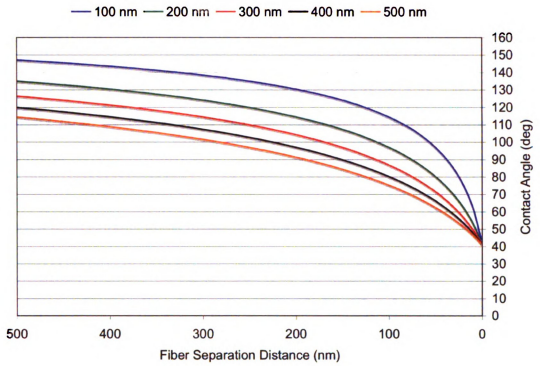

Figure 4.8 Apparent contact angles for electrospun fibers with various diameters and fiber spacing.

The knowledge obtained from ESEM images can be coupled with changes in processing conditions to produce fiber mats with improved wettability. The goal is to use Figure 4.8 as a guide in fiber preparation. A tightly packed network of fibers will reduce the water contact angle, but may have porosity limitations. The Cassie equation can be used as a general guide to estimate the contact angle of the various fiber morphologies, but in the case of the electrospun cellulose nitrate fibers, there may be differences in surface chemistries that would limit its use.

Surface treatments can also be used to further enhance the capillary flow properties.

To reduce the contact angle to an acceptable level that would allow for capillary flow, the fibrous mats were subjected to an oxygen plasma surface treatment.

Table 4.4 Contact angle measurements

Sample Name	Contact Angle
Solvent Cast Cellulose Nitrate Film (θ)	65
Plastic Electrospun Cellulose Nitrate Fibers	131
Glass Electrospun Cellulose Nitrate Fibers	110
Plasma Treated Plastic Electrospun Cellulose Nitrate Fibers	64
Plasma Treated Glass Electrospun Cellulose Nitrate Fibers	12
Solvent Cast Nylon Film [Rutledge]	69
Electrospun Nylon Fibers [Rutledge]	135

The variation in contact angle after plasma treatment can be explained by differences in the surface chemistry of the materials. Aligned electrospun cellulose nitrate fiber mats were exposed to radio frequency (RF) generated O_2 plasma (13.6 MHz, 120 W, 250 mTorr O_2 for 90s). The plasma treatment's effect on contact angle is shown in Figure 4.9. This drastic difference in contact angle was explained by the oxidation of hydroxyl groups on the cellulose backbone to form carboxylate and/or carbonyl functional groups. This transformation did not alter the relative concentrations of atoms present at the surface, but it did alter the type of bonding, which will be explained further in the XPS results section.

Table 4.5 shows that treating both sides of the electrospun fiber mat had little difference on the resultant water contact angle. This data was obtained using the plastic lab ware.

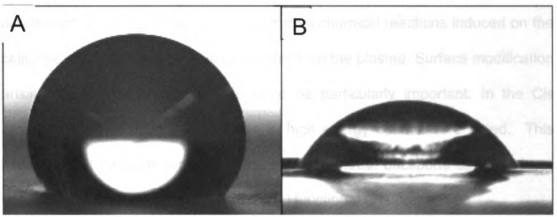

Figure 4.9 Comparison of water on the surface of electrospun cellulose nitrate fibers. The non-wetting behavior is shown in A) neat electrospun fibers and after plasma treatment B) the water droplet wets the surface.

Table 4.5 Water contact angle data showing the effect of plasma treatment

Sample Name	Average Contact Angle (deg)	Standard Deviation
Neat Electrospun CN	131	2.2
Electrospun CN Plasma treated one side (90s)	64.2	13.2
Electrospun CN Plasma treated both sides (90s)	56.4	10.3

X-Ray Photoelectron Spectroscopy

Chemical surface modifications resulted from direct oxidation of the cellulose nitrate surface by the oxygen plasma, or from chemical reactions induced on the cellulose nitrate surface by energy transfer from the plasma. Surface modification arising from oxidation is not thought to be particularly important. In the Cis envelope a broadening and increase in high energy counts were noted. This indicates that the carbon atoms of the cellulose nitrate backbone structure have been oxidized to form carbonyl or carboxyl functional groups.

Figure 4.10 shows the corrected C1s core level spectra for electrospun cellulose nitrate fiber mats that have been plasma treated for 0, 90 and 360 seconds. From these spectra it can be seen that considerable changes in the surface chemistries of the cellulose nitrates has taken place with plasma treatment. There was a reduction in the signal from the C-OH, which appeared at approximately 287 eV. The appearance of a new peak at 289 eV indicates that new carbon functionalities have been introduced with the plasma treatment. The exact identity cannot be determined using XPS, but it is most likely due to the formation of carbonyl (aldehydes and ketones) and carboxylate (acids and esters).

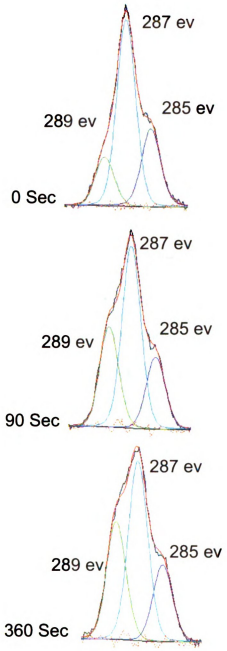

Figure 4.10 Comparison of C1s spectra. An addition of carbonyl and/or carboxylate signal (289 eV) is evident.

The changes observed in the NIs core level cannot be attributed to surface oxidation. The appearance of new nitrogen functionalities at lower binding energy is indicative of surface reduction, not oxidation. Very similar changes in this core level were reported in the argon plasma treatment of cellulose nitrates.[14] Here, direct energy transfer was shown to result in the removal of some nitrate esters from the cellulose nitrate surface, and in the conversion of nitrate esters into new nitrogen functionalities. Surface modification by direct energy transfer was shown to be limited to the outermost 10 angstroms of the surface of polymeric materials.

In the NIs core level there was a reduction in the signal from the nitrate ester, which appeared at about 408 eV, and the appearance of new peaks at 402 and 401 eV. The width of the new nitrogen peaks indicates that at least three new nitrogen functionalities were created by the plasma treatment. Their identity cannot be determined from the spectra alone; however, from a consideration of the binding energy range, possible assignments are N=O and NR_4^+ at 402 eV and N-N, -C≡N, NR_4^+ at 401 eV. The shift in nitrogen peaks is shown in Figure 4.11.

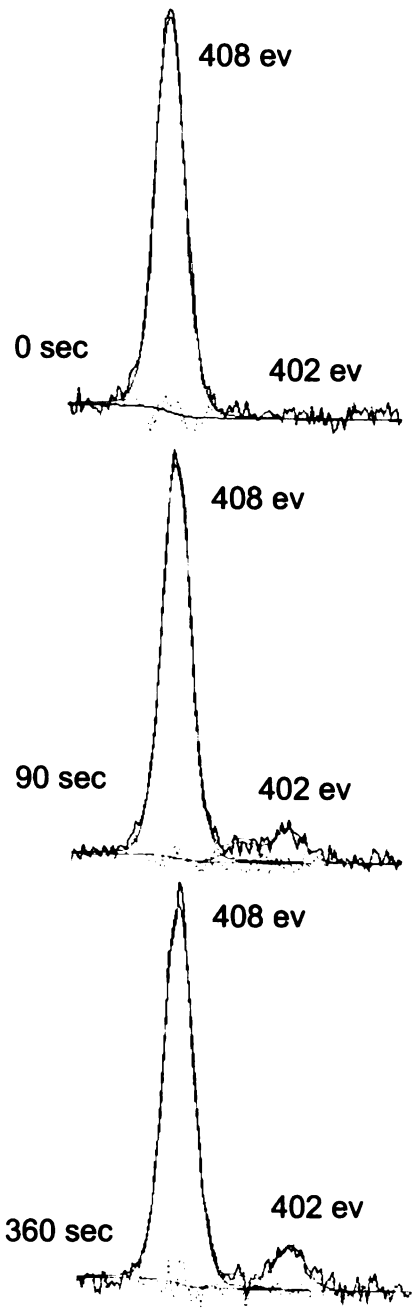

Figure 4.11 N1s XPS spectra, the reduction in nitrate ester signal (408 eV) is evident.

Radiative energy transfer has been shown to be responsible for the conversion of nitrate esters into the new nitrogen functionalities.[14] This occurred on a much slower time-scale than direct energy transfer, but occurred to a much greater depth into the material. In oxygen plasma both direct and radiative energy transfer from the plasma to the surface will occur, and energy transfer brought about changes observed by XPS in the NIs core level spectra. In argon plasma, cellulose nitrates do not etch. However, the modified surface resulting from energy transfer in oxygen plasma was being continually etched. The new surface presented to the plasma, as a result of etching, was also removed by the plasma.[15]

The XPS results are summarized in Table 4.6 below. The relative amounts of carbon, nitrogen and oxygen are not significantly changing with plasma treatment time, but the surface chemistry of the cellulose nitrate is changing. The nitrate functional group is being reduced as evidenced by the shift to lower binding energies. The cellulose nitrate backbone is also being oxidized to form esters, aldehydes or carbonyl structures.

Table 4.6 XPS summary table – relative C,N and O concentrations are constant with plasma treatment, but functionalities have changed

Plasma Treatment Time	Atomic Concentration Percentages									
	N-N 401 ev	N=O 402 ev	NO3 408 ev	C-C 285 ev	C-Q 287 ev	C=O, COC	COOH 289 ev	Element C1s	N1s	O1s
0 s	0	0	100	44.23	55.77	0	0	46.3	10.14	43.52
90 s	8.96	0	91.04	34.19	40.94	16.64	8.23	46.8	8.43	44.73
360 s	7.71	7.54	84.75	38.55	37.41	19.84	4.2	47.3	8.18	44.58

Fourier Transform Infrared Spectroscopy

The purposes of FTIR experiments were to confirm that the bulk chemistry of the cellulose nitrate has not been altered and to validate chemical changes from plasma treatment. Figure 4.12 shows the FTIR spectra for neat electrospun cellulose nitrate and samples that were plasma treated for 90s and 360s. The only significant difference in absorbance occurs with the hydroxyl groups at 3515 cm^{-1} and 3200 cm^{-1} and the carbonyl peak at 1750 cm^{-1}.

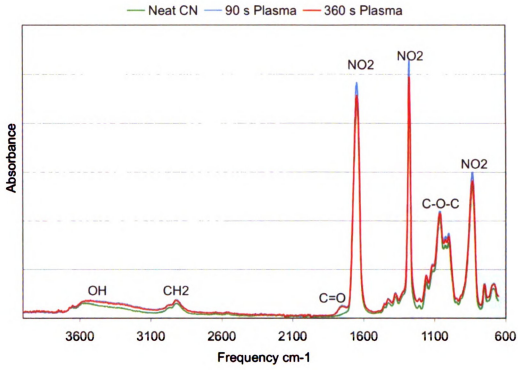

Figure 4.12 Full FTIR scan of neat electrospun cellulose nitrate and 90 s and 360 s plasma treated cellulose nitrate fibers.

The absorption bands for nitrate groups were strongest. Two very strong absorption bands at 1640 and 1275 cm^{-1} were evident due to the asymmetric and symmetric NO_2 vibration frequencies. Other absorption bands related to the nitrate functional groups are found at 830, 740 and 670 cm^{-1}. Figure 4.13 shows that there is not a significant difference in nitro group absorbance for the neat and plasma treated samples.

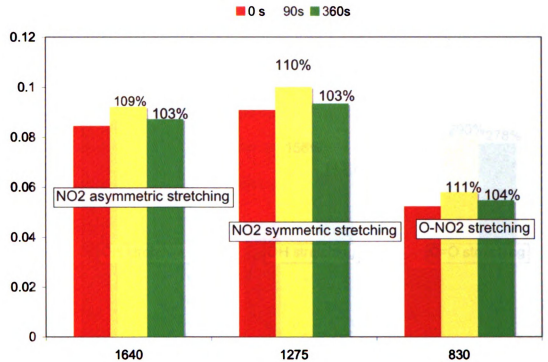

Figure 4.13 FTIR analysis of the nitro functional group absorbencies.

The CH stretching region (2800-3000 cm^{-1}) of Figure 4.12 is characterized by two bands of smaller intensity near 2900 and 2950 cm^{-1}. Based on IR analysis of cellulose the 2950 cm^{-1} band can be assigned to CH_2 stretching mode of nitrocellulose and the 2900 cm^{-1} band to the CH stretching mode.[26] The small peak at 1750 cm^{-1} is due to carbonyl (C=O) stretching. These differences are shown in Figure 4.14 below.

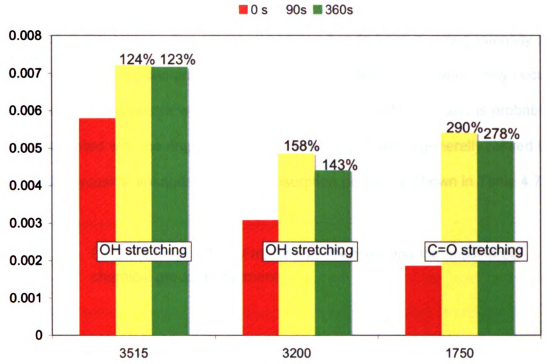

Figure 4.14 FTIR analysis of hydroxyl and carbonyl peaks, showing an increase in absorbance for plasma treated samples.

The very strong 1275 cm-1 band is mainly due to the NO_2 vibration. However, a band of medium intensity is observed at 1365 cm^{-1}, which can be assigned to the CH bending mode. In the 1000-1200 cm^{-1} range a strong IR band is observed at 1150 cm^{-1}. The same band is also observed in IR spectra of cellulose at 1162 cm^{-1} and of collodion at 1158 cm^{-1}. This band has been found in most polysaccharides and is believed to be characteristic of the ring structure, C-O stretching, asymmetric stretching of C1-O-C4' bridge and C-OH bending modes. Another strong band appears in this region at 1060 cm^{-1}. This band, in

the spectrum of native cellulose has been assigned to the C-O stretching mode in the C1-O-C4' bridge. The nitrate absorption bands have a strong intensity in the 740-950 cm^{-1} regions and cover most other vibration bands, which may occur in this region. However, a weak band still appears near 910 cm^{-1} and is probably also associated with the ring skeleton: this absorption band is generally related to α(1 -4)-D-glycosidic linkages. All major absorption peaks are shown in Table 4.7.

Table 4.7 FTIR summary table of major absorbencies and the associated chemical group assignment

Frequency cm-1	Assignment
3550	OH stretching
3200	
2950	CH_2 asymmetric stretching
2920	CH stretching
2850	CH_2 symmetric stretching
1650	C=O stretching
1450	CH_2 bending
1370	CH bending
1275	Si-CH3 stretching
1185	N-CH_3-H deformation
1150	CH_3 deformation
1060	CH_3-H deformation
1005	C-O stretching
995	
940	
835	N-CH_3 symetrical stretching

The pattern observed for plasma treatment using XPS is confirmed with FTIR. The plasma treatment reduces the nitro group and oxidizes the cellulose backbone structure. This is most easily seen with the drastic increase in the carbonyl peak with plasma exposure. FTIR has also been used to verify the cellulose nitrate bulk chemistry and provide a baseline for future work.

Thermal Properties – Thermal Gravimetric Analysis

Thermal analysis identified the presence on water in the resultant fiber network. A solvent system using ethanol and acetone resulted in uniform fibers, but the processing was hindered by the fact that the solvents were too volatile, which resulted in excessive needle clogging, which hindered the throughput of the process. Ethanol has a vapor pressure of 59 mm Hg and a boiling point of 78°C. It has been shown that ethanol is a suitable solvent for electrospinning.[6] Acetone has a vapor pressure of 229 mm Hg and a boiling point of 56°C. The mixture of ethanol and acetone is very volatile and does not result in residual solvent within the electrospun fibers as shown in Figure 4.15.

Another solvent system consisted of a mixture of THF and DMF. THF has a relatively high vapor pressure of 129 mm Hg and a relatively low boiling point of 66 °C. It is expected that all THF will be rapidly evaporated during the electrospinning process. DMF has a low vapor pressure of 3 mm Hg and a high boiling point of 153°C. Due to the high boiling point and low vapor pressure of DMF, it is thought that residual DMF will remain entrapped in the electrospun

fiber network. As Figure 4.15shows, there is only a small amount of water present in fibers that were electrospun from both solvent systems. The onset of degradation occurs at the same temperature, 205°C and the residual value of 1.5 wt% is the same for each solvent system.

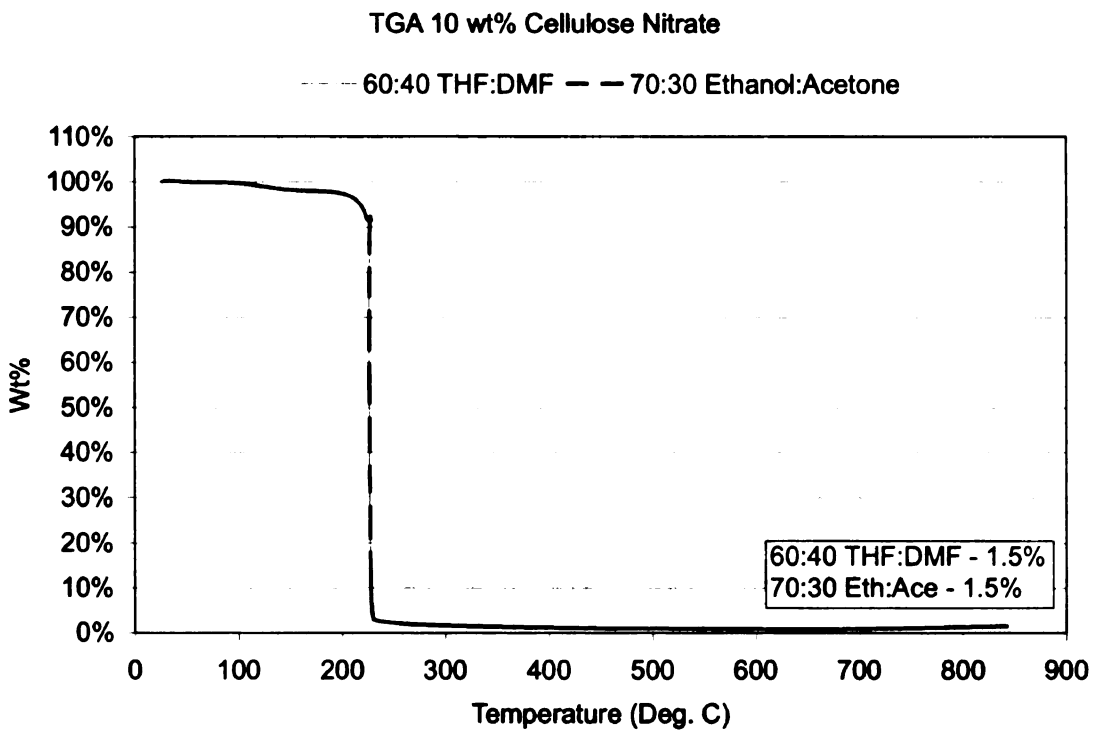

Figure 4.15 TGA thermogram of the electrospun fiber networks prepared from two different solvent systems, 60:40 THF:DMF and 70:30 Ethanol Acetone.

Electrical Properties

Electrical properties of the electrospun fibers were measured to establish a baseline for creating conductive polymer networks. Electrical Impedance Spectroscopy was used to measure the resistance of the fiber network at 1 Hz. This value will be used as a baseline value for the preparation of conductive fibers. It was determined that the neat electrospun cellulose nitrate had a resistance of 5.26E+10 ohms and a conductivity of 1.90E-09 S/cm. As expected, the cellulose nitrate was not conductive.

Mechanical Properties – Dynamic Mechanical Analysis

Mechanical properties were measured to characterize the tensile modulus of the electrospun fiber mats prepared from 8, 10 and 12 wt% solutions of cellulose nitrate in a 60:40 THF:DMF solvent mixture. These values were generated from a collection of five aligned fiber mat samples that were clamped in the DMA using a polycarbonate window frame. The data produced was then compared to literature data, which was only available for film samples.

A summary of tensile modulus as it relates to fiber diameter and more importantly fiber network density is shown as Table 4.8. There is a large difference in the modulus values, due to the considerable variance in fiber packing density. As Figure 4.16 shows, there is a considerable difference in fiber coverage amongst the samples analyzed. In general, it is expected that decreasing the concentration of starting solution from 12 wt% to 8 wt% would

result in more fibers per unit volume and would therefore improve the mechanical behavior. Film samples exhibit tensile modulus values of 1300 MPa, which are much higher than their electrospun fiber counterparts.[27] This is due in part to the volume and density of the fiber mat; the mechanical properties are relatively low due to the discontinuous, microporous nature of the nonwoven fibers

Table 4.8 Mechanical properties of electrospun cellulose nitrate fibrous materials

Solution Concentration (wt%)	Tensile Modulus (MPa)	Fiber Diameter (nm)	Fiber Coverage (%)
8	13.4	180	79
10	13.9	220	79
12	10.2	945	19

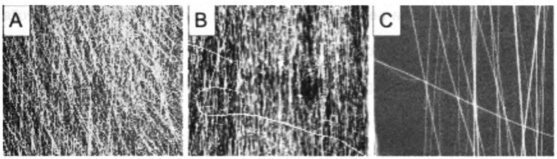

Figure 4.16 ESEM showing fiber coverage differences amongst A) 8 wt%, B) 10 wt% and C) 12 wt% solutions.

Electrospinning resulted in mechanical property values that were lower than films of cellulose nitrate. This was expected since the fiber network is open and porous, and since the bulk density of the electrospun fiber samples were much lower than the films. In summary, it was evident that smaller fibers maximized the space within the volume used for analysis and resulted in the highest modulus. To prepare biosensor capture pads, the fibers must be made to withstand multiple handling, washing and treatment steps, while still providing improvements in terms of surface area.

Conclusions

Cellulose nitrate was electrospun to form fiber mats with individual fiber diameters in the range of 100 to 1,000 nm. A unique rotating collector was designed that allowed for collection of the fibers without sustaining any damage to the fiber mat. Establishing a procedure to control fiber size and alignment will

allow for properties such as pore volume, surface area and capillary flow to be managed. The concentration of cellulose nitrate in solution was found to be the most dominant factor controlling fiber size. Increasing the concentration resulted in increased fiber diameters due to increased viscosity causing more entanglements, leading to a structure that was more resistant to external fiber whipping and stretching forces. Electrospun cellulose nitrate nanofibers are suitable for biosensor applications because they provide a large available surface area and cellulose nitrate is a material with great protein binding ability.

The electrospun cellulose nitrate fiber mats were found to be hydrophobic in nature, due to morphology issues, and were therefore unsuitable for capillary flow biosensor devices. This limitation was overcome by plasma treating the surface of the fibers. A 90 second plasma treatment was found to be most effective for creating surface functional groups that were hydrophilic, thus reducing the water contact angle and improving the capillary flow properties. The plasma treatment process allowed for the formation of carbonyl (aldehydes and ketones) and carboxylate (acids and esters) that were deteced using XPS and FTIR. The surface chemistry modification allowed for improvements in capillary flow by altering the surface functional groups to ones that were more hydrophilic. This technique is ideally suited to electrospun scaffolds because, unlike other physical and chemical modification techniques, it did not compromise the bulk architecture of the material.

A correlation between fiber packing density and mechanical properties was determined. In the case of 8 and 10 wt% cellulose nitrate solutions, the fiber

mats had similar densities and therefore resulted in similar mechanical properties. The 12 wt% solution had larger fibers, but a much more open porous structure and resulted in fiber mats with lower tensile modulus. The mechanical behavior of the fiber mats was lower than films, due to the large amount of void spaces in the fiber mats, with tensile modulus values in the 10 – 13 MPa range.

Thermal analysis was performed to determine if any residual solvent remained in the fiber mat, which may be detrimental. It was determined that the fiber mats did not contain any residual solvent, had a low water composition of 2wt% and the onset of thermal degradation was 205 °C. As expected, the electrical characterization showed that the neat fibers were insulating.

Cellulose nitrate nanofibers were electrospun from a mixed solvent system of 60 wt% THF and 40 wt% DMF. The resulting fiber network was composed of fibers that were approximately 95 nm in diameter and collected on a rotating drum with a PVDC film coating, allowing for easy fiber harvesting and random fiber morphology. These fibers will be used in a biosensor device that requires capillary flow. The neat electrospun fibers were hydrophobic; therefore a plasma treatment was developed to produce a surface that was hydrophilic. The plasma treatment introduced new surface functional groups, such as aldehydes and carbonyl structures on the cellulose nitrate backbone structure to increase wettability and capillary flow.

References

1. Dieter Klemm, B. H. H.-P. F. A. B., Cellulose: Fascinating Biopolymer and Sustainable Raw Material. *Angewandte Chemie International Edition* **2005,** 44, (22), 3358-3393.

2. Liu, H. Q.; Hsieh, Y. L., Ultrafine fibrous cellulose membranes from electrospinning of cellulose acetate. *Journal of Polymer Science Part B-Polymer Physics* **2002,** 40, (18), 2119-2129.

3. Ma, Z. W.; Kotaki, M.; Ramakrishna, S., Electrospun cellulose nanofiber as affinity membrane. *Journal of Membrane Science* **2005,** 265, (1-2), 115-123.

4. Son, W. K.; Youk, J. H.; Lee, T. S.; Park, W. H., Preparation of antimicrobial ultrafine cellulose acetate fibers with silver nanoparticles. *Macromolecular Rapid Communications* **2004,** 25, (18), 1632-1637.

5. Wu, X. H.; Wang, L. G.; Yu, H.; Huang, Y., Effect of solvent on morphology of electrospinning ethyl cellulose fibers. *Journal of Applied Polymer Science* **2005,** 97, (3), 1292-1297.

6. Shukla, S.; Brinley, E.; Cho, H. J.; Seal, S., Electrospinning of hydroxypropyl cellulose fibers and their application in synthesis of nano and submicron tin oxide fibers. *Polymer* **2005,** 46, (26), 12130-12145.

7. Zhou, W.; Li, Z.; Zhang, Q.; Liu, Y.; Wei, F.; Luo, G., Gas Flow-Assisted Alignment of Super Long Electrospun Nanofibers. *Journal of Nanoscience and Nanotechnology* **2007,** 7, 2667-2673.

8. Tong, H.-W.; Wang, M., Electrospinning of Aligned Biodegradable Polymer Fibers and Composite Fibers for Tissue Engineering Applications. *Journal of Nanoscience and Nanotechnology* **2007,** 7, 3834-3840.

9. G. Mathew, J. P. H. J. M. R. D. J. L. C. N., Preparation and anisotropic mechanical behavior of highly-oriented electrospun poly(butylene terephthalate) fibers. *Journal of Applied Polymer Science* **2006,** 101, (3), 2017-2021.

10. Li, D.; Ouyang, G.; McCann, J. T.; Xia, Y. N., Collecting electrospun nanofibers with patterned electrodes. *Nano Letters* **2005,** 5, (5), 913-916.

11. Image-Pro Software - MediaCybernetics - http://www.mediacy.com/.

12. Gu, B. K.; Sohn, K.; Kim, S. J.; Kim, S. I., Fabrications of Nanofibers as Crossed Arrays by Electrospinning. *Journal of Nanoscience and Nanotechnology* **2007,** 7, 4202-4205.

13. Lee, H.; Yoon, H.; Kim, G., Highly oriented electrospun polycaprolactone micro/nanofibers prepared by a field-controllable electrode and rotating collector. *Applied Physics A: Materials Science & Processing.*

14. Short, R. D.; Munro, H. S.; Ward, R. J.; McBriar, I.; Chan, H. S. O.; Tan, K. L., An xps investigation of the radiation-induced degradation reactions of cellulose nitrate .1. Argon plasma induced surface-reactions. *Polymer Degradation and Stability* **1991,** 31, (2), 211-218.

15. Short, R. D.; Munro, H. S.; Ward, R. J.; Chan, H. S. O.; Tan, K. L., An x-ray photoelectron-spectroscopy investigation of the radiation-induced degradation reactions of cellulose nitrate .2. Oxygen plasma-induced reactions. *Polymer Degradation and Stability* **1994,** 43, (1), 67-74.

16. Lafuma, A.; Quere, D., Superhydrophobic states. *Nature Materials* **2003,** 2, (7), 457-460.

17. Ma, M. L.; Gupta, M.; Li, Z.; Zhai, L.; Gleason, K. K.; Cohen, R. E.; Rubner, M. F.; Rutledge, G. C., Decorated electrospun fibers exhibiting superhydrophobicity. *Advanced Materials* **2007,** 19, (2), 255.

18. Zhai, L.; Cebeci, F. C.; Cohen, R. E.; Rubner, M. F., Stable superhydrophobic coatings from polyelectrolyte multilayers. *Nano Letters* **2004,** 4, (7), 1349-1353.

19. Shirtcliffe, N. J.; McHale, G.; Newton, M. I.; Chabrol, G.; Perry, C. C., Dual-scale roughness produces unusually water-repellent surfaces. *Advanced Materials* **2004,** 16, (21), 1929.

20. Herminghaus, S., Roughness-induced non-wetting. *EPL (Europhysics Letters)* **2000**, (2), 165.

21. Nosonovsky, M., Multiscale Roughness and Stability of Superhydrophobic Biomimetic Interfaces. *Langmuir* **2007,** 23, (6), 3157-3161.

22. Tuteja, A.; Choi, W.; Ma, M.; Mabry, J. M.; Mazzella, S. A.; Rutledge, G. C.; McKinley, G. H.; Cohen, R. E., Designing Superoleophobic Surfaces. *Science* **2007,** 318, (5856), 1618-1622.

23. Jian-Lin, L.; Xi-Qiao, F.; Gangfeng, W.; Shou-Wen, Y., Mechanisms of superhydrophobicity on hydrophilic substrates. *Journal of Physics: Condensed Matter* **2007**, (35), 356002.

24. Ma, M.; Hill, R. M.; Rutledge, G. C., A Review of Recent Results on Superhydrophobic Materials Based on Micro- and Nanofibers. *Journal of Adhesion Science and Technology* **2008,** 22, 1799-1817.

25. Ma, M.; Mao, Y.; Gupta, M.; Gleason, K. K.; Rutledge, G. C., Superhydrophobic Fabrics Produced by Electrospinning and Chemical Vapor Deposition. *Macromolecules* **2005,** 38, (23), 9742-9748.

26. Sekkal, M.; Dincq, V.; Legrand, P.; Huvenne, J. P., Investigation of the glycosidic linkages in several oligosaccharides using FT-IR and FT Raman spectroscopies. *Journal of Molecular Structure* **1995,** 349, 349-352.

27. In *Modern Plastics Encyclopedia*, 1999; pp B158 - B216.

CHAPTER 5

BIOSENSOR PERFORMANCE

Abstract

This chapter describes the development of electrospun cellulose nitrate fiber mats for use as a conductimetric biosensor for detecting *Escherichia coli* O157:H7. The biosensor consists of two components: an immunosensor that is based on electrochemical sandwich immunoassay, and a reader for signal measurement. The architecture of the immunosensor utilizes a lateral flow system that allows the liquid sample to move from one pad to another. The biosensor provides a specific, sensitive, low volume, and near real-time detection mechanism. Results are presented to highlight the performance of the biosensor for *Escherichia coli* O157:H7, which is of concern for health and safety issues.

Introduction

Biosensors are a potentially new application for electrospun cellulose based materials since they offer improved surface area over existing technologies. The large available surface area produces higher sensitivity, decreasing the detection time and improving the detection limit of the sensors.

Biosensor development and testing using the electrospun nanofibers were conducted by collaborating students at the Nano-Biosensors Lab. Methods and data on these experiments are presented here to show feasibility of the electrospun nanofibers for use in biosensors.

The performance of the electrospun cellulose nitrate fibers was evaluated using a simple detection mechanism of monitoring changes in resistance over time using a digital multimeter following methods and approaches by Muhammad-Tahir and Alocilja (2004), Pal et al. (2008) and Pal and Alocilja (2009).[1-3] *E. coli* O157:H7 was used in conjunction with the appropriate antibodies and conductive polyaniline complex to evaluate the effectiveness and sensitivity of the electrospun cellulose nitrate materials.

The conductive biosensor operates by using an electrical signal to determine the presence and concentration of a target analyte. The conductimetric biosensor consists of three porous membranes, referred to as the application, capture, and absorption pads (Figure 5.1).[1]

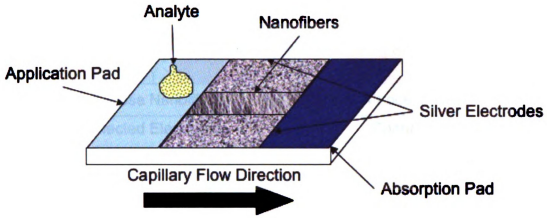

Figure 5.1 Schematic of the biosensor device

To begin detection, a fluid sample containing the antigen (Ag) is mixed with a conjugate of a specific antibody (Ab) and an electrically active polyaniline coated magnetic particle in a phosphate buffered saline solution.[2] Then, the Ag-Ab-polymer complex is re-suspended in sterile deionized water for testing. This solution is applied to the application membrane and flows across the capture pad by capillary action through the membrane pores. Finally, on the capture membrane, an Ab-Ag-Ab-polymer sandwich forms when the Ag-Ab-polymer complex binds to an immobilized Ab on the capture pad (Figure 5.2).[2] The conductive polymer creates an intercalated network bridging the gap between the electrodes, thus completing the circuit. The resistance of an electrical signal applied to the sensor can then be measured, with the resistance being inversely proportional to the Ag concentration of the sample.

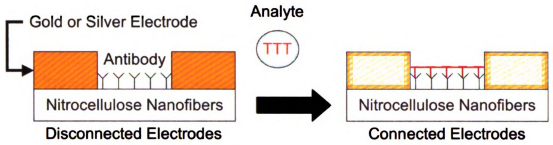

Figure 5.2 Schematic showing a cross section of the capture pad on a test strip.

Experimental

Nitrocellulose Fiber Mat Preparation

Cellulose nitrate was purchased from Scholle Corporation (College Park, GA). Solutions of cellulose nitrate were prepared in a 60:40 (wt:wt) mixture of tetrahydrofuran (THF):N,N-dimethylformamide (DMF). Solvents were purchased from Sigma-Aldrich (St. Louis, MO). Suitable solutions were made by dissolving 8 wt% (cellulose nitrate:total solvent) by magnetic stir bar mixing for 2 hours.

The electrospinning unit was purchased from Kato Tech Co (Kyoto, Japan) and operated with electric field strength of 10 kV, syringe pump rate of 0.01 mm/min, rotating drum speeds of 9 m/min, and collection times up to 4 hours. The collector was a rotating drum type collector wrapped in polyvinylidene dichloride (PVDC) to allow for easy fiber harvesting and resist fiber charge build

up. The separation distance was maintained at 10 cm between the needle tip and drum surface.

The PVDC backed electrospun fiber mats were plasma treated in a Plasma Sciences system for 90 seconds with a gas pressure of 0.29 torr and at a power level of 300W. The plasma treatment reduced water contact angles from the hydrophobic range of approximately 110 degrees to very hydrophilic around 12 degrees. This resulted in a vast improvement in capillary flow. The plasma treated samples were mounted on thin frame made of polycarbonate using spray adhesive. The samples were then cut into rectangular shapes approximately 2 inches by 5 inches for ease of capture pad preparation.

Electrodes were made of colloidal silver ink; which was applied to the capture pads using an airbrush operated at 28 psi. The airbrush deposition of conductive material was found to provide the most uniform electrodes with the least amount of fiber substrate damage. A mask was utilized to create electrodes 2.5 cm long and 1 cm wide with a 0.5 cm wide channel in between for testing. Individual test strips were cut from the capture pad with electrodes so that each test strip was 2.5 cm long with a narrow electrode on each side of the 0.5 cm wide channel. The finished test strips were stored in a sealed Petri dish.

Antibody Attachment To Capture Pad

Gluteraldehyde was used as a linking agent to attach the antibodies to the electrospun fiber mats. The plasma treated electrospun fiber mats were rinsed

with 100 µL of distilled water then let dry for 45 minutes in the biosafety cabinet. Then 20 µL of 0.1% glutaraldehyde ($C_5H_8O_2$) solution per 1.0 in^2 of fiber mat was applied with a hand pipette using a polycarbonate coverslip. This was allowed to dry in the biosafety cabinet for 30 minutes. The antibody attachment was confirmed using fluorescent-tagged antibodies and confocal scanning laser microscopy (CLSM) and the results are shown in Figure 5.3.

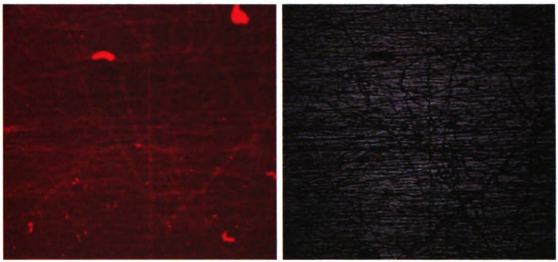

Figure 5.3 CLSM image of neat cellulose nitrate fibers and fibers with fluorescent-tagged antibodies attached.

A thin polycarbonate coverslip was placed on top of the fiber membrane to evenly disperse solution of the entire surface. The coverslip was removed and the fiber mat was allowed to dry for 30 minutes in the biosafety cabinet. After the fiber mat was dried, 20 µL of 0.5mg/ml per 1.0 in^2 of fiber mat of polyclonal *E.coli O157:H7* antibodies diluted in a phosphate buffer solution were applied to

the fiber membranes. A new clean polycarbonate cover slip was placed on top of the fiber mat to ensure even distribution of the antibody solution and promote capillary flow. The fiber mat was then sealed in a Petri dish with Parafilm and incubated for 1 hour at 37 °C to allow the antibodies to bind to the nanofibers.

The antibody coated fiber mats were washed with 20 µL of tris ($C_4H_{11}NO_3$) buffer with 0.1% tween-20 ($C_{58}H_{114}O_{26}$) per 1.0 in^2 of fiber mat. A new clean polycarbonate cover slip was placed on top of the fiber mat to ensure even distribution of the buffer solution. The fiber mats were sealed in Petri dishes and incubated for 45 minutes at 37 °C. The fiber mats were dried for 30 minutes in the fume hood and can be renamed capture pads. The capture pads were stored in a 4 °C refrigerator in a sealed Petri dish when not in use.

Preparing Conjugate Solution

In order to obtain a signal from the test strips, a magnetic conductive polymer must be used to form a bridge between the antibodies and the airbrushed electrodes. The method by Pal et al. (2008) was used to prepare the magnetic conductive polyaniline (PANi) solution.[2] Specifically, 100 µg of magnetic iron oxide (FE_2O_3) and polyaniline (PANi) conjugate were added to a 1.5 mL test tube. Then 1 mL of phosphate buffer solution (PBS) was added to test tube and sonicated for 10 minutes to disperse the particles. The appropriate amount of antibody was added to make the concentration of the solution 0.5 mg/ml. It was incubated in a hybridization oven at 25 °C at 30 rpm for 1 hour.[3]

After incubation, the test tube was vortex mixed and placed in a magnetic separator. After 2 minutes, the supernatant was removed using a micropipette to remove any unbound antibodies. Then 1 mL of tris buffer solution with 0.1% casein was added to the test tube. The test tube was then vortex mixed again, placed in the magnetic separator for 2 minutes, then the supernatant solution was removed with a micropipette. Then 1 mL of tris buffer solution with 0.1% casein was added to the test tube again. After the final rinse, the solution was resuspended in 1 mL PBS. This solution was stored in a 4 °C refrigerator until needed for test solution preparation.

Preparation of Test Solution

In order to obtain test solutions, the bacteria solution was serially diluted in sterilized water. 100 µL of bacteria solution, 800 µL of water, and 100 µL of conjugate solution were added to a 1.5 mL test tube. This solution was vortex mixed and allowed to react for 30 minutes at 20 rpm and 25 °C in a hybridization oven to increase bacteria antibody bonding. The tube was then vortex mixed again and placed in the magnetic separator for 2 minutes. The supernatant containing unbound bacteria was removed using a micropipette and replaced with 1 mL of PBS with 0.1% tween-20. The test tube was vortex mixed and placed in the magnetic separator for 2 minutes. The supernatant was removed and replaced with 1 mL of sterilized water. The final solution was vortex mixed and applied to the test strip by dispensing 50 µL onto strip or until flow across the

channel was deemed sufficient. The resistance of the test strip between electrodes was continually monitored using a multimeter.

Test Strip Construction

Test strips were constructed using the electrospun fiber mats as capture pads and commercially available Kim-wipe materials for application and absorption pads. The test strips were cut to the appropriate length and mounted onto the sensor-testing platform with double-sided tape. The Kim-wipe materials were cut and placed on the platform for application and absorption pads at the top and bottom of the capture pad. The airbrushed electrodes were connected to the test platform electrodes using colloidal silver ink and allowed to dry for 10 minutes. The application pad was attached to the platform and capture pad, and the absorption pad was constructed by placing the Kim-wipe material under the coverslip and a small section of commercially available nitrocellulose membrane material was placed on the Kim-wipe.

The completed test strip was covered with a polycarbonate sheet and held in place using binder clips on a glass slide to provide uniform pressure on the sensor channel. 50 μL of test solution was dispensed onto the application pad. Resistance was continually monitored using an impedance meter with 1-second intervals for 8 minutes and recorded and plotted. Test solution was continually monitored to ensure that the entire area of the test strip was being utilized. Once the lateral flow across the test strip was achieved, the resistance of the device

was stable and ready for analysis. The tests were performed in triplicate and the data was averaged. When the device was operational, the polyaniline complex became bound to the antibody present on the fiber and conductivity increased via a percolated network as shown in Figure 5.4.[4]

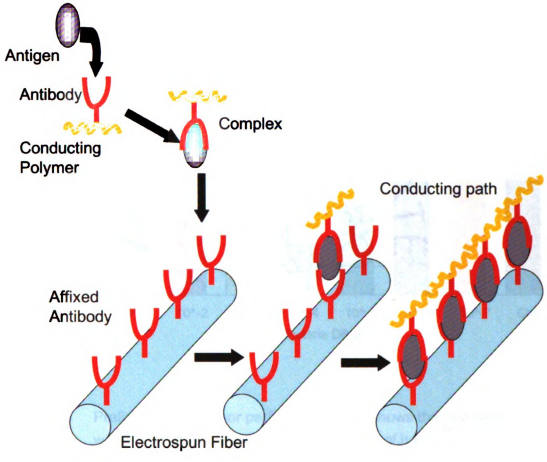

Figure 5.4 Non-Conductive biosensor design.

The preliminary data shows that the sensor works and that it is sensitive to the bacteria concentration (Figure 5.5). The data shows that as storage time increases, the antibodies will denature and be less effective. Using an immediate testing procedure provides the highest sensitivity.

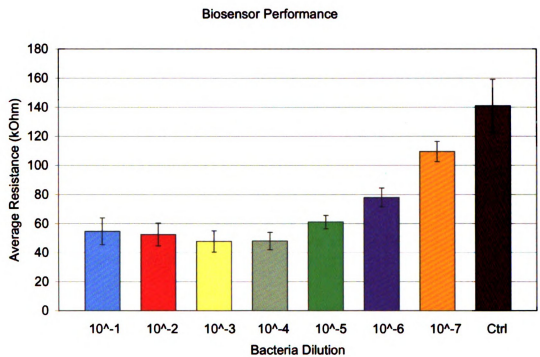

Figure 5.5 Preliminary biosensor performance data shows that the sensor works and is sensitive for several dilutions of bacteria.

Results and Discussion

Figure 5.5 shows the preliminary data as a bar graph. It can be seen that further improvements would help to distinguish between the control sample and

the dilutions. Improvements need to be realized in terms of storage time and testing time. Improvements are needed to increase the resistance of the control solution. This will allow for further dilutions to be accurately detected. A procedure needs to be developed to understand and limit the denaturing effect of the antibodies and provide reliable reproducible data sets.

References

1. Muhammad-Tahir, Z.; Alocilja, E. C., A Disposable Biosensor for Pathogen Detection in Fresh Produce Samples. *Biosystems Engineering* **2004,** 88, (2), 145-151.

2. Pal, S.; Setterington, E. B.; Alocilja, E. C., Electrically active magnetic nanoparticles for concentrating and detecting Bacillus anthracis spores in a direct-charge transfer biosensor. *Ieee Sensors Journal* **2008,** 8, (5-6), 647-654.

3. Pal, S.; Alocilja, E. C., Electrically active polyaniline coated magnetic (EAPM) nanoparticle as novel transducer in biosensor for detection of Bacillus anthracis spores in food samples. *Biosensors & Bioelectronics* **2009,** 24, (5), 1437-1444.

4. Yuk, J. S.; Jin, J. H.; Alocilja, E. C.; Rose, J. B., Performance enhancement of polyaniline-based polymeric wire biosensor. *Biosensors & Bioelectronics* **2009,** 24, (5), 1348-1352.

CHAPTER 6

CONCLUSIONS

Understanding the processing conditions and solution variables that affect the electrospinning process is essential for creating uniform homogenous nanoscale fiber mats. Post treatment processes allow the fiber mats to take advantage of the surface chemistry and capillary flow properties required for sensor applications. Combining the knowledge gained from altering the processing conditions in combination with post-treatment procedures allows for construction of sensor substrates with tunable properties.

It was determined through a series of experiments that varied solvents, solvent ratios and quantities that a mixed solvent system of THF and DMF provided the best results for the electrospinning process in terms of homogenous fiber production, limited operator interaction (no needle clogging) and ease of solution preparation. Specifically the optimal solution was determined to be 8 wt% cellulose nitrate dissolved in a 60:40 (by weight) THF:DMF solvent system. This solution allowed the electrospinning operation to be run continuously, without interruption for up to 12 hours.

The ideal solution could be electrospun onto any type of collector, depending on the desired fiber morphology. A split electrode (c-shaped) collector allowed

the production of aligned fiber mats. A rotating drum that was wrapped in PVDC reduced the alignment, but provided a dramatic improvement in production rate. It was determined that the optimum operating conditions for the Kato-Tech Nanofiber Electrospinning Unit were 10 kV applied to the syringe needle, a needle tip to collector spacing of 10 cm a syringe pump flow rate of 0.01 mm/min and when using the rotating drum, a rotating drum speed of 9 m/min. These processing conditions allowed for uniform fiber mats 2.5 inches wide and 28 inches long to be produced in 4-hour intervals. The use of PVDC on the rotating drum allowed for the fiber mat to be easily transferred from the collector without damaging the fiber network. Increasing the concentration of the cellulose nitrate in solution produced larger diameter fibers, which decreased the surface area of the fiber mat. Slowing the rotation rate of the drum decreased the fiber alignment. Altering the size and morphology of the fibers is important to modify the performance of the sensing device. After removing the PVDC film from the collector, the fibers were subjected to a plasma treatment process.

Plasma treatment was performed on the electrospun fiber mats to increase the capillary flow. Capillary flow is required for adequate biosensor performance. It was determined that 90 seconds of oxygen plasma with a gas pressure of 0.29 torr and power level of 300W provided the optimal capillary flow properties while maintaining good antibody adhesion characteristics. The changes in surface chemistry were observed using XPS and contact angle measurements. Contact angle measurements proved that the surface was becoming more hydrophilic with plasma treatment. The water contact angle was decreased from 110

degrees to 12 degrees after the plasma treatment. The electrospinning equipment had an effect on the contact angle. Plastic syringes were found to produce fiber mats with higher, more hydrophobic, contact angles. This was due to the strong solvents THF and DMF leaching materials from the plastic labware. XPS proved that oxidation was responsible for decreasing the contact angles. The relative amounts of carbon, nitrogen and oxygen were not significantly changing with plasma treatment time, but the surface chemistry of the cellulose nitrate was changing. The nitrate functional group was being oxidized as evidenced by the shift to lower binding energies. The cellulose nitrate backbone was also oxidized to form esters, aldehydes or carbonyl structures. It is recommended that glass lab ware be used to limit contaminants. Plasma treatment should be performed on the PVDC backing to maintain a rigid fiber mat with minimal damage to the cellulose nitrate fibers.

An airbrush was operated with a line pressure of 28 psi to deposit colloidal silver particles on the plasma treated cellulose nitrate fibers. The fiber mats were mounted to polycarbonate sheets using spray adhesive and masked using the rectangular steel mask with 0.5 mm width. It was determined that 4 to 5 inch distance of airbrush gun to fiber sample produced the most uniform paint coverage. The mask was then placed on a large magnet with the sample between the magnet and the mask. This masking method allowed for half of the mask to be used at one time, but significantly limited the stray silver particles in the sensor channel. After electrode deposition, the samples were transferred back to Biosystems Engineering department for treatment and testing.

The procedure was optimized to produce the highest sensitivity and best signal to noise ratio. The samples were rinsed with deionized water twice and allowed to dry for 30 minutes. Then 20 micro liters per square inch of 0.1% gluteraldehyde solution was applied and dried with a coverslip for 30 minutes. Then 20 micro liters per square inch of antibody solution was applied and incubated at 37 ° C for 1 hour. Then 20 micro liters per square inch of tris buffer solution was applied and incubated at 37 ° C for 45 minutes. Silver electrodes were applied to the nanofiber mats using an airbrush.

The next step in fiber mat preparation was to cut individual test strips using a razor blade in a guillotine fashion. The test strips were attached to the testing platform with double sided tape and hand painted silver electrodes. A polycarbonate coverslip was used to ensure proper flow on test solution. The test solution was prepared by adding magnetic polyaniline-antibody solution to control dilution (deionized water), in 10^{-2}, and 10^{-4} dilutions of original culture. These were put in a hybridization oven for 30 minutes at 30 rpm and 25 ° C to increase bacteria antibody bonding. They were then separated three times to concentrate bacteria solution and remove other materials.

Measuring the voltage across the channel continuously for a period of 8 minutes provided the test results. A small Kim wipe at top and bottom below cellulose fiber pads was added to improve sensor performance. A polycarbonate coverslip was placed over the Kim wipes and capture pad regions. Then 50 µL of the test solution was placed onto application pad (cellulose pad cut in half) and results were logged and recorded.

It was determined that the sensor was sensitive to various *E. coli* O157:H7 bacteria concentrations, but improvements still need to be realized. The sensitivity and testing/storage time limitations need to be improved. Reducing the time between sensor pad constructions and testing can realize improvements in sensitivity.

Future Work

Electrospun fiber mat production rate can be improved by increasing the number of syringes within the electrospinning unit. Glass syringes should be added with a minimal spacing of 5 cm between the needle tips to limit the interactions. In order to improve alignment using the rotating drum, higher rotational speeds must be realized. This is only possible with a higher speed motor or altering the pulley ratio on the electrospinning unit. Fiber sizes can be increased by increasing solution concentration and by changing fiber sizes in conjunction with processing variables; changes in fiber mat porosity can be realized. Alterations of porosity may have an impact on the sensor sensitivity.

Understanding the time degradation behavior of test solutions and the electrospun fiber materials will allow for testing procedure optimization. By improving the testing procedure, sensor performance improvements can be achieved. A study of various fiber sizes, which will lead to fiber mat porosity changes and capillary flow differences, should be studied to understand the optimal conditions necessary to realize the most sensitive device.